ADAPTIVE CONSTRUCTION MODELLING WITHIN WHOLE BUILDING DYNAMIC SIMULATION

Abdullatif E. Nakhi

A thesis submitted for the
Degree of Doctor of Philosophy

Department of Mechanical Engineering
Energy Systems Research Unit
University of Strathclyde
Glasgow, UK.

October 1995

Dedicated
To My

Parents, Eisa and Maliha
wife, Masoumah
children, Sarah, Saleh and Hajar

Table of Contents

ACKNOWLEDGEMENTS

This thesis could not have been completed without the help and the support of many individuals and institutions to whom I am grateful.

My gratitude is sincerely expressed to Professor J. A. Clarke for his guidance, expert knowledge and never ending stream of ideas while this study was undertaken.

My thanks go to the government of Kuwait, particularly the Puplic Authorities for Applied Education and Training (PAAET), for their financial support

I wish to thank my colleges E. Aasem, M. Evans, T. Chow, J. Hand, J. Hensen, M. Janak, N. Kelly, M. Lindsay, I. Macdonald, J. MacQueen, C. Negrao, P. Strachan and M. van der Laan.

Finally, I am grateful to my family for their support and help while this thesis was being produced. I dedicate this thesis to them.

Abstract

In today's climate of energy, environment and health awareness, it is important to design buildings which respect to the threefold goals of efficient energy use, protection of the environment and human health. This can best be achieved if overall building performance is considered within the building design process. However, because the energy/environmental performance of buildings is dynamic and complex, simulation tools should be employed within the design process. In order to service this need, simulation model accuracy and applicability should be improved.

While the state-of-the-art for environmental building performance simulation has been substantially enhanced for most processes, building fabric modelling is not well performed. Many simplifying assumptions are adopted in multi-layered construction modelling. For example, thermophysical properties are often assumed constant, heat flow through building constructions is considered to be one dimensional, and moisture transport through porous building materials is not considered.

This thesis is concerned with the development of new simulation schemes for adaptive building construction modelling. These schemes are integrated within a state-of-the-art energy simulation environment so that it can be effectively employed in practice.

After addressing the theory underlying heat and moisture diffusion within porous media, three approach to adaptive building fabric simulation are presented. These are: multi-dimensional, variable resolution, error based building fabric modelling; variable thermophysical properties simulation and combined heat and moisture transport simulation. The numerical model, implementation and solution methods of these schemes are discussed in detail.

The validation of these schemes is then performed, after their integration with the whole building simulation environment, ESP-r. This is done using a comprehensive validation methodology, which includes the elements of theory checking, source code inspection, analytical conformance, inter-model comparison and empirical verification.

The applicability of the developed schemes is then presented in the context of a typical Scottish house design. It is concluded that the application potential and robustness of environmental building performance tools have been increased.

Finally, the future work required to increase the applicability and accuracy of building simulation tools is elaborated in terms of the required integration with other technical sub-systems and related computer aided design tools.

LIST OF SYMBOLS

A	area	$[m^2]$
a	scale factor	[–]
Bi	Biot number	[–]
c	specific heat	$[J/kgK]$
D	mass diffusivition coefficient	
d	layer thickness	$[m]$
e	error vector	
F	mass diffusion driving potential	
Fo	Fourier number	[–]
f	geometric view factor	[–]
f	surface temperature factor	[–]
G	heat source term	$[W]$
g	heat source term	$[W/m^3]$
g	acceleration due to gravity	$[m/s^2]$
Gr	Grashof number	[–]
h	enthalpy	$[J/kg]$
h	heat transfer coefficient	$[W/m^2K]$
I	chemical species phase change source	$[kg/m^3s]$
J	mass flux	$[kg/m^2s]$
L	heat of transformation	$[J/kg]$
l_c	characteristic length	$[m]$
M_a	molecular mass of air (28.964)	$[kg/kmole]$
M_w	molecular mass of water (18.016)	$[kg/kmole]$
m	number of nodes per layer	
m	mass	$[kg/m^3]$
P	partial water vapour pressure	$[Pa]$
Pr	Prandtl number	[–]
q	heat flux	$[W/m^2]$
R	universal gas constant (8314.4)	$[J/kmole\ K]$
S	moisture source term	$[kg/s]$
s	moisture specific source term	$[kg/m^3s]$

Sc	Schmidt number	[–]
t	time	$[s]$
T	temperature	$[^oC]$
u	moisture content	$[kg/kg_{material}]$
$\mathbf{u}$	internl energy	$[J/kg]$
V	volume	$[m^3]$
w	moisture content	$[kg/m^3]$
x	vapour ratio	$[kg/kg_{air}]$
z	hight	$[m]$

Greek symbols

Λ	thermophysical property	
Φ	total hydraulic head	$[m]$
Ψ	eigenvector	
Θ	inverse of thermal storage term	$[K/J]$
Υ	hydraulic potential	$[m^2/s^2]$
α	thermal diffusivity	$[m^2/s]$
β	convective mass transfer coefficient	$[s/m]$
χ	volume fraction of air-filled open pores	[–]
δ	water vapour permeability	$[s]$
ε	stopping criterion	
γ	implicitness degree	[–]
κ	material hydraulic conductivity	$[m/s]$
λ	heat conductivity	$[W/mK]$
μ	vapour resistance factor	[–]
ν	kinematic viscosity	$[m^2/s]$
ω	eigenvalue	
ϕ	relative humidity	[–]
ψ	eigenvalue	
ρ	density	$[kg/m^3]$
θ	moisture content	$[m^3/m^3]$
υ	tortuosity factor	[–]
ξ	moisture storage capacity	$[kg/kg]$
ζ	linear thermal transmittance	$[W/m\ K]$

Subscripts

c	convective
g	gravity
l	liquid
m	matrix
o	dry
P	pressure as the driving potential
r	radiative
r	reference
s	saturation
T	temperature as the driving potential
tot	total
v	vapour

Superscrips

D	molecular diffusion
P	pressure as the second driving potential
P_{tot}	filtration motion
T	thermal diffusion
T	temperature as the second driving potential
$\rightarrow$	vector
.	per unit time
–	average

CHAPTER 1

Introduction

1.1 The need for building energy simulation

A fundamental change in the characteristics of our energy consumption is urgently needed in order to combat the ever increasing energy related challenges such as pollution, waste, the exhausting of fossil fuel resources, local thermal pollution, global warming, and the depletion of the ozone layer (Tolba *et al*, 1992; IEA, 1994). In general, energy related activities are either contributing constituents in, or the main causes of, considerable environmental concerns.

There are three main approaches that can be used to reduce the environmental impact of energy related activities: emission control, use of less polluting energy sources, and increasing energy efficiency. Energy conservation § is the most effective approach since it leads to both energy security and desirable environmental goals, particularly the reduction of the carbon dioxide emissions that contribute to global warming (IEA, 1991).

In most of the industrialised and developing countries nearly half of the national energy consumption is in buildings. For example, some 56% of the total British annual energy consumption is used in buildings (Bunn, 1990). On the other hand, the UK Department of Energy estimates that the better design of new buildings could produce energy consumption reductions of 50% and that appropriate design intervention in the existing stock of buildings could result in a 25% reduction in energy consumption (Clarke and Maver, 1991). Therefore, there is a significant potential for energy conservation in buildings.

The major potential for energy conservation in buildings is in the reduction in the use of heating, ventilating, and air-conditioning (HVAC) systems since more than 60% of the building energy consumption is used to condition the indoor environment (Gandrille and Hammond, 1988) and the energy consumption of HVAC systems is increasing (Rousseau and Mathews, 1993).

§ energy conservation is defined as the strategy of adjusting and optimising energy use in order to reduce energy use per person (unit of output) without causing disruption in life styles (or affecting socio-economic development).

Energy conservation in HVAC systems can be achieved through optimisation, and through improved building thermal performance. This can best be achieved if the building's thermal performance, HVAC system sizing and optimisation of controls are considered together within the building design process (Hokoi and Matsumoto, 1993). However, buildings and their environmental control systems are complex (multi-dimensional and highly interactive) making this optimisation task non-trivial. The various flow paths (and their interactions) commonly encountered in buildings are presented in detail by Clarke (1993) who stated that the energy sub-system is inherently complex because it is:

- dynamic: associated variables change with time and at different rates.
- non-linear: most of the flow paths are related to temperature in a non-linear manner.
- systemmic: different heat transfer mechanisms interact in a complex manner.

In order to accommodate this complexity, and provide effective design decision support, building energy simulation has received growing attention in recent years. This is because simulation tools can be used directly and indirectly to achieve energy efficient buildings. Computer modelling can be used directly within the building design process, or indirectly through research and code of practice, to accomplish environment friendly buildings.

1.2 The evolution of building energy simulation tools

The evolution of building energy simulation tools, from the traditional to the present day simulation approach, is summarised in Table 1.1. In the early 1960s, the HVAC systems in buildings were designed in order to meet thermal comfort requirements, architectural needs, and constructional budgets. Very simplified manual methods, such as the degree day method (ASHRAE, 1993), were used to predict building energy consumption. Accordingly, HVAC systems were usually over designed and mechanical and/or electrical control systems were used to maintain the indoor thermal comfort. In the late 1960s, and early 1970s, programs were developed to automate these manual load calculation methods. These programs represent the first generation of building energy simulation tools.

The world energy crisis of 1973-74 boosted the development and use of automated energy calculation tools. Consequently, the 2nd generation emerged, by which building energy models were able to predict the dynamic thermal performance of buildings instead of just calculating the peak thermal loads. Commonly, these programs were established to operate on an hourly basis. This required more computing power, which became available due to the rapid advances in computer technology.

The second world energy crises (1979-80) moved energy conservation in buildings from an important, but optional extra, to a basic requirement. Because of that, and the development in computing power, the 3rd generation of building energy simulation tools emerged. The main feature of this generation is the recognition of the importance of energy flow path integration, for which

Table 1.1 The evolution of building energy simulation tools (from Clarke and Maver, 1991)

1 st Generation	• Handbook oriented • Simplified • Piecemeal	• Indicative • Applications limited • Difficult to use
2 nd Generation	• Dynamics important • Less simplified • Still piecemeal	
3 rd Generation	• Field problem approach • Numerical methods • Integrared energy sub-systems • Heat and mass transfer considered • Better user interface • Partial CABD integration	
Next Generation	• CABD integration • Advanced numerical methods • Intelligent knowledge based • Advanced software engineering	• Predictive • Generalised • Easy to use

numerical methods were adopted.

The need for energy conservation, and building energy modelling, grew by the third world energy crisis in the late 1980s. Unlike the first two crises, this was related to environmental issues. Effectively, this called for the integration of thermal performance within the building design process. As a result several projects were launched for the development of computer aided building design such as within the Computer Models for the Building Industry in Europe (COMBINE) project (Augenbroe, 1992). These projects represent the trends for the 4th simulation generation.

Measures employed for energy conservation in buildings have affected indoor air quality. The concentration of a wide range of impurities, such as micro-organisms, in the occupied space have increased. This contributes to the phenomenon of building related illness, known as Sick Building Syndrome. The air impurity concentration is regulated by the rate of fresh air introduction, and the rate of generation of impurity elements. In the pursuit of energy conservation, designers adopted lower fresh air supply regimes. In addition, improper insulation installation often created thermal

bridges. Taken together, these factors establish localised micro-climates suitable for the germination and growth of micro-organisms (Rowan *et al*, 1995). This issue not only magnified the need for integrated building design, but also raised the need for a higher thermal simulation resolution in order to better model three dimensional phenomena such as thermal bridging.

1.3 The need for accurate building fabric modelling

On the other hand, the need for more accurate building energy simulation increased because of the adoption of passive solar and naturally ventilated buildings. For such buildings, simulation tools are expected to predict accurately (i.e. within an acceptable margin of error) the time varying demands and internal temperatures (Bunn, 1995).

The building energy simulation research community is continuously working to bridge the gap between computer aided building design tools and practice. In recent years, intensive research has been performed in order to ensure that the quality of these prediction tools is high. Three major approaches are extant. First, the development of new mathematical models for a better representation of the heat and mass transfer processes occurring within the building/plant system. Second, by increasing the simulation resolution in order to reduce the number of simplifying assumptions which are often invalid. Third, by elaborating a comprehensive validation methodology which includes all stages of simulation program development.

The simulation of most of the heat and mass transfer processes occurring within the building/plant system have been significantly improved. For example, Negrao (1995) coupled computational fluid dynamics with a whole building environmental performance tool (ESP-r) in such a way that the CFD model operates in conjunction with ESP-r's air flow network (Cockroft, 1979; Clarke, 1985; Hensen, 1991). In the approach, CFD provides discretised information about the mass, energy and momentum state of a space. Hence, detailed information about the air flow within a space can be achieved. Therefore, this project allows dynamic simulation of air flow through the entire building with variable resolution.

While the state-of-the-art for environmental building performance simulation has been substantially enhanced for most processes, building fabric modelling is not well performed. Many simplifying assumptions are adopted in multi-layered construction modelling. For example, thermophysical properties are often assumed constant, heat flow through building constructions is considered to be one dimensional, and moisture transport through porous building materials is not considered.

Conduction modelling is one of the main physical processes in building thermal simulation and its integration with other processes, such as solar gain and convective air flow, dominates the overall performance. In contemporary models, these integrations are usually performed in such a way that the conduction algorithm is at the core of the calculation procedure. Hence, errors in conduction may have a compound effect on the accuracy of a simulation. For example, conduction errors may affect

the surface temperature prediction and so, indirectly, affect the action of a control system. Therefore, the acceptable accuracy for conduction modelling in isolation is not necessarily acceptable for conduction modelling when placed within a building energy simulation package.

Modelling of conduction heat flow through porous building materials is a macroscopic process involving one or more of the following:

- conduction through the material matrix
- conduction through the pore filling gas
- convection in wide pores
- radiation in the pores
- conduction via the absorbed and capillary condensed water
- heat flow through the pore filling moisture.

Therefore, in building applications, conduction heat flow is a complex process for which empirical based information on the material's hygrothermal properties are used in order to simplify it. Several recent validation projects (e.g. CEC, 1989; Bloomfield, 1992) have demonstrated the importance of accurate modelling in order to bring together experimental results and predictions. Therefore, conduction analysis assumptions have to be reconsidered for the case of building combined heat, air and moisture transfer.

The need for accurate building energy simulation is not only associated with aspects related to energy conservation and thermal comfort, but also to building fabric and environmental health. This is because accurate predictions of the dynamic temperature distribution at the inside surface of the building envelop (i.e. where the highest potential for condensation occurs) is of primary importance for condensation, which can cause structural damages, result in surfaces disfiguring, and boost germination and mould growth (Pel, 1995; Rowan *et al*, 1995).

1.4 Objective and outline of the present work

The objective of the present work is to develop and enhance building environmental performance evaluation tools in terms of adaptive fabric modelling within whole building dynamic simulation. This is achieved by means of adaptive building fabric gridding, facilitating variable thermophysical properties simulation, and combined heat and moisture transport simulation.

The development of these schemes requires a clear understanding of heat and mass diffusion in porous materials. The fundamentals of heat and mass diffusion in solids are presented in Chapter 2. The technique of adaptive gridding is presented in Chapter 3 where a multi-dimensional, variable resolution, error based gridding technique is developed. Chapter 4 is concerned with the effect of a material's temperature and/or moisture content variation on its thermophysical properties. It covers

the linear temperature and/or moisture content dependence of thermal conductivity, and the nonlinear temperature dependence of thermophysical properties. A mathematical model of combined heat and moisture transport within building constructions is presented in Chapter 5. The developed schemes are validated in Chapter 6. Then, practical applications for the developed schemes are demonstrated in Chapter 7. Finally, in Chapter 8, conclusions and recommendations for future work are presented.

References

American society of Heating, Refrigeration, and Air-Conditioning Engineers 1993. in *ASHRAE HANDBOOK: Fundamentals*, Atlanta,USA.

Augenbroe, G 1992. ''Integrated building performance evaluation in the early design stages,'' *Building and Environment*, vol. 27, no. 2, pp. 149-161.

Ayres, J M and E Stamper 1995. ''Historical Development of Building Energy Calculations,'' *ASHRAE journal*, vol. 37, no. 2, pp. 47-55.

Bloomfield, D P 1992. ''IEA Annex 21 Technical Briefing: Calculation of Energy and Environment performance in Buildings,'' in *Proc. IEA Energy Conservation in Buildings and Community Systems*, Maastricht.

Bunn, R 1990. ''Going Green,'' *Building Services the CIBSE Journal*, vol. 12, no. 10.

Bunn, R 1995. ''Simulation Models: Tower of Babel or The Promised Land,'' *Building Services The CIBSE Journal*, vol. 17, no. 1.

CEC 1989. *The PASSYS Project Phase 1*, Commission of the European Communities, Research and Development, Brussels..

Clarke, J. A. 1985. *Energy simulation in building design*, Adam Hilger Ltd, Bristol,UK.

Clarke, J A and T W Maver 1991. ''Advanced Design Tools for Energy Conscious Building Design: Development and Dissemination,'' *Building and Environment*, vol. 26, no. 1, pp. 25-34.

Cockroft, J P 1979. ''Heat transfer and air flow in buildings,'' *PhD thesis University of Glasgow*.

Gandrille, T and G P Hammond 1988. ''An intermediate-level model of external convection for building energy simulation,'' *Energy and Buildings*, vol. 12, pp. 53-66.

Hensen, J.L.M. 1991. ''On the thermal interaction of building structure and heating and ventilating system,'' Ph.D. Thesis, Eindhoven University of Technology.

Hokoi, S and M Matsumoto 1993. ''An Analysis of Stochastic Properties of Room Temperature, Cooling Load and Air-conditioning Systems,'' *Energy and Environment*, vol. 28, no. 4, pp. 497-508.

IEA1991. , *Energy Efficiency and the Environment*. OECD/IEA

IEA1994. , *World Energy Outlook*.

Johnson, P D1994. , *Reducing Carbon Dioxide Emissions and Improving Comfort in New Build Low Energy Housing*. Proceedings of the First International Conference on Buildings and the Environment. session: energy, paper 10

Masters, G M 1991. *Introduction to Environmental Engineering and Science*, Prentice Hall, Inc, USA.

Negrao, C 1995. ‘‘Conflation of Computational Fluid Dynamics and Building Thermal Simulation,’’ *Phd thesis, University of Strathclyde*.

Oreszczyn, T 1992. ‘‘Insulating the existing housing stock: mould growth and cold bridging,’’ in *Energy Efficient Building: A Design Guide*, ed. S Roaf and M Hancock.

Pel, L 1995. ‘‘Moisture Transport in Porous Building MaterialsPhD Thesis,’’ *PhD Thesis, Eindhoven University of Technology*, The Netherland.

Rousseau, P G and E H Mathews 1993. ‘‘Needs and Trends in Integrated Building and HVAC Thermal Design Tools,’’ *Energy and Environment*, vol. 28, no. 4, pp. 439-452.

Rowan, N, J A Clarke, J E Smith, J G A Anderson, A Nakhi, N Kelly, R McClain, and J L M Hensen1995. , *Development of a prototype technique for the prediction/alleviation of conditions leading to mould growth in houses*, Glasgow. ESRU report

Shaw, M R and K W Treadaway 1994. ‘‘The Energy Related Environmental Issues Research Programme,’’ in *Proceedings of Building Environmental Performance: Facing the Future*, pp. S-49 - S-63.

Tolba, M K, O A El-Kholy, and E El-Hinnawi 1992. in *The World environment 1972-1992 : two decades of challenge*, Chapman & Hall, New York.

CHAPTER 2

Review of Heat and Moisture Transport within Porous Materials

In Chapter 1, the need for more accurate building fabric modelling was highlighted and three areas for development were defined as the objective of the current work. The developments require a clear understanding of the related theory. In this chapter, the fundamentals of heat and mass diffusion are presented after a brief description of numerical simulation. This is followed by a literature review for the three development areas.

2.1 Building energy simulation

The building energy system is complex. It encounters various interacting, dynamic flow paths as shown in Figure 2.1. In order to simulate these flow paths, a mathematical model must be developed. From a mathematical point of view, the flow paths must be expressed by some governing equations. After that, a numerical model is generated. As a result, the building energy system is represented by an equivalent network of time-dependent resistances and capacitances subjected to varying driving potentials (such as temperature and pressure gradients). In general, the numerical simulation is performed as a three stages process: discretisation of the problem, derivation of simulation equations for the discrete system, and solution (simultaneous) of this set of equations.

As an introduction to the simulation of heat and mass transport through the building fabric, the mathematical, numerical and computational approaches for heat and mass diffusion are presented in this section.

2.1.1 Heat conduction

Heat is the form of energy that is transferred between two system boundaries by virtue of a temperature difference, from the boundary at the higher temperature to the boundary at the lower one. It is a transient phenomenon. That is, it occurs only when it crosses the system boundary.

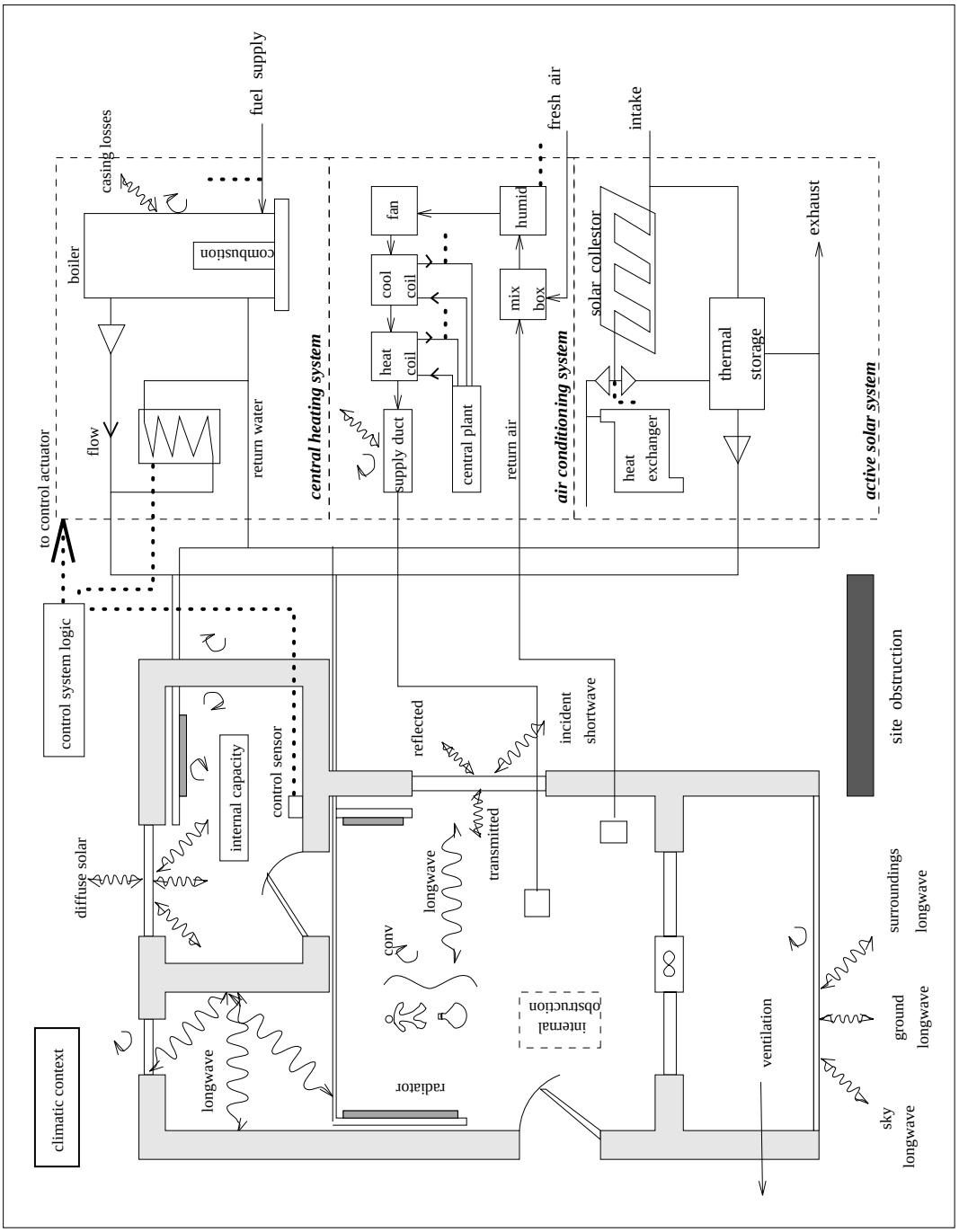

Figure 2.1 Energy flow paths in buildings (from Clarke, 1985).

Fourier's law of conduction gives the relationship between heat flow and the temperature gradient for a homogeneous, isotropic§ solid in steady state. It can be written in the form

§ Diffusion coefficient (e.g. thermal conductivity) is independent of direction.

$$\vec{q}(\vec{r},t) = -\lambda\,\nabla T(\vec{r},t) \tag{2.1}$$

where $\vec{q}(\vec{r},t)$ is the heat flux vector in the direction of the decreasing temperature, $\nabla T(\vec{r},t)$ is the temperature gradient vector, and the constant of proportionality, λ, is the thermal conductivity of the material. It is a positive, scalar quantity. The minus sign is to make the heat flow a positive quantity since it points in the direction of decreasing temperature. In SI units, the heat flux is in W/m^2, the temperature gradient is in K/m, and thermal conductivity is in $W/m\ K$.

Thermal conductivity, λ, is a property of the conducting material and of its state. It is sometimes called a transport property because, for a given temperature gradient, heat flux is directly proportional to thermal conductivity. Thus, thermal conductivity is an important property in thermal analysis. Furthermore, the accuracy of a thermal analysis is strongly dependent on the thermal conductivity's estimation accuracy.

Differential equation of heat conduction

Usually, heat conduction occurring in buildings is transient. That is because of the changing boundary conditions which is affected by the outside climate, plant operation, occupant's activity, etc. For a transient thermal assessment, the differential equation of heat conduction is required. In order to derive such an equation, the energy conservation law can be applied for a small control volume. For the stationary, homogeneous and isotropic control volume (C.V.) shown in Figure 2.2, with internal heat generation and constant thermophysical properties, the energy conservation law is stated as

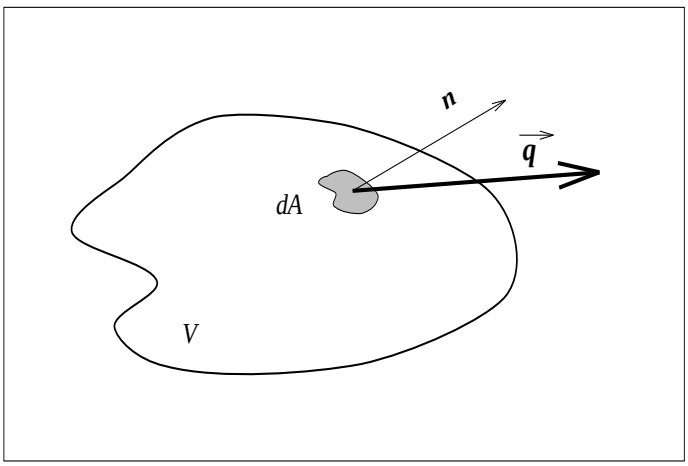

Figure 2.2 Differential element for heat conduction analysis.

$$\begin{bmatrix} \textit{The rate of} \\ \textit{heat storage} \\ \textit{in the C.V.} \end{bmatrix} = \begin{bmatrix} \textit{The rate of heat} \\ \textit{entering through C.V.} \\ \textit{bounding surface} \end{bmatrix} + \begin{bmatrix} \textit{The rate of} \\ \textit{heat generation} \\ \textit{in the C.V.} \end{bmatrix} \tag{2.2}$$

Therefore, equation (2.2) can be rewritten as

$$\int_V \rho\, c_p\, \frac{\partial T(\vec{r},t)}{\partial t}\, dV = -\int_V \nabla \,.\, \vec{q}\; dV + \int_V g(\vec{r},t)\; dV \tag{2.3}$$

where the surface integral has been converted to a volume integral by using the divergence theorem

$$\int_V \nabla \,.\, \vec{q}\; dV = \int_A \vec{q}.\vec{n}\; dA \quad .$$

For a small control volume, the integrals in equation (2.3) can be removed:

$$\rho\, c_p\, \frac{\partial T(\vec{r},t)}{\partial t} = -\nabla \,.\, \vec{q} + g(\vec{r},t) \quad . \tag{2.4}$$

The heat flux vector $\vec{q}$ is usually the summation of several heat flux vectors $\vec{q}_i$. Therefore, equation (2.4) can be rewritten as

$$\rho\, c_p\, \frac{\partial T(\vec{r},t)}{\partial t} = -\sum_i \nabla \,.\, \vec{q}_i + g(\vec{r},t) \tag{2.5}$$

The heat flux can be due to heat conduction, convection or radiation. Therefore, it is estimated by equation (2.1) for conduction heat flux. Convection and radiation heat fluxes are estimated by Newton's law of cooling and the Stefan-Boltzmann law of thermal radiation respectively. That is

$$\vec{q}_{convection} = h\; \Delta T \tag{2.6a}$$

$$\vec{q}_{radiation} = \sigma\; T^4 \quad . \tag{2.6b}$$

For a conduction only heat flux, equation (2.5) becomes

$$\rho\, c_p\, \frac{\partial T(\vec{r},t)}{\partial t} = \nabla \,.\, [\; \lambda\; \nabla T(\vec{r},t)\;] + g(\vec{r},t) \tag{2.7}$$

and for constant thermal conductivity, equation (2.7) simplifies to

$$\frac{1}{\alpha}\, \frac{\partial T(\vec{r},t)}{\partial t} = \nabla^2 T(\vec{r},t) + \frac{1}{\lambda}\; g(\vec{r},t) \tag{2.8}$$

where α is thermal diffusivity defined by

$$\alpha = \frac{\lambda}{\rho\, c_p} \quad .$$

For a domain without internal heat generation, equation (2.8) simplifies to the diffusion (Fourier) equation. In turn, the Fourier equation simplifies to the Laplace equation for a steady state problem.

Boundary conditions

While the differential equation for heat conduction indicates the way in which the dependent variable (i.e. temperature) depends on the independent variables (i.e. x, y, z and t), the solution of this differential equation for any particular physical circumstance requires defining a set of boundary conditions and an initial condition (for a time dependent problem). The boundary conditions designate the temperature or the heat flow at the boundaries of the domain. On the other hand, the initial condition designates the temperature distribution in the domain at some specific time, usually at the origin of the time dimension ($t = 0$).

Boundary conditions can be classified into linear and nonlinear. Three types of linear boundary conditions exist. These are the boundary condition corresponding to a prescribed temperature distribution, a prescribed heat flux distribution, and a heat exchange by convection with prescribed ambient temperature. The mathematical representation of the general case for the three boundary condition types can be written, respectively, as

$$T = f_i(\vec{r}, t) \qquad on\ S_i$$

$$\frac{\partial T}{\partial n_i} = f_i(\vec{r}, t) \qquad on\ S_i$$

$$\lambda_i \frac{\partial T}{\partial n_i} + h_i = f_i(\vec{r}, t) \qquad on\ S_i \ .$$

The homogeneous case for each of these types can be formulated by vanishing the function (i.e. $f_i(\vec{r}, t) = 0$). For example, the homogeneous case for the boundary condition of the second type is given by

$$\frac{\partial T}{\partial n_i} = 0$$

This represents the adiabatic (i.e. no heat flow) boundary.

On the other hand, there are different types of nonlinear boundary conditions, such as the thermal radiation boundary condition which is a function of the fourth-power temperature. In order to simplify nonlinear boundary conditions, linearisation techniques can be used as shown in Chapter 4.

Numerical model

Many methods for the numerical formulation of partial differential equations exist. The control volume approach is adapted in the present work because of its simplicity of formulation and physical elegance. The method also allows easy extension to multi-dimensional problems, consideration of complicated boundary conditions, and adoption of variable gridding and thermophysical properties.

The control volume formulation is achieved by integrating the associated partial differential equation (2.4) over a small control volume V (Figure 2.2). That is

$$\int_V \rho\, c_p\, \frac{\partial T}{\partial t}\, dV = -\int_V \nabla \,.\, \vec{q}\, dV + \int_V g\, dV \quad . \tag{2.9}$$

Applying the mean value theorem, equation (2.9) becomes

$$\rho\, c_p\, V\, \frac{\partial \bar{T}}{\partial t} = -\int_V \nabla \,.\, \vec{q}\, dV + V\, \bar{g} \tag{2.10}$$

where $\bar{T}$ and $\bar{g}$ are the average temperature and heat generation rate over the control volume respectively. Using the divergence theorem, the volume integral can be transformed to a surface integral. That is

$$\rho\, c_p\, V\, \frac{\partial \bar{T}}{\partial t} = -\int_S \vec{q} \,.\, \vec{n}\, dS + V\, \bar{g} \quad . \tag{2.11}$$

For a polyhedron control volume, with homogeneous material and uniform boundary at each surface, equation (2.11) can be rewritten as

$$\rho\, c_p\, V\, \frac{\partial \bar{T}}{\partial t} = -\sum_{s=1}^{N} A_s\, \vec{q}_s \,.\, \vec{n} + V\, \bar{g} \tag{2.12}$$

where for a boxed control volume, N is given by

$$N = \begin{cases} 2 & 1D \text{ heat conduction} \\ 4 & 2D \text{ heat conduction} \\ 6 & 3D \text{ heat conduction} \end{cases}$$

For a structured (uniform or non-uniform) mesh, equation (2.12) simplifies to

$$\rho\, c_p\, V\, \frac{\partial \bar{T}}{\partial t} = \sum_{s=1}^{N} A_s\, q_s + V\, \bar{g} \quad . \tag{2.13}$$

In order to generate the characteristic equations based on the control volume formulation, the domain space must be discretised. The employed gridding approach is an important factor for space discretisation. The importance of this factor becomes clearer for non-uniform meshes. In building

applications, non-uniform meshes are commonly used as the building constructions are composed of multiple layers which usually differ in their thermophysical properties and dimensions.

There are mainly two practices for space discretisation:

- Establishing control volumes after locating the grid points. Usually, the control volume surfaces are located midway between grid points.
- Identifying the grid point positions after defining the control volumes. Usually the grid points are located at the geometric centres of the control volumes.

The distinct advantage of the second approach is that a better node location, in terms of representing the average temperature of the associated control volume, can be achieved. On the other hand, the first approach can provide greater accuracy in estimating the heat flux through the control volume surfaces. This is because, in the first approach, the nodes are positioned first. This allows nodes to be located at each layer's interface (i.e. thermophysical property discontinuity). Therefore, continuity in the transport property (i.e. thermal conductivity) is assured between nodes. In Chapter 3 another approach is presented which combines the advantages of both approaches.

Beside the gridding approach, the particular finite differencing scheme must be defined in order to derive the finite difference approximations for the governing equations. The two point formulae is used in the current work for the following reasons:

- In the time dimension, it requires less storage.
- Faster convergence is expected in iterative solution methods.
- Its simplicity in deriving the finite difference approximation, in truncation error estimation for uniform and non-uniform grids, and in coding effort.

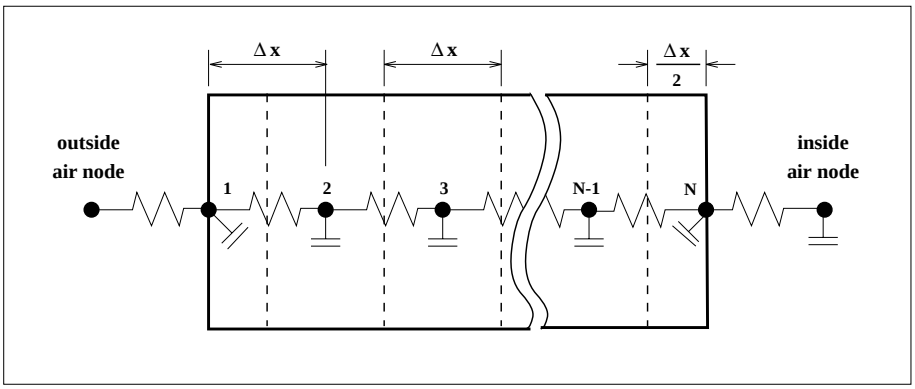

Figure 2.3 A space discretisation approach.

For the discretised slab shown in Figure 2.3, the characteristic equations for the interconstructional nodes are given by

$$a_i^{n+1}\ T_i^{n+1} + a_{i-1}^{n+1}\ T_{i-1}^{n+1} + a_{i+1}^{n+1}\ T_{i+1}^{n+1} - \gamma\ G_i^{n+1}\ \Delta t =$$

$$a_i^{n}\ T_i^{n} + a_{i-1}^{n}\ T_{i-1}^{n} + a_{i+1}^{n}\ T_{i+1}^{n} + (\ 1 - \gamma\ )\ G_i^{n}\ \Delta t \tag{2.14}$$

where,

$$a_j^{n+1} = \frac{-\ \gamma\ A\ \lambda_{j\to i}\ \Delta t}{\Delta X_{j\to i}}$$

$$a_j^{n} = \frac{(\ 1 - \gamma\ )\ A\ \lambda_{j\to i}\ \Delta t}{\Delta X_{j\to i}}$$

$$a_i^{k} = \rho_o\ c_p\ V - a_{i-1}^{k} - a_{i+1}^{k}$$

$$G^k = V\ g^k = V\ (\ g_s^k + g_p^k\ )$$

where g_s is the shortwave energy absorption (for transparent materials), and g_p is the energy absorption by plant interaction (all measured in W/m^3). For an exposed surface (internal or external) node, the convective heat transfer path is numerically represented by modifying the a coefficients for the convective connection:

$$a_j^{n+1} = -\ \gamma\ A\ h_{j\to i}^{n+1}\ \Delta t$$

$$a_j^{n} = (\ 1 - \gamma\ )\ A\ h_{j\to i}^{n}\ \Delta t$$

where h is the convective heat transfer coefficient. The same modification is valid for air gap surface nodes (if explicit air gap modelling is required). Furthermore, a surface node may have radiative heat transfer coefficients for which the heat generation term G [§] must be modified to

$$G^k = V\ g^k = V\ (\ g_s^k + g_p^k + g_l^k + g_r^k\ )$$

where g_l is the longwave energy exchange with the surrounding, and g_r is the radiant energy from casual sources. In general, other energy terms can be added to account for complexities such as phase change.

The format of the characteristic equation (2.14) has the following advantages

§ For simplicity, radiation flux is calculated based on the latest available temperature distribution.

- suitable for modelling massless nodes. This is more important for moisture flow modelling since its effective penetration depth is usually small.
- The generated system matrix will be symmetric for which special storage and solution techniques exist that requires less CPU time and storage.
- The terms are in Joules which is the base units for energy. Physically this help to check and confirm energy conservation within the domain.

Solution method

By deriving a characteristic equation for each node, a set of algebraic equations will emerge. Originally, these equation are nonlinear for which direct solution methods are not directly applicable. In addition, convergence instabilities and divergence are expected to occur with iterative solution methods (depending on the nonlinearity type and degree). Linearisation schemes (see Chapter 4) can be used to simplify the iterative solution methods and allow direct solution methods.

On the other hand, several methods exist for the simultaneous solution of a set of linear algebraic equations (equation (2.14)), such as the direct Gaussian elimination method and the iterative Gauss-Siedal method (Smith, 1985).

2.1.2 Mass diffusion

Mass diffusion through a solid domain occurs by the motion of quantities of adsorbate mass through the adsorbent solid material. Mass diffusion may occur as a result of several driving forces and physical mechanisms, such as pressure, temperature, concentration and external forces. The density of mass flow rate (i.e. mass flux) due to any driving force through a homogeneous, isotropic[§] solid in steady state is given by Fick's law as

$$\vec{J}_i^F = - D_F \nabla F \tag{2.15}$$

where $\vec{J}_i^F$ is the *ith* chemical species mass flux vector in the direction of the decreasing driving potential F, ∇F is the driving potential gradient vector and the constant of proportionality D_F is the mass diffusion coefficient for the driving potential F, which is a positive, scalar quantity. The minus sign is to make the mass flux a positive quantity since it points in the direction of decreasing driving potential. In SI units, the mass flux is usually expressed in mass per unit area and time (i.e. $kg/m^2 s$). However, the units for the mass diffusion coefficient are dependent on the driving force. For example, if the driving force is pressure, then ∇F is expressed in $kg/m^2\ s^2$, and D_F is expressed in seconds.

§ Where the *mass* diffusion coefficient is independent of direction.

Differential equation of mass diffusion

Similar to heat conduction, mass transport occurring in buildings is a transient phenomenon since the boundary conditions are usually fluctuating. For the stationary, homogeneous, and isotropic control volume (C.V.) shown in Figure 2.4, with internal mass generation and without phase change, the mass conservation law is stated as

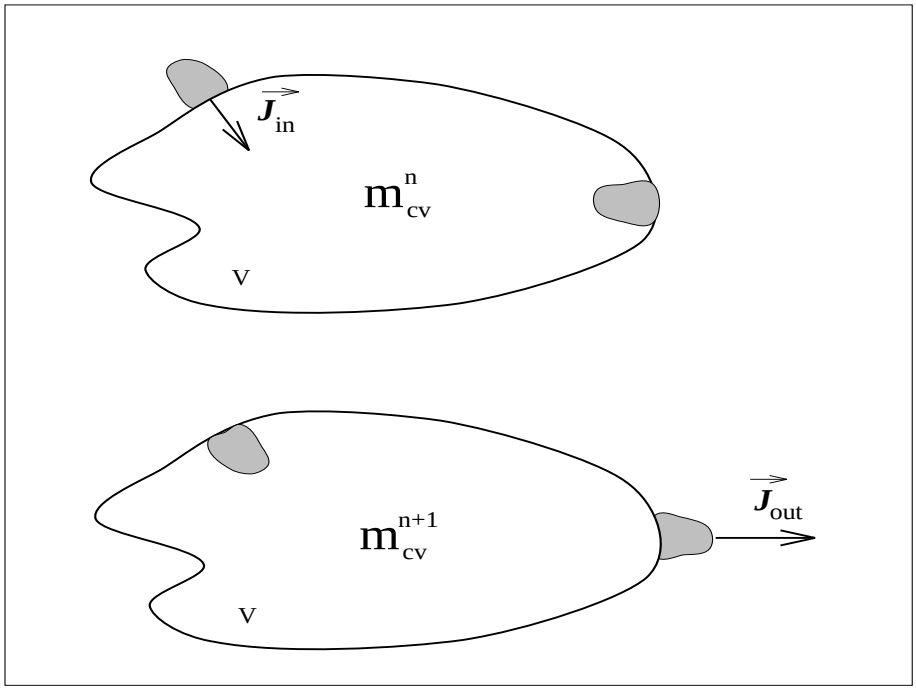

Figure 2.4 Differential element for mass diffusion analysis.

$$\begin{bmatrix} \textit{The rate of} \\ \textit{the ith species} \\ \textit{mass storage} \\ \textit{in the C.V.} \end{bmatrix} = \begin{bmatrix} \textit{The rate of the ith} \\ \textit{species mass entering} \\ \textit{through the C.V.} \\ \textit{bounding surface} \end{bmatrix} + \begin{bmatrix} \textit{The rate of} \\ \textit{ith species} \\ \textit{mass generation} \\ \textit{in the C.V.} \end{bmatrix} \tag{2.16}$$

Therefore, equation (2.16) can be written as

$$\rho_o \frac{\partial u_i}{\partial t} = -\nabla \cdot \vec{J}_i^F + s_i \ . \tag{2.17}$$

Substituting equation (2.15) into equation (2.17), the differential equation of mass diffusion is derived as

$$\rho_o \frac{\partial u_i}{\partial t} = \nabla \cdot [\, D_F \, \nabla F \,] + s_i \ . \tag{2.18}$$

For a constant diffusion coefficient, equation (2.18) simplifies to

$$\rho_o \frac{\partial u_i}{\partial t} = D_F \nabla^2 F + s_i \quad . \tag{2.19}$$

The mass generation term, s_i, can be proceeded by a summation sign to account for different sources of mass generation (or removal) such as a phase change process.

Boundary conditions

The three linear boundary conditions presented for heat conduction are also applicable for moisture transport after replacing the thermal coefficients and variables by mass diffusion terms. For example, the adiabatic boundary for heat conduction problems is defined mathematically by $(\partial T / \partial n_i = 0)$. In order to represent a zero mass transport surface, the thermal variable T is replaced by the mass diffusion variable F, mathematically expressed by $(\partial F / \partial n_i = 0)$.

Solution method

Although mass diffusion is analogous to heat conduction, a mass diffusion problem is usually nonlinear because of the nonlinear dependence of the diffusion coefficient on the mass diffusion variables. In addition, the complexity of mass diffusion problems may be worsened by the occurrence of a phase change. Therefore, an iterative solution method should be employed.

2.2 Adaptive gridding

It is usual for building energy simulation programs to employ uni-directional thermal conduction models. That is, lateral heat flows are not considered, or are implicitly considered by introducing correction factors[§] which are usually based on a simplified analytical analysis (Hassid, 1991). The uni-directional assumption is acceptable in cases where the temperature difference and thermal unit conductance (i.e. the inverse of the total resistance) in the perpendicular direction is significantly higher than in the lateral directions. The correction factor employed may be acceptable for the specific cases on which the correction factor equation determination is based.

In general, such an approach can lead to significant errors in the predicted loads and temperature distribution. For example, in well insulated buildings, the unit conductance difference is significantly reduced due to the reduction in the perpendicular unit conductance. This is exemplified by Figures 2.5 and 2.6 where the addition of insulation to a homogeneous wall converts heat conduction through the wall near the junction from uni-directional to 2-dimensional (although the overall heat flow rate is reduced as indicated by the heat flow line density).

§ an implicit representation of a flow path (e.g. lateral).

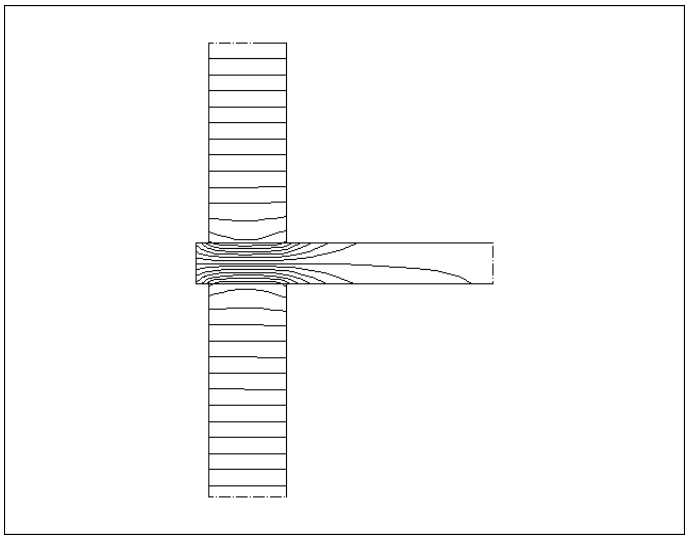

Figure 2.5 Isotherms and heat flow lines for a homogeneous wall-floor junction.

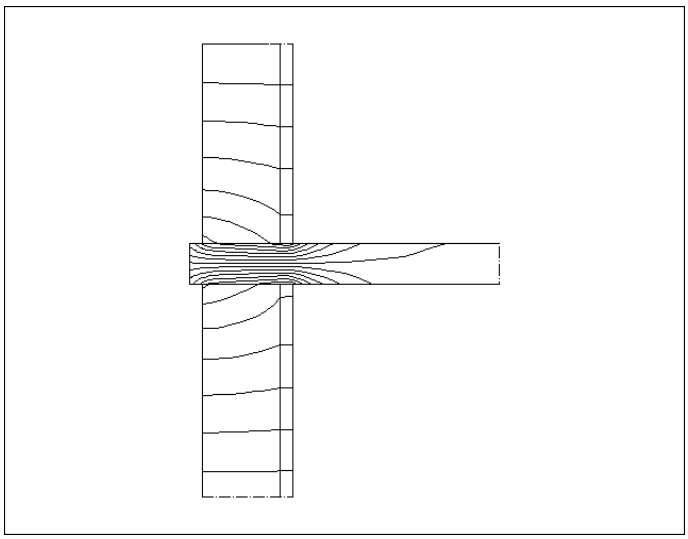

Figure 2.6 Isotherms and heat flow lines for internally insulated wall-floor junction.

The 2- and 3-dimensional heat flows in buildings are associated with thermal bridges which are parts of the building envelope where the unit thermal conductance is higher than the surrounding unit conductance. Although thermal bridges may occur as a uni-directional phenomena, the existence of a thermal bridge usually gives rise to complex 2- or 3-dimensional conduction heat flow. Hence, the rate of heat flow of the otherwise one-dimensional heat flow will change, as will the internal surface

temperature. These two parameters are important in energy conservation, thermal comfort, condensation and mould growth analysis. In buildings, thermal bridges can occur as a result of one or more of the following:

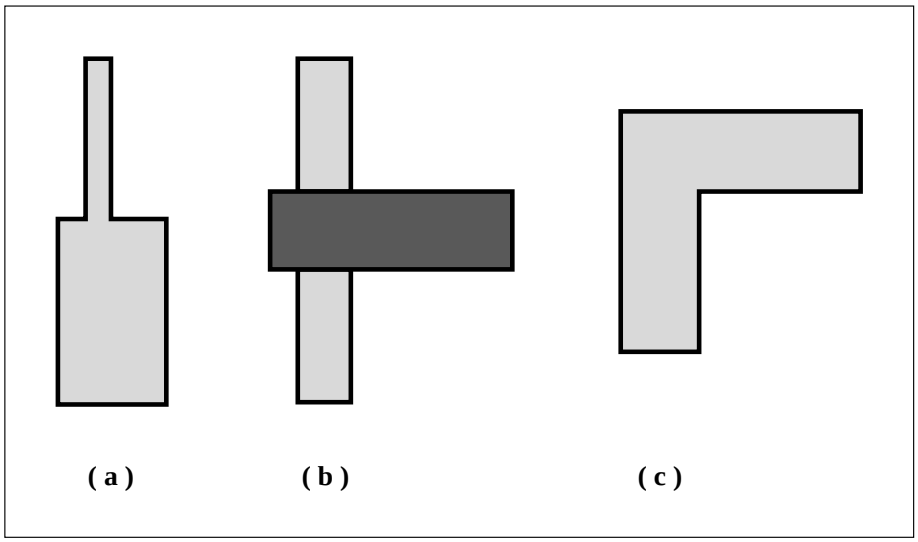

Figure 2.7 Thermal bridges types.

- a change in the thickness of a construction (Figure 2.7a)
- a partial or full penetration of the building envelope by materials with different thermophysical properties (Figure 2.7b)
- a range of geometric factors such as the difference between internal and external areas of the building envelope surfaces (Figure 2.7c).

In most western countries, thermal insulation was introduced in buildings in order to achieve the following:

- to reduce building energy consumption (i.e. HVAC systems)
- to improve thermal comfort (e.g. by achieving a uniform temperature distribution throughout a zone)
- to reduce condensation and mould growth risk during the heating season.

Although the first two targets have been achieved, the third has not. In fact, the condensation and mould growth cases have increased in renovated and newly insulated buildings. This is due to two main reasons:

1. The introduction of thermal insulation coincided with the reduction in ventilation and infiltration rates, by installing air tight windows and doors, which increase the indoor relative

humidity.

2. The improper installation of insulation created and worsened thermal (or cold) bridges. For example, Aasem (1986) has reported a 20% increase in the flow of heat through insulated walls due to corner effects, while Standaert (1985) stated that for the traditional insulated cavity wall construction, the conductive heat losses exceed the one dimensionally calculated heat losses by 30% to 40%. The improper installation of insulation is because:

   2.1. Insulating materials used in buildings are commonly not rigid, therefore they cannot fulfill a structural role.

   2.2. The existence of windows.

Although most designers and building technologists have a general understanding of the issues relating to thermal bridges, and how to avoid severe cases, an alarming number of new buildings suffer from significant problems. According to statistical information (IEA, 1991), some 20% of the social housing stock is affected in Belgium, some 15% in the Netherlands, with some 25 to 30% of low income housing in the United Kingdom being affected by condensation and mould growth. This highlights the need for tools to predict condensation at the early design stages. Although some general rules exist for avoiding thermal bridges, these are usually not applicable because of the complexity of building components, i.e. wall, edge, corner, etc. Traditionally, there are two main types of tools for assessing thermal bridges in buildings.

Firstly, there are building thermal catalogues containing sketches of different building component details, with some thermal data, such as the temperature factor[§] which is used as an index of the likelihood of moisture condensation. These give general guidance on the problems that can result from, and the methods for avoiding, thermal bridges in specific construction types. The main advantage of these catalogues is that they do not require detailed knowledge of building physics. However, not all building details are given in these catalogues, and the user has to search for the nearest match which may have different thermal behaviour despite the geometric similarity. Not only may it be difficult to decide how closely a specific construction matches the catalogue, but also it is impossible to investigate the effect of modifications. In addition, it is difficult to obtain quantitative information on energy loss or surface temperatures that are likely to lead to condensation risk.

Secondly, there are general purpose computer packages such as PHOENICS (Spalding 1991). These can simulate thermal behaviour of almost any building component. On the other hand, they are difficult to use and require considerable input from experienced users before structures can be specified or modified. It is also possible for plausible answers to emerge without their accuracy being clear.

§ refer to appendix E.

There have been several recent initiatives aimed at improving the current situation, such as the use of improved thermal bridge assessment techniques in the early design stage, or for remedial action through retrofits to assess the overall impact of energy losses and condensation risk. This is enabled through an EC-supported development of the EUROKOBRA database of 2-D thermal bridges, in conjunction with a software package for their selection, manipulation and analysis (refer to Appendix E).

Although computerised thermal bridge catalogues are user friendly, flexible and sophisticated in presenting the results, they require some professionality in defining the domain geometry. This is because the user has to define the locations for adiabatic surfaces. This can be a difficult task. In addition, heat flow through the building component is simulated in isolation, ignoring the complex interaction between the processes occurring within buildings such as air flow. For detailed studies, it is clear that these heat losses need to be integrated more fully into dynamic simulation program which attempt to model the overall building performance.

Although, in principle, it is easy to formulate the discretised equations for 3-D conduction (Clarke, 1985), in practice, until recently, they have not been implemented. The reasons for this are twofold. With regard to the computational effort, 3-D modelling results in a significantly larger program size, much longer simulation times, and time consuming model specification. On the other hand, it was considered that other uncertainties in thermal simulation gave rise to greater errors than those caused by the 1-D conduction approximation. This perspective may be changing, as computing power and user interfaces improve, and thermal bridging and ground modelling assume a more important role within the overall building response.

This need for improvement was clearly demonstrated in a major European research programme called PASSYS (Vandaele and Wouters, 1994). Within PASSYS, the edge loss problem was addressed with the use of extra "edge constructions" within the model which attempted to account for the heat transfer in the edges of the test cell (refer to Appendix F).

Although successful in the case of the PASSYS programme, it is clear that the use of a separate 3-D steady state program and/or the use of detailed experimental data and analysis is not a useful general tool for dynamic modelling. Although the PASSYS test cell is an extreme example of important 3-D conduction heat flow, there are other cases where a full 3-D modelling capability would be useful, e.g. ground modelling, and where it is required to predict surface temperatures near the corners of rooms.

The development of a multi-dimensional, variable resolution, error based[§] conduction model within an environmental building performance program, ESP-r, is presented in Chapter 3.

§ based on gridding technique which allows minimising or controlling numerical simulation errors.

2.3 Thermophysical properties

Accurate modelling of the thermophysical properties is of prime importance in conduction heat transfer simulation. For dynamic heat conduction, thermophysical properties can be classified into transport and storage properties. Thermal conductivity is the thermal transport property, while density and specific heat capacity are the thermal storage properties. In order to achieve accurate thermophysical property modelling, dependence on the state variables must be considered, especially temperature and moisture content. More attention should be given to thermal conductivity as it is considered in transient and steady state conduction modes.

Usually in building energy simulation packages, the thermophysical properties of building construction are assumed to be constant throughout the time domain. In principle, this assumption is acceptable for the case where the variation in the dependent variables (i.e. temperature, and partial vapour pressure or moisture content) are relatively small, or within the range of their variation the thermophysical properties are essentially independent. However, as was reported within several validation projects such as PASSYS (Baker *et al*, 1992), it is advisable to consider the temperature and/or moisture content dependence for at least some materials within a simulation. With regard to temperature, the dependence for building materials may be linear, nonlinear (e.g. as with some insulation materials) or discontinuous (e.g. as with some "*intelligent*" materials). In addition, in buildings it is possible to have localised high temperature variations due to plant interaction or passive solar elements such as transparent insulation material. As for moisture in building applications, there is potential for steep (i.e. exponential) moisture content variations due to capillary condensation as shown in Figure 2.8.

Several studies have shown the temperature and/or moisture content dependence of a material's thermophysical properties, and the effect on the predicted temperature and heat flux distributions. Temperature and heat flux distributions are of importance in many fields in addition to energy conservation. For example, the analysis of thermal stress requires the knowledge of the temperature distribution. From the knowledge of how the temperature at a point varies with time, the metallurgical conditions can be defined. Tseng and Chu (1992) investigated the effect of variable thermal conductivity on transient conduction and radiation in an absorbing, emitting and anisotropically scattering slab. Their results showed that the temperature dependence of thermal conductivity of the medium has a significant effect on both temperature and heat flow distribution. Tao, Besant and Rezkallah (1992) have shown that the effects of hygroscopicity on the transient temperature distribution are significant for a slab with one boundary open to moist air.

As shown in Figure 2.9, thermal conductivity of various engineering materials extends over a large range from about 0.001 to about 500 $W/m\ K$. The effect of temperature on thermal conductivity is not the same for all materials. While for most pure metals thermal conductivity decreases with increasing temperature, it increases with temperature for most insulating materials. From the physical

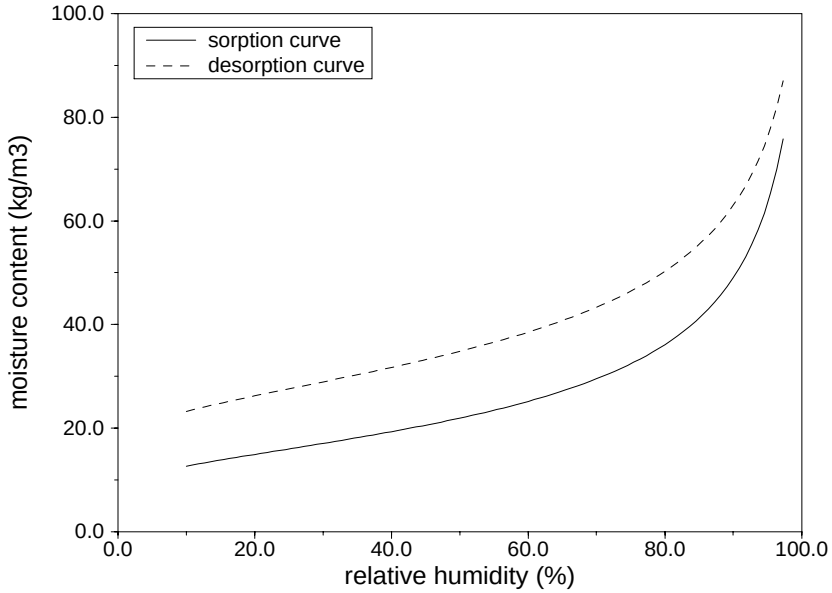

Figure 2.8 Sorption isotherm for light weight concrete.

point of view, there are two main mechanisms for thermal conduction in solids: one is associated with the flow of free electrons [§] , the other is due to lattice vibrations. In general, the latter mode of heat conduction is not as significant as the former one. Thermal conductivity and its temperature dependence are physical properties of the material in question. In general, the thermal conductivity of materials which have relatively few free electrons, such as insulators, increase as the material's mean temperature increases. This is because lattice vibrations increase with increased temperature. On the other hand, thermal conductivity of materials which are good electrical conductors, such as pure metals, decreases as their mean temperature rises. This is because the increase in lattice vibrations obstructs the free electrons motion at a higher rate than the increase in thermal conductivity due to greater lattice vibrations.

The thermal conductivity of most non metal materials has a near to linear relationship with temperature (Carslaw and Jaeger, 1947). However, a general polynomial equation can be used to estimate the thermophysical properties of solid materials as a function of temperature, especially when subjected to large temperature differences. For example, Durand (1985) suggested a third degree polynomial equation for determining the thermal conductivity of some insulating materials, such as mineral wool, as a function of temperature, and supplied the temperature range for which the constant coefficients are valid. On the other hand, Buck and Danbert (1990) suggested a fourth degree polynomial equation to describe the temperature dependence of the density and heat capacity of solids. Their

§ Materials which are good electrical conductors are also good thermal conductors.

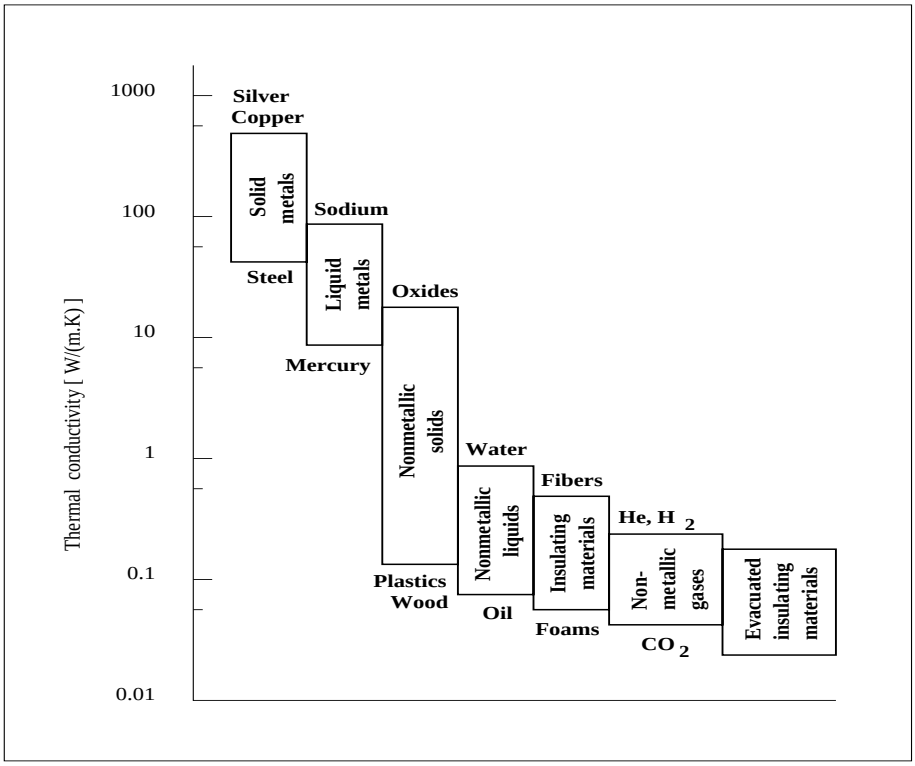

Figure 2.9 Thermal conductivity for different materials.

suggested formula is a result of the data compilation project by the Design Institute for Physical Property Data which compiled pure component thermophysical property data for 1249 chemical compounds (the compilation contains 25 single valued properties and 13 temperature dependent properties for each chemical compound).

Density is an important hygrothermal property as it affects heat and moisture transport. It is defined as the weight of one unit volume. In building applications, the density typically ranges from 10 kg/m^3 for the lightest insulation material to 2700-11000 kg/m^3 for metallic materials. Despite its importance in transient hygrothermal simulation, its dependence on temperature is usually not considered in building energy simulation. This is because of its complex nature and its interaction with other properties and processes. For example, the density changes for a closed system at constant pressure are associated with volume changes. This may require readjustment for the total thermal conductance between two points to account for changes in construction dimensions. In addition, the actual volume change and its details (i.e. directions) require simultaneous stress analysis which is beyond the scope of most thermal programs and this work. Furthermore, the thermal conductivity is a function of a material's density.

The specific heat capacity is the heat required for a unit change in the temperature of a unit mass of dry material. The range for the specific heat capacity encountered in building applications is much smaller than that for density. It is from about 100 $J/kg\ K$ for some metallic materials to 2000 $J/kg\ K$ for some wood based materials.

On the other hand, it is almost universally agreed that the thermophysical properties are linearly dependent on the moisture content (at least for the expected temperature and moisture content in building applications). The upgraded version of the International Energy Agency's Annex 14 Catalogue of material properties defines the moisture content dependence for thermal conductivity as

$$\lambda = a + b\ u \quad . \tag{2.20a}$$

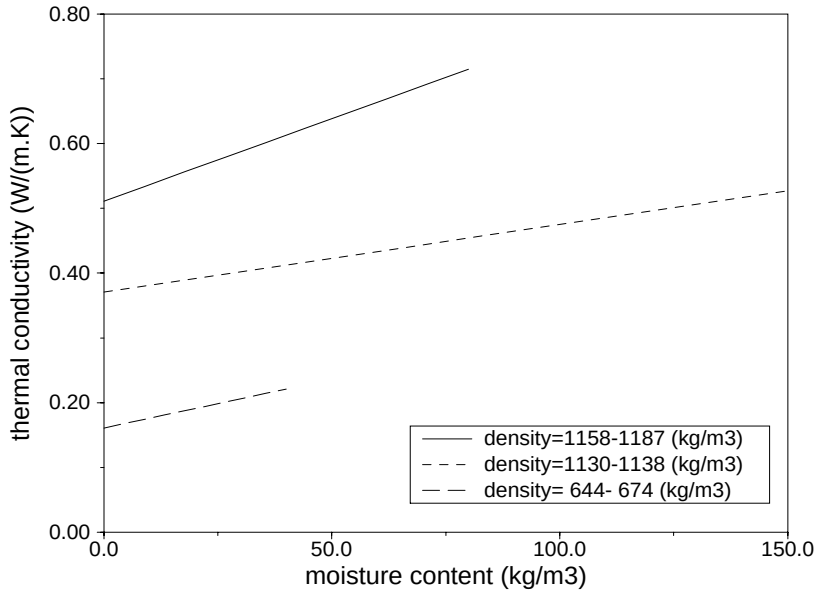

Figure 2.10 Thermal conductivity for lightweight concrete vs moisture content.

Thermal conductivity for lightweight concrete as a function of its moisture content is shown in Figure 2.10. This figure also shows the relation between thermal conductivity and density. Some researchers algebraically combine the temperature and moisture content dependencies for solid thermal conductivity. That is

$$\lambda = a + b\ u + c\ (\ T - T_r\ ) \tag{2.20b}$$

where a is the dry material thermal conductivity at reference temperature T_r, b is the moisture content dependence and c is the temperature dependence. The moisture content dependence of a material's heat capacity can be defined by the perfect gas law. According to this law, the enthalpy of a moist

solid matrix is equal to the sum of the enthalpies of both the solid matrix and moisture. In addition, the enthalpy is a function of temperature only. Assuming thermodynamic equilibrium, the heat capacity for a moist material is defined by

$$c_p = c_{p,dry} + u\, c_{p,moisture} \quad . \tag{2.21}$$

The simulation of variable thermophysical properties is discussed in Chapter 4. This scheme is able to model the linear, nonlinear, continuous and discontinuous temperature dependence of thermophysical properties. Furthermore, linear moisture content dependence for thermal conductivity is considered also.

2.4 Combined heat and moisture transport

Moisture transport through porous media has received considerable attention for several decades. This is because of its significance in numerous fields, such as petroleum engineering and building science. Both short and long term building performance is affected by moisture in relation to the building's construction and structure, its contents and the health and comfort of occupants.

According to Pel (1995), moisture plays a major role in building construction deterioration. This can result from moisture freezing and construction drying. Clearly, the former may cause structural damage as the volume of water increases on freezing; while construction drying may cause salt crystallisation. Contaminants, such as soluble salts, may be transported through the construction by water flow and salt crystallisation may occur at the surface, resulting in surface disfiguring, or within the construction, where it may lead to structural damage. In addition, the existence of moisture in building materials, such as insulation, may affect their thermal and other properties temporarily or permanently.

Building contents and systems are also affected by moisture. For example, the operation of an air-conditioning system is affected in that the sorption properties of the room air, contents, walls, etc. can significantly increase the start-up cooling load associated with the dehumidifying process. Sorption properties are therefore an important factor when the air-conditioning operation is intermittent, or when the indoor humidity is not controlled.

In addition to its effect on the occupant's thermal comfort, moisture transport has an important role in indoor air quality (IAQ). A substantial percentage of buildings in Britain experience condensation mould growth. For example, the Scottish House Condition Survey of 1991 stated that around 12.3% of Scottish houses were affected by mould. Mould growth can lead to a number of psychological conditions and physiological illnesses in the occupants (mainly children) as was reported by the Medical Research Council's Epidemiology Unit at the Royal Edinburgh Hospital in 1989. They reported that children in damp and mouldy houses had considerably more wheezing coughs, sore throats, persistent headaches, fevers and runny noses compared to children in well conditioned houses.

Adults in damp houses were significantly more likely to have symptoms of nausea, vomiting, constipation, blocked nose, breathlessness, backache, and nervous complaints than adults in dry houses. It should be mentioned here that statistical techniques were adopted in that study in order to minimise or eliminate the effects of other variables. The Department of Health (Environmental Committee 1991) also reported that damp and mouldy surfaces can lead to hypersensitivity with severe reactions, including breathing difficulties. Other national, European and North American bodies have reported similar findings (Dale *et al*, 1991; Henry and Cole, 1993; Watkinson, 1995).

The integration of moisture transfer within a building energy simulation package is required not only for condensation prediction, which is a major IAQ factor, but also for more accurate energy modelling. Moisture diffusion affects the process of heat transfer by several means, although, in building science one or more of the following effects are considered:

- heat absorption or dissipation due to moisture phase change
- enthalpy of diffused moisture
- dependence of thermophysical properties of building construction materials and zone air on their moisture content.

While there is a general understanding of heat and moisture flows between designers and building technologists, building energy simulation packages are needed to assist understanding of the dynamic interaction between building structure and materials with their environment, occupants and contents.

Combined moisture and heat transfer in building construction simulation has received considerable world-wide attention over several years. At the present time the UK building regulations propose a steady state method (Glaser, 1959) for the prediction of moisture transfer. This method is deficient in that it does not account for the absorption and desorption of moisture by building materials. Hence, the numerical methods within current transient simulation models should be extented to cater for the complexity of the transient diffusion problem.

The physics of moisture transport through building constructions has been known since the eighteenth century. The development of combined heat and mass transport models were first introduced by Philip and De Vries (1957). In 1966, Luikov (1975) developed the coupled equations for heat and mass transfer. His equations are based on the mass, momentum and energy conservation laws. Many transient Heat-Air-Moisture (HAM) transport models are based on Luikov's equations, using different assumptions to simplify the experimental evaluation of the transport coefficients. In 1991, a joint project was initiated by the International Energy Agencies (IEA): *Annex 24 on Heat-Air-Moisture Transport in Insulated Envelope Parts* (HAMTIE). It divided the existing HAM models into 9 types, ranging from steady state heat conduction and vapour diffusion models to transient heat, air and moisture transfer models. The current work adds to these types by developing and integrating a

moisture transport model within a whole building energy simulation program.

2.4.1 Moisture transport in porous building materials

One of the important mass diffusion processes occurring in buildings is moisture transport. It is a complicated process due to material porosity. However, it can be simplified by employing empirical based diffusion coefficients.

According to Rose (Galbraith, 1992) there are four distinct stages in the wetting process of a porous system:

- absorption: at very low relative humidities vapour arriving due to surface diffusion is absorbed to form a complete absorbed monolayer.
- vapour transfer: in this stage unblocked vapour transfer occurs.
- vapour and liquid transfer: this stage involves capillary condensation of vapour within material pores creating some liquid islands. Therefore, both vapour and liquid transfer occur at this stage. Furthermore, vapour transfer is enhanced by the existence of liquid islands which act as bridges (short circuit) for vapour transfer.
- liquid transfer: this stage occurs at high relative humidity. At this stage the liquid phase will be continuous. Therefore, only liquid transfer occurs.

Therefore, in order to model moisture transport through building materials both water vapour, and liquid water transfer should be considered. In addition, all driving potentials should be considered. Then, the total moisture flux will be found by vector summation of the individual fluxes.

Vapour transfer

Moisture transfer may occur via molecular diffusion, thermal diffusion, or filtration motion. Molecular diffusion is governed by the concentration gradient. Using Fick's law, this molecular diffusion is defined by

$$\vec{J}_v^D = - D_{\rho_v} \nabla \rho_v \tag{2.22}$$

where,

$\vec{J}_v^D$: diffusion vapour flux ($kg/m^2 s$)

ρ_v: vapour concentration (kg/m^3)

D_{ρ_v}: diffusion coefficient of vapour in porous medium (m^2/s), and

$$D_{\rho_v} = \upsilon \, \chi \, D_v$$

where,

υ: tortuosity factor

χ: volume fraction of air-filled open pores

D_v: diffusion coefficient of vapour in air (m^2/s).

In building applications, vapour behaves as an ideal gas, therefore, the ideal gas state equation can be applied as

$$\rho_v = \frac{P_v}{R_v T} \tag{2.23}$$

where,

P_v: partial water vapour pressure (N/m^2)

R_v: gas constant for water vapour, 461.52 ($J/kg\ K$)

T: absolute temperature (K).

Substituting equation (2.23) into equation (2.22) gives

$$\vec{J}_v^D = - \frac{D_{\rho_v}}{R_v T} \nabla P_v + \frac{D_{\rho_v} P_v}{R_v T^2} \nabla T \quad . \tag{2.24}$$

Some authors argue the validity of density gradient as the driving force for vapour molecular diffusion. Everdell (1965) stated that chemical potential is the true driving potential for vapour diffusion.

Thermal vapour diffusion is the diffusion caused solely by the temperature gradient and through porous materials is defined by

$$\vec{J}_v^T = - D_T \nabla T \tag{2.25}$$

where D_T is vapour thermal diffusion coefficient ($kg/m\ s\ K$).

Filtration flow of vapour occurs when there is a total pressure gradient. Using Fick's law, vapour filtration flow through porous bodies is given by

$$\vec{J}_v^{P_{tot}} = - D_{P_{tot}} \nabla P_{tot} \tag{2.26}$$

where D_{P_t} is vapour filtration coefficient (s).

Liquid transfer

Liquid transfer may occur via molecular diffusion, thermal diffusion or filtration motion. Molecular diffusion liquid transfer through saturated porous materials can be expressed by Darcy's law as

$$\vec{J}_l^D = - \rho_l \kappa \nabla \Phi \tag{2.27}$$

where,

J_l^D: liquid flux due to molecular diffusion (kg/m^2s)

ρ_l: water density (kg/m^3)

κ: material hydraulic conductivity (m/s)

Φ: total hydraulic head (m).

For unsaturated media, Childs and Collis-George (Galbraith, 1992) stated that a modified form of Darcy's law can be used as follows

$$\vec{J}_l^D = - \rho_l \, D_{l,\Upsilon} \, \nabla \Upsilon \tag{2.28}$$

where $D_{l,\Upsilon}$ is the liquid permeability (s), and Υ is the hydraulic potential expressed in m^2/s^2. It is composed of two elements: the matrix potential, Υ_m, which is related to the pore water pressure caused by capillary effects, and the gravity potential, Υ_g, which is related to gravitational effect. Hence

$$\Upsilon = \Upsilon_m + \Upsilon_g \tag{2.29a}$$

or

$$\Upsilon = \frac{P_l}{\rho_l} + z \, \mathbf{g} \, \vec{k} \tag{2.29b}$$

where,

P_l: pore water pressure (N/m^2)

$\mathbf{g}$: gravitational acceleration (m/s^2)

z: height over a reference level (m)

$\vec{k}$: unit vector in the positive z-direction.

Substituting equation (2.29) into equation (2.28) gives

$$J_l^D = - D_{l,\Upsilon} \, \nabla P_l - D_{l,\Upsilon} \, \rho_l \, \mathbf{g} \, \vec{k} \, \Delta z \tag{2.30a}$$

or

$$J_l^D = - D_{l,P_l} \, \nabla P_l - D_{l,z} \, \Delta z \quad . \tag{2.30b}$$

Which is in Fick's law format. It should be noted that liquid molecular diffusion due to the gravity force gradient may be in a lateral direction for some building components such as walls for which 2D analysis is required.

On the other hand, liquid thermal diffusion in porous materials is estimated by

$$\vec{J}_l^T = - D_{l,T} \, \nabla T \tag{2.31}$$

where $D_{l,T}$ is the thermal liquid diffusion coefficient ($kg/m\ s\ K$). Liquid filtration flow occurs when there is a total pressure gradient. The liquid filtration flux can be estimated by utilising an empirical diffusion coefficient, $D_{l,P_{tot}}$, expressed in units of seconds as

$$\vec{J}_l^{P_{tot}} = - D_{l,P_{tot}} \nabla P_{tot} \quad . \tag{2.32}$$

Clearly, all the diffusion flux types can be expressed by Fick's law, for which the diffusion coefficients are empirical. If liquid molecular diffusion due to the gravitational force, and vapour and liquid filtration flows are neglected, then the total moisture transport is estimated by

$$\vec{j}_{tot} = \vec{J}_v + \vec{J}_l = \vec{J}_v^D + \vec{J}_v^T + \vec{J}_l^D + \vec{J}_l^T \tag{2.33a}$$

or

$$\vec{j}_{tot} = - \frac{D_{\rho_v}}{R_v T} \nabla P_v + \left(\frac{D_{\rho_v} P_v}{R_v T^2} - D_T - D_{l,T} \right) \nabla T - D_{l,P_l} \nabla P_l \quad . \tag{2.33b}$$

This equation contains three dependent variables (i.e. P_v, T and P_l). Using the approach presented by Galbraith and McLean (1993), the number of variables can be reduced to two. They derived a formula (based on Kelvin equation) which relates the vapour pressure gradient to the liquid pressure gradient as

$$\nabla P_l = \frac{R_v\ T\ \rho_l}{P_v} \nabla P_v + R_v\ \rho l \left[\ln \phi - \frac{L}{R_v\ T} \right] \nabla T \tag{2.34}$$

where,

ϕ: relative humidity, $\phi = P_v / P_s$

P_s: vapour saturation pressure (N/m^2)

L: latent heat of vapourisation (J/kg)

Substituting equation (2.34) into equation (2.33) will reduce the dependent variables to P_v and T. Therefore, equation (2.33) can be re-expressed in a simplified form as

$$\vec{j}_{tot} = - D_{p_v}^T \nabla P_v - D_T^{p_v} \nabla T \tag{2.35}$$

where $D_{p_v}^T$ is a moisture diffusion coefficient due to the vapour pressure gradient when the second driving potential is temperature gradient. Similarly, $D_T^{p_v}$ is a moisture diffusion coefficient due to the temperature gradient when the second driving potential is the vapour pressure gradient. Therefore, when dealing with a diffusion coefficient, it is important to check for the set of driving potentials. For example, the moisture diffusion coefficient due to temperature gradient $D_T^{p_v}$ in equation (2.35) is not the same as D_T^u in

$$\vec{j}_{tot} = - D_u^T \nabla u - D_T^u \nabla T \quad .$$

2.4.2 Differential equations for combined heat and moisture transport

In the real world, moisture transport and heat transfer are inter-related. Moisture flow will convect energy, and phase change will involve latent heat. On the other hand, temperature gradient will result in thermal moisture diffusion. Furthermore, thermal transport and storage properties are affected by moisture distribution; similarly, hygroscopic transport and storage properties are affected by temperature distribution. Therefore, this problem should be described by a combined approach.

The system of differential equations for combined moisture and heat transfer can be achieved by applying both mass and energy conservation laws on a small control volume (C.V.) of the domain. For the stationary, homogeneous and isotropic control volume shown in Figure 2.11, with internal energy and moisture generation:

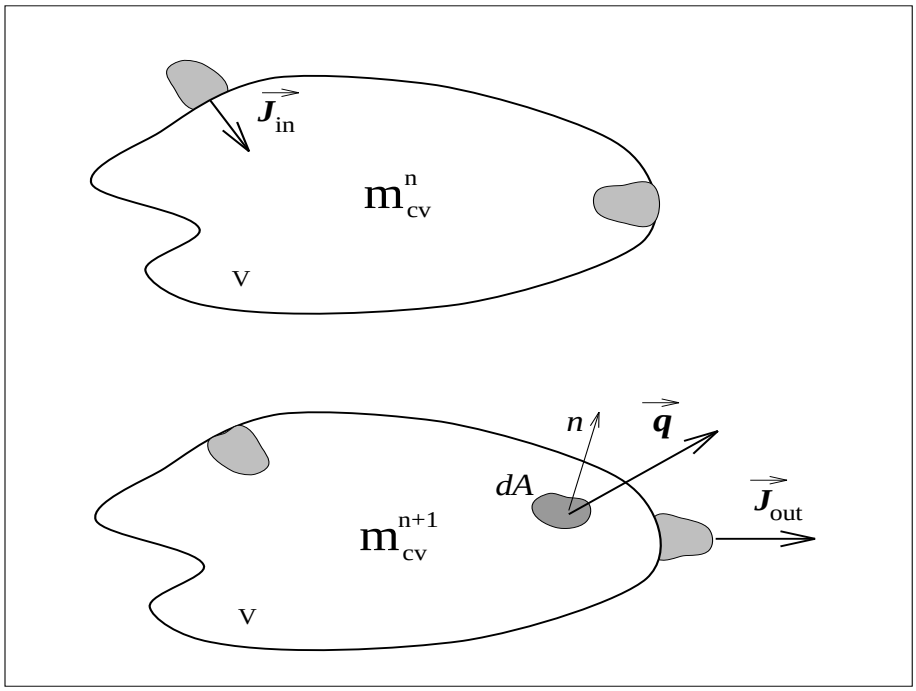

Figure 2.11 Differential element for combined heat and moisture transport analysis.

$$\begin{bmatrix} \textit{The rate of the} \\ \textit{ith phase mass} \\ \textit{storage in the} \\ \textit{control volume} \end{bmatrix} = \begin{bmatrix} \textit{The rate of the ith} \\ \textit{phase mass entering} \\ \textit{through C.V.} \\ \textit{bounding surface} \end{bmatrix} +$$

$$\begin{bmatrix} \textit{The rate of the} \\ \textit{ith phase mass} \\ \textit{generation due to} \\ \textit{phase change} \end{bmatrix} + \begin{bmatrix} \textit{The rate of the} \\ \textit{ith phase mass} \\ \textit{generation due to} \\ \textit{plant interaction} \end{bmatrix} \tag{2.36}$$

$$\begin{bmatrix} \textit{The rate of} \\ \textit{heat storage} \\ \textit{in the} \\ \textit{control volume} \end{bmatrix} = \begin{bmatrix} \textit{The rate of heat} \\ \textit{entering through C.V.} \\ \textit{bounding surface} \\ \textit{by conduction} \end{bmatrix} +$$

$$\begin{bmatrix} \textit{The rate of heat} \\ \textit{entering through C.V.} \\ \textit{bounding surface} \\ \textit{by moisture transfer} \end{bmatrix} + \begin{bmatrix} \textit{The rate of} \\ \textit{heat generation} \\ \textit{in C.V. due} \\ \textit{to plant interaction} \end{bmatrix} \tag{2.37}$$

Assuming all vapour and liquid moisture flow within the domain is slow enough to achieve thermodynamic equilibrium between the four phases and the building construction, their temperatures can be assumed equal. Therefore, equations (2.36) and (2.37) can be written as

$$\rho_o \frac{\partial u_i}{\partial t} = -\nabla \cdot \vec{J}_i + I_i + s_i \qquad i = 1, 2 \tag{2.38}$$

where

$$\sum_{i=1}^{2} I_i = 0$$

and

$$\sum_{i=0}^{2} \frac{\partial\, \rho_i \mathbf{h}_i}{\partial t} = -\nabla \cdot \vec{q} - \sum_{i=1}^{2} \nabla \cdot \mathbf{h}_i \vec{J}_i + g \tag{2.39a}$$

or

$$\sum_{i=0}^{2} \left(\rho_i \frac{\partial \mathbf{h}_i}{\partial t} + \mathbf{h}_i \frac{\partial \rho_i}{\partial t} \right) = -\nabla \cdot \vec{q} - \sum_{i=1}^{2} \nabla \cdot \mathbf{h}_i \vec{J}_i + g \tag{2.39b}$$

where the subscripts 0,1,2 denote dry solid domain and vapour and liquid water respectively, **h** is the enthalpy and *g* accounts for heat and moisture plant interaction.

Based on the foregoing theory, a dynamic, 1D combined heat and moisture transport model is developed and integrated within ESP-r as described in Chapter 5.

References

Aasem, I O 1986. ‘‘The Effect of Corners on the Heat Flow Through Insulated Walls,’’ *Technical Report*. Kuwait Institute For Scientific Research

Buck, E. and T. Danbert 1990. ‘‘Project 801: The DIPPR data compilation project,’’ *AIChE Symposium Series 275*, vol. 86, pp. 5-14.

Carslaw, H. and J. Jaeger 1947. *Conduction of heat in solids*, Clarendon press, UK.

CEC 1989. *The PASSYS Project Phase 1*, Commission of the European Communities, Research and Development, Brussels..

Clarke, J. A. 1985. *Energy simulation in building design*, Adam Hilger Ltd, Bristol,UK.

Dales, R E, H Zwanenburg, R Burnett, and C A Franklin 1991. ‘‘Respiratory health effects of home dampness and molds among Canadian children,’’ *American Journal of Epidemiology*, vol. 11134, pp. 196-206.

Durand, A. 1985. ‘‘Thermal conductivity of some insulating materials as a function of temperature,’’ *chemical Engineering*, no. May 27, pp. 153-154.

Environments, International Workshop on Health Implications of Fungi in Indoor1992. , The Netherlands.

Everdell, M H 1965. *Introduction to chemical thermodynamics*, The English Universities Press Ltd.

Galbraith, G1992. , *Heat and Mass Transfer Within Porous Building Materials*, Glasgow. PhD University of Strathclyde

Galbraith, G H and R C McLean 1993. ‘‘The Determination of Vapour and Liquid Transport Coefficients as Input to Combined Heat and Mass Transfer Models,’’ in *Proceedings of 3rd international Building Performance Simulation Association*, pp. 413-419, Adelaide.

Gebhart, B 1993. *Heat conduction and Mass Diffusion*, McGraw-Hill, Inc., USA.

Hassid, S 1991. ‘‘Algorithms for Multi-Dimensional Heat Transfer Simulation in Buildings,’’ *Building Simulation 91*, pp. 9-13, France.

Hendry, K M and E C Cole 1993. ‘‘A review of mycotoxins in indoor air,’’ *Journal of Toxicology and Environmental Health*, vol. 38, pp. 183-198.

Homes, Scottish Edinburgh. ‘‘Scottish Housing Condition Survey 1991,’’ *A report to the Scottish Office and Scottish Homes Board*.

IEA 1991. ‘‘Condensation and energy: Sourcebook, Report Annex XIV,’’ *International Energy Agency, Energy Conservation in Buildings and Community System Programme*, vol. 1.

Laan, M J van der 1994. ‘‘A model for combined heat and vapour transfer in building constructions,’’ *PhD Progress Report, Einhoven University of Technology*.

Luikov, A. V. 1975. ‘‘Systems of differential equations of heat and mass transfer in capillary-porous bodies,’’ *international journal of heat and mass transfer*, vol. 18, pp. 1-14.

McLean, R C1988. , *Interstitial Condensation and the Vapour Transmission Performance of Building Materials*. MPhil Thesis, University of Strathclyde

Ozisik, M.N. 1993. *Heat Conduction*, John Wiley, USA.

Pel, L 1995. ‘‘Moisture Transport in Porous Building MaterialsPhD Thesis,’’ *PhD Thesis, Eindhoven University of Technology*, The Netherland.

Spalding, D B 1991. *The PHOENICS Beginner’s Guide*, Heat and Momentum Ltd.

Standaert, P 1985. ‘‘Thermal Bridges: a Two-Dimensional and Three-Dimensional transient Thermal Analysis,’’ *Thermal Performance of the Exterior Envelopes of Buildings III*, Florida.

Tao, Y, R Besant, and K Rezkallah 1992. ‘‘The transient thermal response of a glass-fiber insulation slab with hygroscopic effects,’’ *International Journal of Heat and Mass Transfer*, vol. 35, pp. 1155-67.

Tseng, C. and H. Chu 1992. ‘‘Transient combined conduction and radiation in an absorbing, emitting, and anisotropically-scattering medium with variable thermal conductivity,’’ *Int. J. Heat Mass transfer*, vol. 35, no. 7, pp. 1844-1847.

Vandaele, L and P Wouters1994. , *The PASSYS Services: Summary Report*. European Commission Publication No EUR 15113 EN

Watkinson, S 1995. ‘‘The physiology and morphology of fungal decay in buildings,’’ in *Building Mycology*, ed. J Singh, pp. 54-75, London.

CHAPTER 3

Adaptive Building Fabric Gridding

This chapter is concerned with developing an adaptive building fabric gridding technique which is multi-dimensional (enables simulation of multi-dimensional phenomenon such as thermal bridges), flexible (facilitates variable modelling resolution in order to reduce CPU requirements) and error based (allows controlling simulation accuracy). First, the associated theory is presented. Then, the associated numerical representation is derived, followed by a discussion on how to implement the adaptive gridding scheme within a whole building energy simulation environment. After that, the solution method is presented. Finally, conclusions are given.

3.1 Mathematical model

The theory associated with numerical error sources is discussed in this section. This is followed by simulation examples to illustrate this theory. After that, lumped formulation is presented. Finally, based on the theory an adaptive gridding technique for multi-layered building constructions is presented.

3.1.1 Numerical error sources

At each step in time there will be a difference between the exact solution of the equation (2.4) and the numerical approximation according to equations (2.14). The total per step error is a combination of rounding errors, truncation errors and stability errors. The rounding errors arise from performing the required computational operations with numerical values having a limited number of significant digits. This type of error is expected to be directly proportional to the number of computational operations. Accordingly, iterative methods for the simultaneous solution of a set of linear algebraic equations will produce lower rounding errors than the direct methods as the rounding off errors in iterative solution methods are associated with the last iteration only. On the other hand, rounding errors can be minimised or controlled by using double precision arithmetic. In general, rounding errors are not significant as long as mathematical stability is satisfied.

Truncation errors result from replacing the derivatives in the governing equation by finite differences (i.e. numerical approximations). This type of errors can be minimised by using difference schemes of higher truncation error order such as three points formula (Ozisik, 1993), or by reducing the time or space steps as this will reduce variable variations. The local truncation error for any finite difference scheme can be estimated by replacing the temperatures involved by their Taylor-series expansion centred at $(i\Delta x, n\Delta t)$. For example, the heat conduction equation for a domain with homogeneous and constant thermophysical properties, and without heat generation (refer to Chapter 2), may be written in the form

$$\frac{\partial T(\vec{r},t)}{\partial t} = \alpha \, \nabla^2 T(\vec{r},t) \tag{3.1}$$

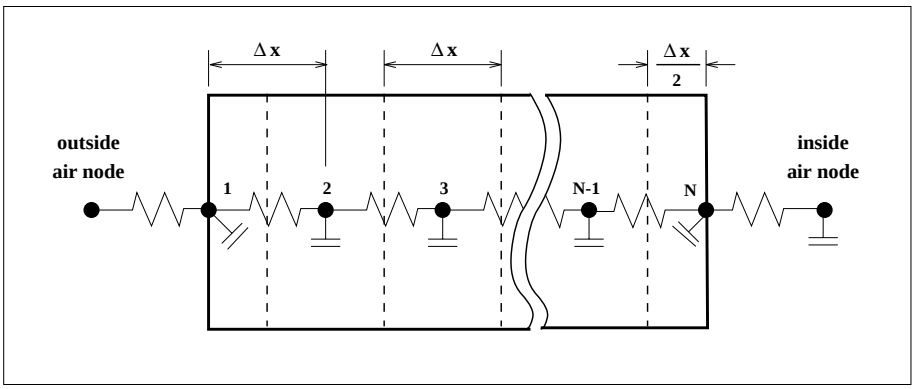

Figure 3.1 ESP-r space discretisation approach.

Recalling the space discretisation adopted in Chapter 2 (Figure 3.1), the numerical representation for internal nodes can be written as

$$T_i^{n+1} - T_i^n = \gamma \, F_o \left[\, T_{i-1}^{n+1} - 2 \, T_i^{n+1} + T_{i+1}^{n+1} \, \right] + (1-\gamma) \, F_o \left[\, T_{i-1}^{n} - 2 \, T_i^{n} + T_{i+1}^{n} \, \right] \tag{3.2a}$$

While for boundary nodes it is

$$T_i^{n+1} - T_i^n = 2 \, \gamma \, F_o \left[\, Bi \, T_{i-1}^{n+1} - (1+Bi) \, T_i^{n+1} + T_{i+1}^{n+1} \, \right] +$$

$$2 \, (1-\gamma) \, F_o \left[\, Bi \, T_{i-1}^{n} - (1+Bi) \, T_i^{n} + T_{i+1}^{n} \, \right] \tag{3.2b}$$

where $T_i^n = T(i\Delta x, n\Delta t)$, and F_o and Bi are the Fourier and *boundary node* Biot numbers respectively. The Fourier number is the ratio of the rate of heat conduction through the control volume to the rate of heat storage within the control volume. The Biot number is the ratio of internal to external thermal

resistance for the boundary node. That is

$$F_o = \frac{\left(\frac{\lambda\ A}{\Delta x}\right)}{\left(\frac{\rho\ c_p\ V}{\Delta t}\right)} = \frac{\alpha\ \Delta t}{\Delta x^2} \tag{3.3}$$

$$Bi = \frac{h_c}{\left(\frac{\lambda}{\Delta x}\right)} = \frac{h_c\ \Delta x}{\lambda}\ . \tag{3.4}$$

The implicitness degree γ is a dimensionless parameter which must be chosen to be within the range $0 \le \gamma \le 1$. Setting γ =0.0, 0.5 or 1.0 results in, respectively, the classic explicit, partially implicit (Crank-Nicolson) or fully implicit discretisation scheme.

Therefore, the truncation error for the numerical equations (3.2), assuming equal spacing, are respectively

$$E = \left[\ F_o\ (\frac{1}{2} - \gamma) - \frac{\alpha}{12}\ \right] \frac{\Delta x^2}{\alpha}\ \frac{\partial^2 T}{\partial t^2} +$$

$$\left[\ F_o^2\ (\frac{1}{6} - \frac{\gamma}{2}\ ) - \frac{\gamma\ F_o \alpha}{12} - \frac{\alpha^2}{360}\ \right] \frac{\Delta x^4}{\alpha^2}\ \frac{\partial^3 T}{\partial t^3} + O(\Delta x^6) \tag{3.5a}$$

$$E = \left[\ 1 - \gamma\ (\ 1 + Bi\ )\ \right] \frac{\partial T}{\partial t} + \left[\ \frac{\Delta t}{2} - \gamma\ (\ 1 + Bi\ )\ [\ \Delta t + \frac{\Delta x^2}{12}\ ]\ \right] \frac{\partial^2 T}{\partial t^2} +$$

$$\left[\ \frac{\Delta t^2}{6} - \gamma\ (\ 1 + Bi\ )\ [\ \frac{\Delta t^2}{2} + \frac{\Delta x^2\ \Delta t}{12} + \frac{\Delta x^4}{360}\ ]\ \right] \frac{\partial^3 T}{\partial t^3} -$$

$$\left[\ \frac{2\ \gamma F_o\ \Delta x\ (\ 1 - Bi\ )}{\Delta t}\ \right] \frac{\partial T}{\partial x} - \left[\ \gamma\ \Delta x\ (\ 1 - Bi\ )\ [\ 2\ F_o + \frac{1}{3}\ ]\ \right] \frac{\partial^2 T}{\partial t\ \partial x} -$$

$$\left[\ \gamma\ \Delta x\ (\ 1 - Bi\ )\ [\ F_o\ \Delta t + \frac{\Delta t}{3} + \frac{\Delta x^2}{60}\ ]\ \right] \frac{\partial^3 T}{\partial t^2\ \partial x} \tag{3.5b}$$

Building constructions are composed of multi-layers with different thermophysical properties and thicknesses which usually cannot be modelled by equal spaced mesh. For the unequal mesh spacing shown in Figure 3.2, the truncation error at node i can be estimated by using the Taylor series expansion about node i (Ozisik, 1993). The forward and backward Taylor series expansion of the temperature are respectively given by

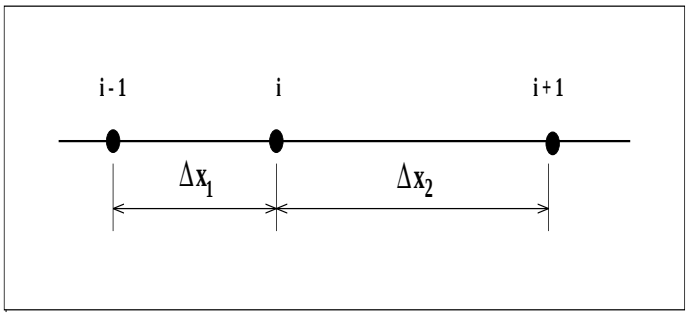

Figure 3.2 Unequal space mesh.

$$T_{i+1} = T_i + \Delta x_2 \frac{dT}{dx} + \frac{(\Delta x_2)^2}{2!} \frac{d^2T}{dx^2} + \frac{(\Delta x_2)^3}{3!} \frac{d^3T}{dx^3} + O\left[(\Delta x_2)^4\right] \tag{3.6a}$$

$$T_{i-1} = T_i - \Delta x_1 \frac{dT}{dx} + \frac{(\Delta x_1)^2}{2!} \frac{d^2T}{dx^2} - \frac{(\Delta x_1)^3}{3!} \frac{d^3T}{dx^3} + O\left[(\Delta x_1)^4\right] \tag{3.6b}$$

By multipling equation (3.6b) by $(\Delta x_2 / \Delta x_1)^2$, then adding the resulting expression to equation (3.6a), we get

$$T_{i+1} + a^2\, T_{i-1} = (1 + a^2)\, T_i + (1 - a)\, \Delta x_2 \frac{dT}{dx} + (\Delta x_2)^2 \frac{d^2T}{dx^2} +$$

$$\frac{(\Delta x_2 - \Delta x_1)\, (\Delta x_2)^2}{6} \frac{d^3T}{dx^3} + O\left[(\Delta x)^4\right] \tag{3.7}$$

where $a = \Delta x_2 / \Delta x_1$, and

$$O\left[(\Delta x)^4\right] = \textit{maximum} \left\{ O\left[(\Delta x_1)^4\right], O\left[(\Delta x_2)^4\right] \right\}$$

From equation (3.7), the finite difference approximation for the second derivative can be determined as

$$\frac{d^2T}{dx^2} = \frac{T_{i+1} - (1 + a^2)\, T_i + a^2\, T_{i-1}}{(\Delta x_2)^2} - \frac{1 - a}{\Delta x_2} \frac{dT}{dx} + O\left[(\Delta x_2 - \Delta x_1)\right] . \tag{3.8}$$

This indicates that the truncation error for a changing mesh spacing is related to the rate of space step change. Therefore, to achieve acceptable accuracy, the rate of mesh spacing changing should be slow.

In an attempt to reduce truncation error, Waters and Wright (1985) came to the conclusion that the best strategy for distributing nodes in a multi-layer wall should be based on a two step approach.

First, a node should be placed on each internal boundary (i.e., interface of layers). Then additional nodes should be placed within the layers in such a way as to approach, as nearly as possible, the condition defined by

$$m_i \approx m_r \sqrt{\frac{\alpha_r \; d_i^2}{\alpha_i \; d_r^2}} \tag{3.9}$$

where m is the number of nodes per layer (boundary nodes are counted as one half node), α is thermal diffusivity, and d is layer thickness. The subscript r denotes the reference layer which is the layer with maximum (α / d^2) value. The approximation sign used in the equation is because the number of nodes in a layer must be an integer value.

On the other hand, Alvarez, Molina and Cejudo (1993) presented a three step discretisation procedure. First, the simulation time step Δt is selected based on the available time basis of the input functions and with the frequency required for the output result. This time step should be lower than the time constant (d^2 / α) of the reference layer, which is the layer with maximum time constant. After that, the space step Δx is defined for the reference layer as

$$\Delta x_r = \sqrt{6 \; \alpha_r \; \Delta t} \quad . \tag{3.10}$$

Finally, the space step for other layers is estimated from

$$\Delta x_i = \Delta x_r \sqrt{\frac{\alpha_i}{\alpha_r}} \quad . \tag{3.11}$$

Clearly, this equation is similar to equation (3.9)

Stability errors are due to errors introduced in the preceding time steps. For that, it is sometimes called history errors (Hensen and Nakhi, 1994). In order to show how stability errors occur, a simple problem may be studied. A homogeneous slab with known surfaces temperature is considered. The equal spacing node distribution for this problem is shown in Figure 3.3, the node numbering starts from 0 in order to simplify the associated mathematical formulae. The numerical representations associated with the nodes, equation (3.2), are rearranged and presented in matrix form as

$$\mathbf{F} \; \mathbf{T}^{n+1} = \mathbf{P} \; \mathbf{T}^{n} + \mathbf{B} \tag{3.12}$$

where,

$$\mathbf{F} = \mathbf{I} - \gamma \; F_o \mathbf{C}^{n+1}$$

$$\mathbf{P} = \mathbf{I} + (1 - \gamma) \; F_o \; \mathbf{C}^{n}$$

Hence,

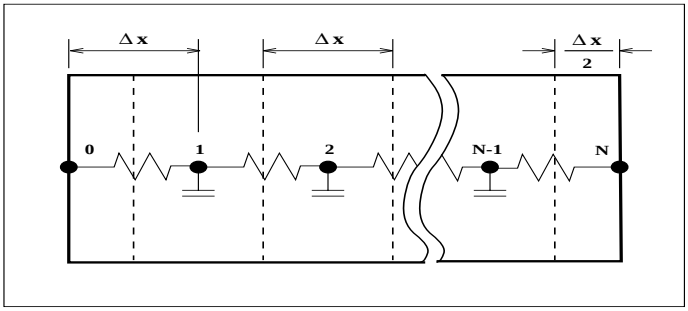

Figure 3.3 Electrical analogue for a slab with known surface temperature.

$$\mathbf{T}^{n+1} = \mathbf{A}\,\mathbf{T}^{n} + \mathbf{E} \tag{3.13}$$

where,

$$\mathbf{A} = \mathbf{F}^{-1}\mathbf{P}$$

$$\mathbf{E} = \mathbf{F}^{-1}\mathbf{B}$$

The number of equations are N-1 as the temperature profiles in the time dimension for nodes 0 and N are known.

There are two standard methods (Smith, 1985) for stability analysis for a set of finite difference equations: matrix method and the Fourier series (Neumann) method. The matrix method is more rigorous as the Neumann method does not count for the boundary conditions.

Applying the matrix method, the boundary vector **B** can be eliminated as it is assumed to be independent of the variables (i.e. temperature of nodes 1 to N-1). However the effect of boundary conditions will be encountered in the stability analysis via the coefficient matrix **A**. The numerical stability and stability errors of the set of equations defined by equations (3.2) are dependent on their associated growth factors ψ which are the eigenvalues of matrix **A**. The numerical behaviour of a set of equations can be classified according to the value of the growth factor into four categories:

-	1	<	ψ			: unbounded growth.
-	0	<	ψ	<	1	: steady decay.
-	-1	≤	ψ	<	0	: stable oscillation.
-			ψ	<	-1	: unstable oscillation.

That is, for $|\psi| < 1$ the problem will be stable, and for $\psi < 0$ oscillation **may** occur.

In the neighbourhoods of discontinuity in the initial values, boundary values, or between initial values and boundary values, the truncation error is usually severe. Therefore, if the growth factor at those points of discontinuity were negative, then an oscillation in the temperature value is expected to occur whose rate of decay is dependent on the magnitude of the growth factors. In general, whenever there is a per step error, the rate of decay or growth of that error in the following steps is dependent on the growth factors to the power of the number of time steps after the step at which the error occurred. That is

$$\mathbf{e}^n = \mathbf{A}^n\ \mathbf{e}^o = \sum_{i=1}^{N-1} c_i\ \psi_i^n\ \Psi_i \tag{3.14}$$

where **e** is the error vector, Ψ_i are the eigenvectors of matrix **A**, c_i are constants, N+1 ($0 \rightarrow N$)) is the number of nodes representing the slab. For known surfaces temperature, fixed time and space steps, and homogeneous domain with no heat generation, the eigenvalues for the set of equations generated by one of the difference schemes defined by equations (3.2) can be easily determined since for that problem the resulted present and future coefficient matrices, **P** and **F**, will be tridiagonal of the form {b,a,c}, That is

$$\mathbf{P} = \begin{bmatrix} [1-2\,(1-\gamma)\,F_o\,] & (1-\gamma)\,F_o & 0 \\ (1-\gamma)\,F_o & [1-2\,(1-\gamma)\,F_o\,] & (1-\gamma)\,F_o \\ 0 & (1-\gamma)\,F_o & [1-2\,(1-\gamma)\,F_o\,] \end{bmatrix}$$

$$\mathbf{F} = \begin{bmatrix} [1+2\,\gamma\,F_o\,] & -\gamma\,F_o & 0 \\ -\gamma\,F_o & [1+2\,\gamma\,F_o\,] & -\gamma\,F_o \\ 0 & -\gamma\,F_o & [1+2\,\gamma\,F_o\,] \end{bmatrix}$$

Accordingly, for constant thermophysical properties, the coefficient matrices $\mathbf{C}^n$ and $\mathbf{C}^{n+1}$ are equal and defined by

$$\mathbf{C} = \begin{bmatrix} -2 & 1 & 0 \\ 1 & -2 & 1 \\ 0 & 1 & -2 \end{bmatrix}$$

The eigenvalues, ω, for a tridiagonal matrix, of the form {b,a,c}, are given by

$$\omega_i = a + 2\,b\left(\frac{c}{b}\right)^{0.5}\cos\left(\frac{i\pi}{N}\right), \quad i = 1, 2, \ldots, N-1 \tag{3.15a}$$

or

$$\omega_i = a + 2\,b\left(\frac{c}{b}\right)^{0.5}\left(1 - 2\sin^2\left(\frac{i\pi}{2\,N}\right)\right), \quad i = 1, 2, \ldots, N-1 \tag{3.15b}$$

Knowing the eigenvalues for matrix **C**, the eigenvalues for matrix **A** can be determined as the eigenvalues for matrix **A** = f (**C**) is defined by (Bickley and Thompson, 1964)

$$\psi_i = \frac{1 + (1 - \gamma)\, F_o\, \omega_i}{1 - \gamma\, F_o \omega_i} \quad , \quad i = 1, 2, \ldots, N - 1 \tag{3.16a}$$

Therefore, the growth factors for known surface temperature condition are given by

$$\psi_i = \frac{1 - 4\,(1 - \gamma)\, F_o \sin^2\left(\dfrac{i\pi}{2\,N}\right)}{1 + 4\,\gamma\, F_o \sin^2\left(\dfrac{i\pi}{2\,N}\right)} \quad , \quad i = 1, 2, \ldots, N - 1 \tag{3.16b}$$

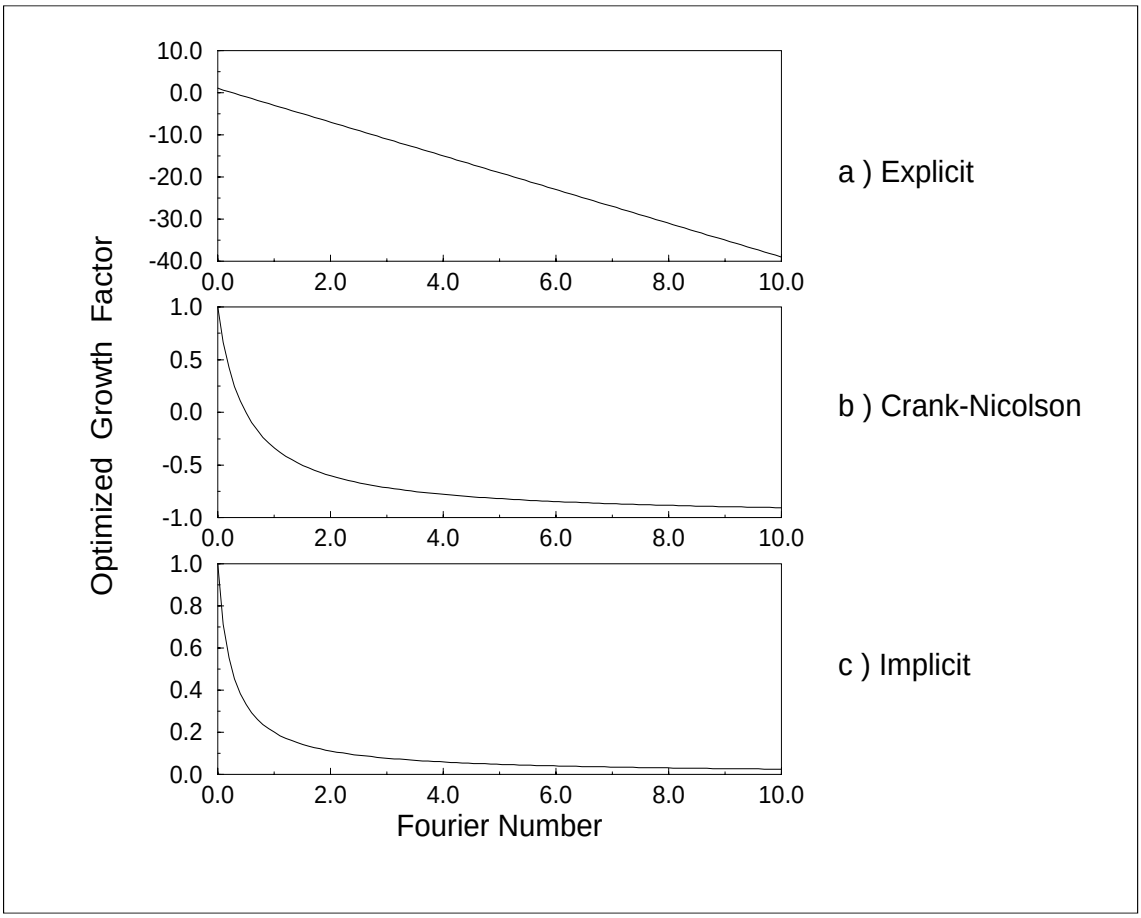

Figure 3.4 Most oscillatory growth factor as a function of Fourier number.

Clearly, the most oscillatory growth factor is associated with the largest node number as its sine approaches one. Therefore, for the current problem, the numerical stability behaviour can be defined by the eigenvalue associated with the largest node. For large number of nodes, the growth factor

associated with the largest node number is a function of the Fourier number and implicitness degree. For the explicit, Crank-Nicolson, and fully implicit schemes, the relationship between the Fourier number and the optimised growth factor is shown in Figure 3.4. From the figure it can be seen that, for the current problem, as $F_o \rightarrow \infty$ the growth factor goes to $-\infty$, -1 and 0 for the explicit, Crank-Nicolson[§], and fully implicit methods respectively. In addition, the optimised growth factor for the Crank-Nicolson method goes to zero when F_o = 0.5. In general, oscillation in the simulation result could be prevented if the growth factors were maintained positive. In other words

$$1 - 4\,(1-\gamma)\,F_o\,\sin^2\left(\frac{i\pi}{2\,N}\right) \geq\ 0$$

or

$$F_o\ \leq\ \frac{1}{4\,(1-\gamma)} \tag{3.17a}$$

where

$$0 \leq \sin^2\left(\frac{i\pi}{2\,N}\right) <\ 1.0$$

Similarly, unstable oscillations can be prevented by maintaining the growth factors greater than or equal to -1.0. Applying this to equation (3.16) we get

$$F_o\ \leq\ \frac{1}{2\,(1-2\gamma)} \tag{3.17b}$$

with the lower limit for steady decay (ψ = 1.0) defined by $F_o \geq 0$.

As shown in Figure 3.5 three areas are defined for the current problem: unstable oscillation, stable oscillation and steady decay, while unbounded growth requires a negative Fourier number which is not acceptable.

For convective boundary problems, the growth factor cannot be determined as directly as for the case of known surfaces temperature. However, by using Brauer's theorem (which is based on Gerschgorin's theorem) (Smith, 1985), the range of the associated eigenvalues can be determined. The Brauer's circle theorem (Figure 3.6) states that each eigenvalue of a matrix lies inside or on the boundary of at least one of the circles defined by $|\psi - a_{i,i}| = R_i$, where $a_{i,i}$ is the diagonal element of row i and R_i is the sum of the elements along the ith row excluding $a_{i,i}$. That is the eigenvalues are defined by

$$|\psi - a_{i,i}| \leq \sum_{\substack{j=1 \\ j\neq i}}^{N-1} |\ a_{i,j}\ | \tag{3.18}$$

§ On the other hand the truncation error order becomes O (Δx^4).

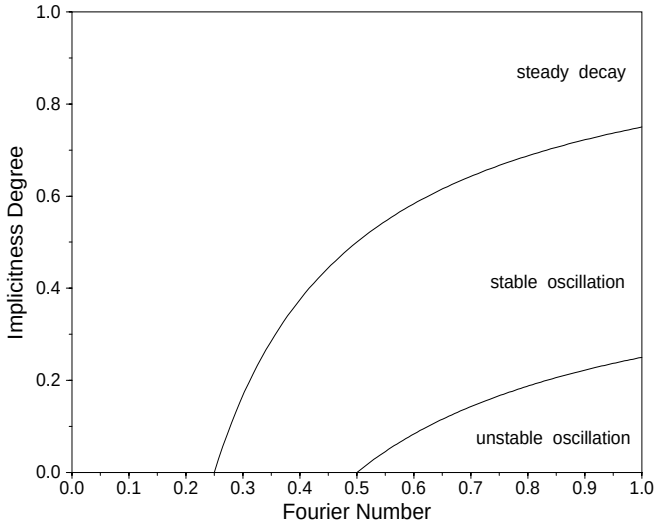

Figure 3.5 Growth factor for known surface temperature (from Crandall, 1955).

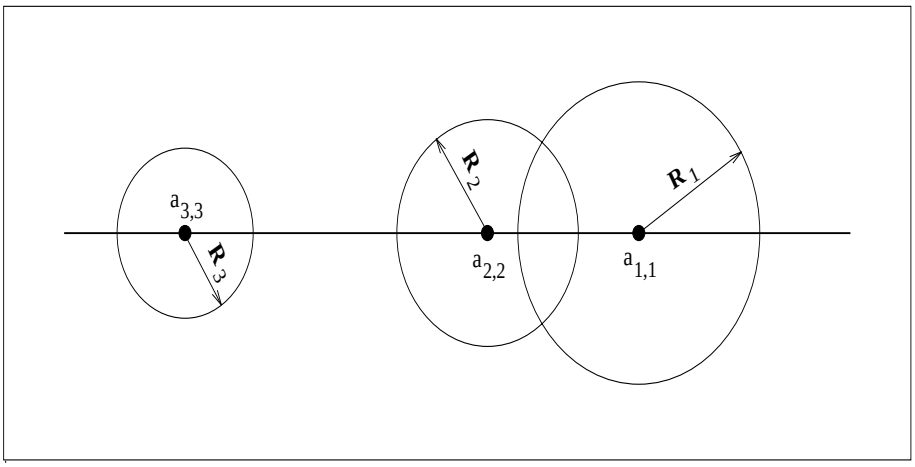

Figure 3.6 Brauer's theorem.

For example, for the convective boundary problem shown in Figure 3.1, the present and future coefficient matrices (**P** and **F**) are defined by

$$\mathbf{P} = \begin{bmatrix} [1 - 2\,(1-\gamma)\,F_o\,(1+Bi)\,] & 2\,(1-\gamma)\,F_o & 0 \\ (1-\gamma)\,F_o & [1 - 2\,(1-\gamma)\,F_o\,] & (1-\gamma)\,F_o \\ 0 & 2\,(1-\gamma)\,F_o & [1 - 2\,(1-\gamma)\,F_o\,(1+Bi)\,] \end{bmatrix}$$

$$\mathbf{F} = \begin{bmatrix} [1 + 2\,\gamma\,F_o\,(1 + Bi)\,] & -2\,\gamma\,F_o & 0 \\ -\gamma\,F_o & [1 + 2\,\gamma\,F_o\,] & -\gamma\,F_o \\ 0 & -2\,\gamma\,F_o & [1 + 2\,\gamma\,F_o\,(1 + Bi)\,] \end{bmatrix}$$

Accordingly, matrix **A** can be defined by

$$A = \frac{\mathbf{I} - (1 - \gamma)\,F_o\,\mathbf{C}}{\mathbf{I} + \gamma\,F_o\,\mathbf{C}} \tag{3.19}$$

where

$$\mathbf{C} = \begin{bmatrix} 2\,(1 + Bi) & -2 & 0 \\ -1 & 2 & -1 \\ 0 & -2 & 2\,(1 + Bi) \end{bmatrix}$$

The growth factors ψ for matrix **A** are defined by

$$\psi_i = \frac{1 - (1 - \gamma)\,F_o\,\omega_i}{1 + \gamma\,F_o\,\omega_i} \tag{3.20}$$

where ω is the eigenvalues for matrix **C**. For the Crank-Nicolson method, Brauer's theorem can be applied more directly by rearranging equation (3.19):

$$A = \frac{\mathbf{I} - 0.5\,F_o\,\mathbf{C}}{\mathbf{I} + 0.5\,F_o\,\mathbf{C}} = \frac{2\,\mathbf{I} - \mathbf{F}}{\mathbf{F}} = 2\,\mathbf{F}^{-1} - \mathbf{I}\ . \tag{3.21}$$

Therefore, the stability condition can be satisfied when matrix **F** eigenvalues, ω_F, are defined by

$$\left| \frac{2}{\omega_F} - 1 \right| \le 1$$

or

$$\omega_F\ \ge\ 1\ .$$

Applying Brauer's theorem for matrix **F**, its eigenvalues can be defined by

$$\left|\ \omega_F - [\ 1 + F_o\,(1 + Bi)\ ]\ \right|\ \le\ F_o \tag{3.22a}$$

for the boundary nodes, and for internal nodes by

$$\left|\ \omega_F - [\ 1 + F_o\ ]\ \right|\ \le\ F_o\ . \tag{3.22b}$$

These can be rearranged , respectively, into

$$1 + F_o\,Bi\ \le\ \omega_F\ \le\ 1 + F_o\,(2 + Bi) \tag{3.22c}$$

$$1 \leq \omega_F \leq 1 + 2\, F_o \ . \tag{3.22d}$$

Clearly, ($\omega_F \geq 1$) is always satisfied for non-negative values for $F_o\ Bi$. This method also indicates that by increasing the Fourier number, the system growth factor goes from 1 to zero to -1. Furthermore, similar effects are expected for increased Biot numbers. Therefore, for convective boundary problems, the growth factors not only are functions of the Fourier number but also the Biot number.

However, numerical methods can also be used to determine the eigenvalues such as the iterative power method. This can be integrated in building energy simulation codes in order to determine the eigenvalues of the system matrix. However, the coefficients of the system matrix usually vary with time due to adapting variable thermophysical properties, or due to the dynamic nature of the boundary conditions and plant interaction. Therefore, the integration should be dynamic. That is the system matrix eigenvalues should be determined at each time step to check if the growth factors are within the acceptable range.

Therefore, it can be concluded from the above theory that the thermal model accuracy not only depends on the number of nodes and time step but also on the thermal storage and transport properties of the domain. Furthermore, the traditional view that more accurate numerical results can be achieved by increasing the number of nodes is not always true.

3.1.2 Numerical investigation

The above theory may best be illustrated by some practical demonstrations. Typical homogeneous constructions which are quite common for building applications are used for this purpose. The material properties are collected in Table 3.1. For each construction a number of simulations were performed. In the first investigation, the temperature is prescribed along the wall surfaces. Although the eigenvalues for this type of problem can be defined by equation (3.20), it does not provide great flexibility for investigating the effect of changing the space step as this is associated with changes in the problem or node location. On the other hand, boundary conditions of the third kind (i.e. convective) allow greater flexibility if the convective surface temperature is selected as the investigation parameter.

The first case concerned a sudden (i.e. step-wise) change in surface temperature on both sides from the initial condition to zero. Initially the wall is at steady state and at $20\ ^oC$. The initial and boundary conditions can be presented as

$$T(x,t) = 20.0 \qquad , 0 \leq x \leq d \ \ , \ \ t = 0$$

$$T(x,t) = 0 \qquad , x = 0 \ \ , \ \ t > 0$$

$$T(x,t) = 0 \qquad , x = d \ \ , \ \ t > 0$$

Table 3.1 Construction materials properties.

Property	unit	Mineral Wool	Styropor	Rubber Tile
thickness, d	m	0.2	0.1	0.2
conductivity, λ	$\frac{W}{m\ K}$	0.045	0.04	0.3
density, ρ	$\frac{kg}{m^3}$	50.0	33.0	1600.0
specific heat, c_p	$\frac{J}{kg\ K}$	840.0	850.0	2000.0
thermal diffusivity, α	$10^{-6}\ \frac{m^2}{s}$	1.07	1.43	0.09

The analytical solution procedure for the problem is shown in Appendix B for which the exact solution is given by

$$T(x,t) = \frac{2\ T_o}{d} \sum_{m=1}^{\infty} e^{-\alpha\ \omega_m^2\ t}\ \frac{\sin(\omega_m\ x)\left[\ 1 - \cos(\omega_m\ d)\ \right]}{\omega_m}$$

where ω_m are the roots of the following equation

$$\sin(\omega_m\ d) = 0$$

or

$$\omega_m = \frac{m\ \pi}{d}$$

The mineral wool layer is represented by 21 nodes of which 19 nodes are associated with full internal control volumes, and 2 associated with two half boundary control volume nodes. Similar to the theoretical analysis, the (N-1) node is selected for the numerical examination as maximum truncation error is expected there. The temperature evolution for the (N-1) node for mineral wool is shown in Figure 3.7. The Crank-Nicolson method was adopted for these simulations. The Fourier number for the 3600s and 60s simulations are 38.6 and 0.6 respectively. For the Crank-Nicolson method the oscillation limit as defined by equation (3.20) is 0.5. Based on this limit, oscillation should occur for both cases but for the 60s simulation it will damp out rapidly as its Fourier number is near to 0.5. The numerical results shown in Figure 3.7 agree with the theoretical expectations. The 60s simulation curve overlaps the exact analytical solution. This is because reducing the time step not only reduced the truncation errors but also reduced the stability errors.

It can be concluded from Figure 3.7 that the stable oscillation reduces as the Fourier number decreases by lessening the time step. The other way for ceasing the oscillation is by using the fully

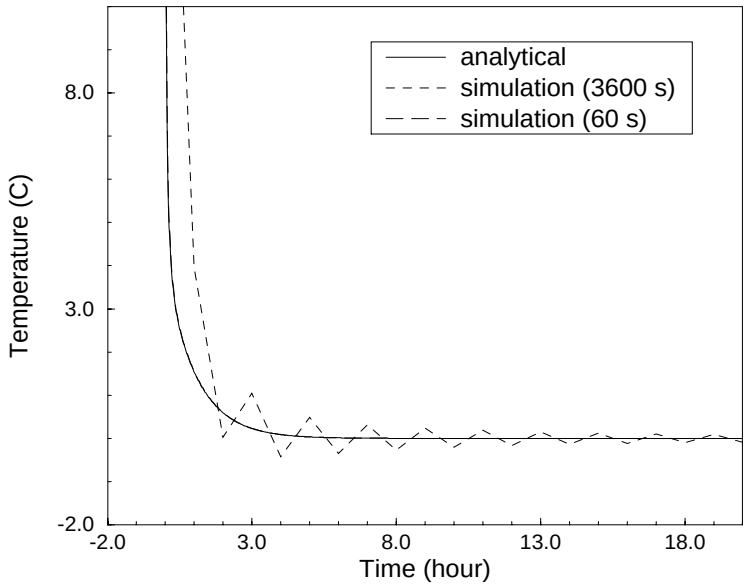

Figure 3.7 Temperature evolution for the (N-1) node of the mineral wool slab.

implicit method as shown in Figure 3.8. The per step total error for the Crank-Nicolson method is higher than that for the fully implicit method despite the higher truncation accuracy associated with the Crank-Nicolson method. The advantage shown here for the implicit method resulted in some researchers (Alvarez *et al*, 1993) recommending the adoption of the fully implicit scheme in building energy simulation codes.

On the other hand, the numerical behaviour is not uniform throughout the domain as shown in Figure 3.9. This is mainly because the temperature is not constant in the space dimension, and the stability error is not the same for all nodes based on equation (3.20). It should be mentioned that the numerical behaviour of any node is affected by its adjacent (i.e. directly or indirectly linked) nodes. This is why large differences in growth factors may occur between nodes but not between their associated per step total errors.

The case being studied for the following numerical experimentations concerned a sudden (i.e. step-wise) change in ambient temperature on one side (x=d) when the other side (x=0) is adiabatic. Initially there is a steady state situation in which all temperatures (ambient and inside the construction) are equal to 20 ^{o}C. At some point in time (say at t=0), the ambient air temperature is suddenly reduced to 0 ^{o}C. There is no radiant heat exchange, and the convective heat transfer coefficient h_c is assumed to be 3 W / (m^2 K). The initial and boundary conditions are given by

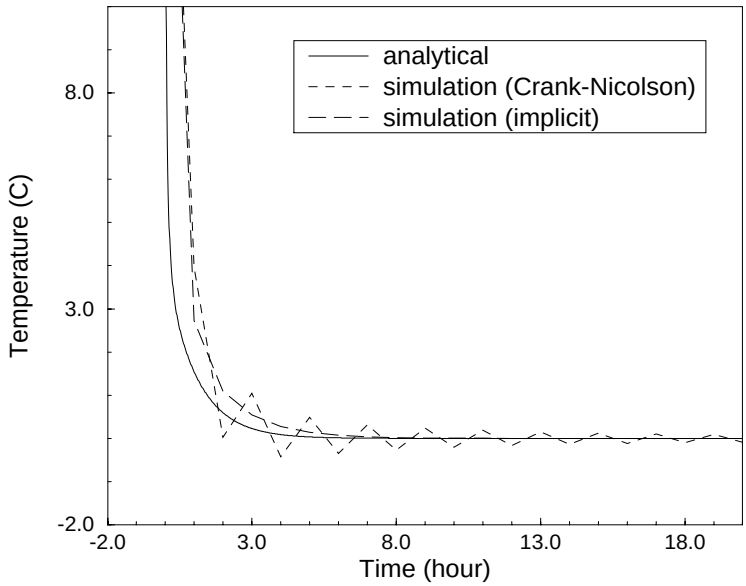

Figure 3.8 Temperature evolution for the (N-1) node of the mineral wool slab.

$$T(x,t) = 20.0 \qquad , 0 \le x \le d \ , \ t = 0$$

$$\frac{\partial T}{\partial x} = 0 \qquad , x = 0 \ , \ t > 0$$

$$\lambda \frac{\partial T}{\partial x} + h_c \, T = 0 \qquad , x = d \ , \ t > 0$$

The analytical solution procedure for the problem is shown in Appendix B for which the exact solution is given by

$$T(x,t) = 2 \, T_o \sum_{m=1}^{\infty} \frac{e^{-\alpha \, \omega_m^2 \, t} \cos (\omega_m \, x) \sin (\omega_m \, d)}{\omega_m \left[\dfrac{\sin (\omega_m \, d) \cos (\omega_m \, d)}{\omega_m} + d \right]}$$

Where ω_m are the roots of the following equation

$$\omega_m \tan (\omega_m \, d) = \frac{h_c}{\lambda} \ .$$

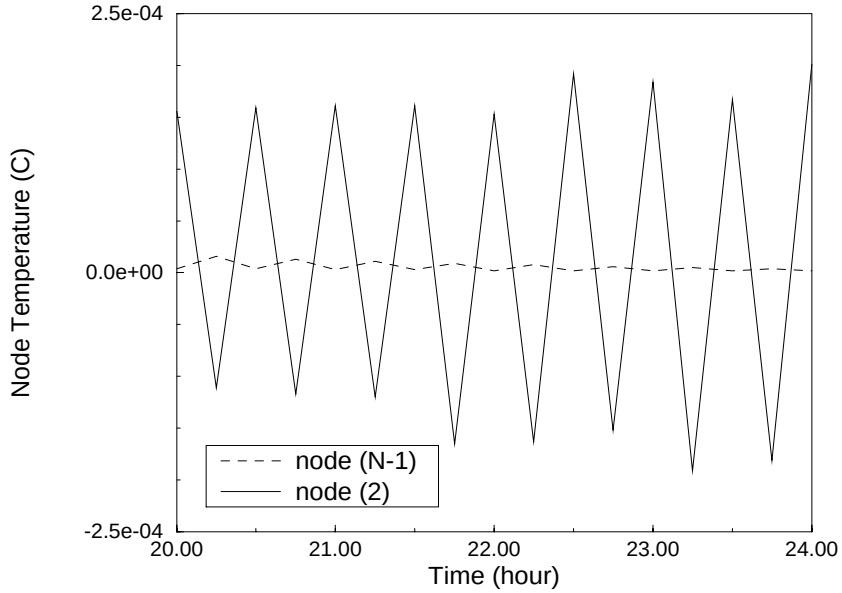

Figure 3.9 Temperature evolution for the nodes 2 and (N-1) of the mineral wool slab.

The convective surface temperature evolution for the homogeneous styropor wall is shown in Figure 3.10. The Fourier number for the 2, 4 and 6 nodes simulations are 2.0, 8.2 and 18.5 respectively. Two important points are clarified by this figure. The first point is that the magnitude of the growth factor increases as the space step is reduced by increasing the number of nodes. The 2 nodes simulation result damps out faster than the 4 and 6 nodes results. The second point is related to the truncation error. As expected, the truncation error decreases as the space step is reduced (as long as the rounding errors are negligible). This can be concluded from noticing that in case of 2 nodes simulation the peak and trough of the first oscillation is deeper than in case of the 4 and 6 nodes simulation.

Therefore, reducing the space step may increase the simulation errors not only by introducing higher rounding off errors, but also by increasing the stability errors. Accordingly, numerical lumping of constructions may produce simulation results with higher accuracy than its equivalent discretised modelling. This is because lumped formulation may decrease the stability and rounding off errors at a higher rate than the rate of truncations error increase.

The effect of negative growth factors was examined in the previous investigation. The last example investigates the effect of positive growth factors. For the rubber tile, three simulation results are compared with their equivalent exact solution in Figure 3.11. The accuracy of the 2 nodes, and 3600s simulation result is usually not acceptable. In order to increase the prediction accuracy, the time step is reduced. However, the increase in the accuracy is not significant even for the 60s time

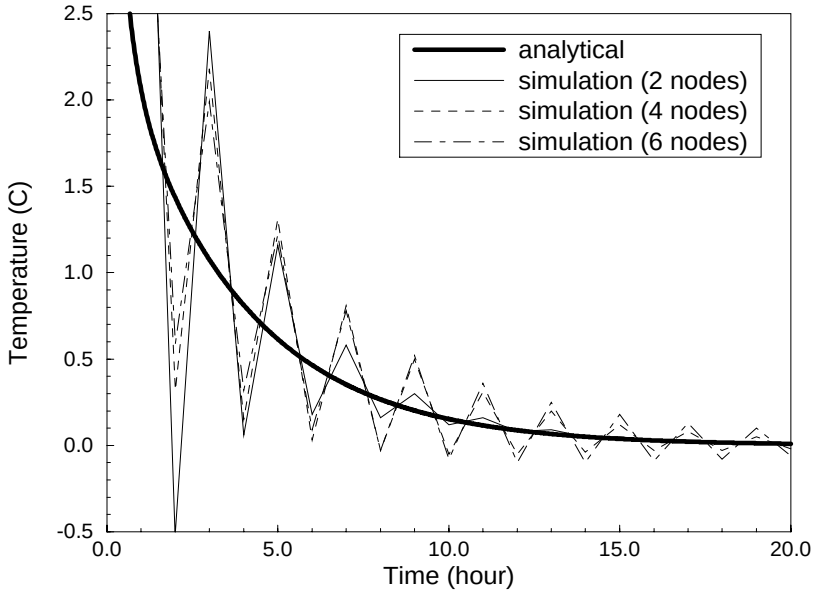

Figure 3.10 Convective surface temperature evolution for the styropor slab.

step. On the other hand, the simulation accuracy improves considerably when the space step is reduced to half its original value.

From the numerical viewpoint, the reason for the high simulation errors for the 2 nodes, 3600s run is that the very low Fourier number associated with this run (0.03) creates positive growth factors less than but approximately equal to 1. This generates un-oscillating stability errors. Similar to the oscillating stability errors, these errors damp out by time depending on the magnitude of the growth factors. Decreasing the time step will decrease the Fourier number. However, the simulation accuracy may be improved if the time step reduction is associated with a higher decrease in the truncation errors than the increase in the growth factors and their associated stability errors. This is why the 2 nodes, 60s simulation has better accuracy than the 2 nodes, 3600s one. On the other hand, if reducing the space step decreases the magnitude of the growth factor via increasing the Fourier number, then better simulation accuracy will be achieved. It should be mentioned that reduction in the growth factors magnitude may be associated with change in the sign but still a better simulation accuracy may be achieved. This explains the improvement in the simulation accuracy for the 4 nodes, 3600s run.

From the physical point of view, when the thermal penetration depth does not include at least the first (boundary) control volume, the associated excitation will not be sensed by the numerical model. Accordingly, reducing the time step will not improve the results as this will decrease the thermal penetration depth. On the other hand, reducing the space step causes a higher portion of the

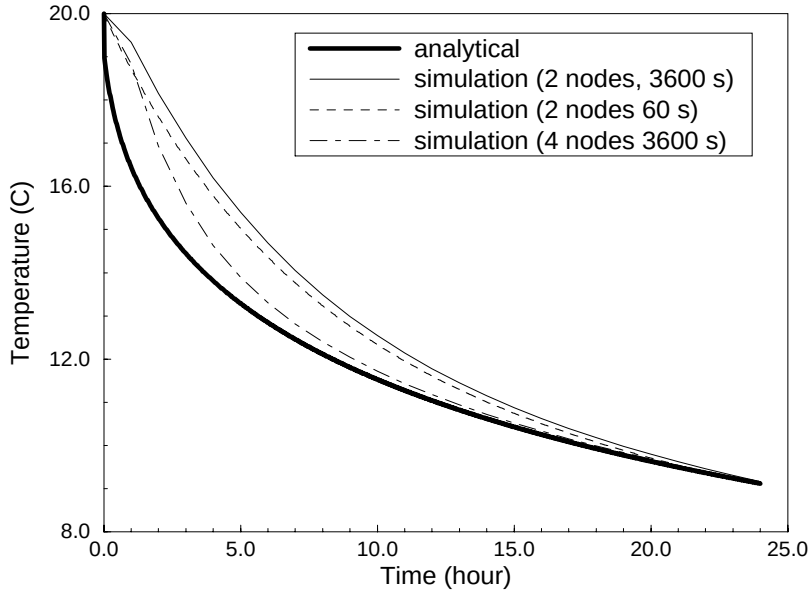

Figure 3.11 Convective surface temperature evolution for the rubber tile.

boundary control volume to be included in the thermal penetration length.

3.1.3 Lumped formulation

Very often, 3-dimensional modelling is not required and lower-dimension can be used for modelling heat flow through building components. When temperature variation in a particular direction is negligible, simulation of heat flow in that direction can be ignored. However, lumped formulation can be used as an inter-mediate case between the two extremes (i.e. 3-dimensional and lower-dimension). Furthermore, lumped formulation may produce more accurate simulation results by minimising stability errors as was shown in the previous sections.

The theory related to analytical lumped formulation of a homogeneous domain with uniform boundary condition and no heat generation can be found in the literature (Holman, 1989). In this section, the validity of lumped formulation is numerically investigated for multi-layered building constructions.

In building energy simulation, truncation is usually the main source for errors. This is because the rounding off errors are not significant as long as the mathematical stability is preserved. In addition, the stability errors are not original error sources as they will have no effect if the truncation and rounding off errors are zero. Furthermore, the growth factors for a real building simulation cannot be

estimated before the simulation as the domain and its associated system matrix are compoundly dynamic. Therefore, problem discretisation should be based on the truncation errors. Then it should be evaluated with respect to the rounding and stability errors. With regard to truncation errors, the space and time discretisation should be related inversely to the rate (in both time and space dimensions) of the dependent variable variation.

There are three main methods for analysing the heat conduction equation: discretised, partially lumped and fully lumped. These methods are applicable for both analytical and numerical solution methods. When all space dimensions used to define the domain geometry are considered in the governing heat conduction equation, the solution method is said to be discretised. If the temperature (i.e. the dependent variable) is not a function of any space dimension, the solution method is called fully lumped. Whereas, a partial lumping formulation occurs when the number of space dimensions used in the governing equation is not zero but less than the geometry space dimensions.

It should be noted that space lumping does not mean reducing the number of heat flow dimensions as the number and type of boundary conditions are not altered by the lumping process. For example, in real building, constructions are 3-dimensional objects, with a thermal analysis usually performed with respect to only one space dimension (i.e. perpendicular to the wall). Although this is usually acceptable for uninsulated constructions, a partial space lumping formulation, where the two lateral dimensions are lumped, is a better representation of heat flow as it will maintain the 3-dimensionality of the heat flow (but with reduced accuracy relative to the discretised formulation). In other words, lumping a space dimension takes out the temperature variation from the analysis, but not the heat flow path in that direction.

The partial or full lumped formulation is usually preferred due to the simplicity it offers in solving analytical problems and because of the reduction in CPU requirements in numerical solutions. Full lumped formulations are most appropriated for analytical solutions of transient problems. This is because the governing partial differential equation, regardless of the geometry complexity, reduces to an ordinary differential equation defined by

$$h\ A\ (T_{\infty} - T(t)) = \rho\ C_p\ V\ \frac{dT(t)}{dt} \tag{3.23}$$

where T_{∞} is the ambient temperature, and the domain temperature $T(t)$ is a function of time. Only the partial lumped formulation can be applied for a steady state conditions, otherwise no independent variable will exist in the governing equation.

As stated in many textbooks, simplicity of approach is often a good starting point. In light of this, the lumped formulation is the most appropriate if the exact temperature profile over the domain is not required, such as for heating load calculations. However, space dimension(s) lumped formulation (partial lumping or full lumping) is not always applicable due to accuracy restrictions. This is because

the mathematical lumping of a space variable means that the dependent variable (i.e. temperature) is independent of that lumped space dimension, that is, the temperature is uniform in that direction. Accordingly, unless the physical statement is true, the mathematical lumping is not acceptable.

Usually, the Biot number, Bi[§], is used as the deciding factor for the applicability of the lumped method. It is a dimensionless factor which is defined as the ratio of internal thermal resistance to the external thermal resistance. That is

$$B_i = \frac{(l_c \,/\, \lambda\ A)}{(1 \,/\, h\ A)} = \frac{h\ l_c}{\lambda} \tag{3.24}$$

where l_c is the characteristic length, and for a homogeneous domain with uniform convective boundary, it is defined by

$$l_c = \frac{total\ volume}{convective\ surface\ area} \quad .$$

From an engineering viewpoint, the lumped formulation can be implemented for the solution of transient heat conduction problems subjected to convective boundary if the Biot number Bi < 0.1. In other words, the lumped formulation can be used when the external thermal resistance is much higher (e.g. 100 times) than the internal resistance. Accordingly, the exact analytical solutions (i.e. physical behaviour) is expected to show less than 5% temperature variation throughout the lumped dimensions.

While the Biot number is used for dynamic applications, it does not account for the density and heat capacity of the domain. However, this does not affect the applicability of the Biot number criterion. This is because, for the homogeneous domain, the storage properties affect only the overall domain temperature, whereas, the thermal conductivity and heat transfer coefficient define the temperature profile throughout the domain. This can be exemplified by comparing the temperature profile of two problems which differ only in the domain's thermal storage properties. Two 0.5 m thick homogeneous brick slabs initially at 20 ^oC were submerged into an environment at 0 ^oC. The storage property (i.e. $\rho\ c_p$) for slab (b) is 1000 times higher than that for slab (a). The temperature profiles after one hour is shown for both slabs in Figure 3.12. As shown in the figure, the absolute variation in the temperature profiles for both cases is approximately $0.06\ ^oC$ despite the difference in their mean temperature.

Basically, the Biot number rule is limited to homogeneous domains with uniform boundaries and no heat generation. However, these conditions are usually not satisfied in building applications because:

- Heat generation via plant interaction, and shortwave and longwave radiation absorption is possible.

§ This is different from the boundary node Biot number introduced in Section (3.1.1).

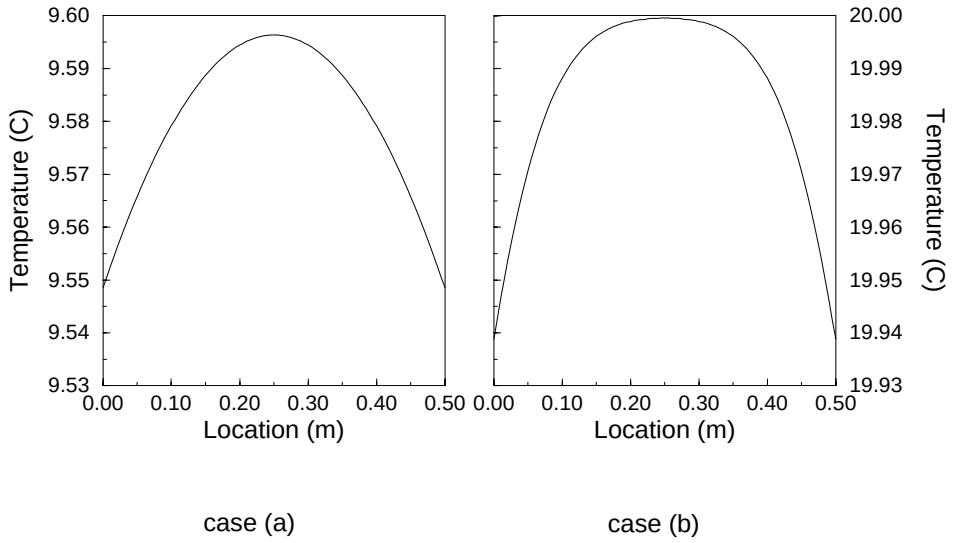

Figure 3.12 The effect of thermal storage properties on temperature distribution.

- Building constructions are usually composed of different materials.
- The internal and external boundaries are expected to be different due to the difference in the ambient temperature and/or convective heat transfer coefficients.

Therefore, the effect of these factors on the applicability of the Biot rule in building applications must be investigated.

In principle, if the internal thermal resistance of the domain is negligible, the temperature distribution within the solid remains acceptably uniform in the time domain. In addition, in order to assure that this remains true even for very short periods after the occurrence of the external boundary condition, the external (i.e. convective) heat transfer coefficient should be much lower than the internal heat heat transfer coefficient (i.e. conductivity). This is what the Biot number rule is based on. Clearly, this rule cannot ensure temperature uniformity if the internal excitation (i.e. heat generation) occurs. This is because the effect of the excitation will not be dampened by the convective heat transfer coefficient. However, the non-uniformity will occur only for a short period from the initiation of the internal excitation. Therefore, for building energy simulation purposes, where relatively large time steps are employed, this will not affect the applicability of the Biot rule.

Different ambient temperatures are expected to create temperature variation even for steady state conditions. This mainly depends on the magnitude of thermal resistance which is equal to the

slope (i.e. variation) of temperature in the space dimension. In building applications, however, thermal conductivity is expected to be large if the Biot rule is satisfied. Otherwise, the convective heat transfer coefficients will be very small.

The characteristic length is the nearest distance between the adiabatic point, line, or surface to the boundary. Therefore, for a homogeneous slab (wall) with uniform boundary conditions on both sides, the characteristic length is equal to the slab thickness divided by 2 (equation (3.24)). However, for a slab with different convective heat transfer coefficients at the boundaries (i.e. similar to external building walls), the characteristic length cannot be easily defined due to difficulties in locating the adiabatic line. That is because the adiabatic surface is expected to be dynamic. This is shown in Figure 3.13 for a homogeneous slab with two heat transfer coefficients 5 and 10 at x=0 and L, initially at 20^oC with the ambient temperature at both sides changing from 20^oC to 0^oC at time t = 0. The temperature profiles throughout the slab for the first 12 hours are shown. The peak of the temperature profile (i.e. the adiabatic line) moves, with time, nearer to the boundary with the lower heat transfer coefficient. In order to unravel this, the convective heat transfer coefficients are assumed to be equal to the largest one. By this, some cases which accept lumping may be not recognised but the inverse is not true.

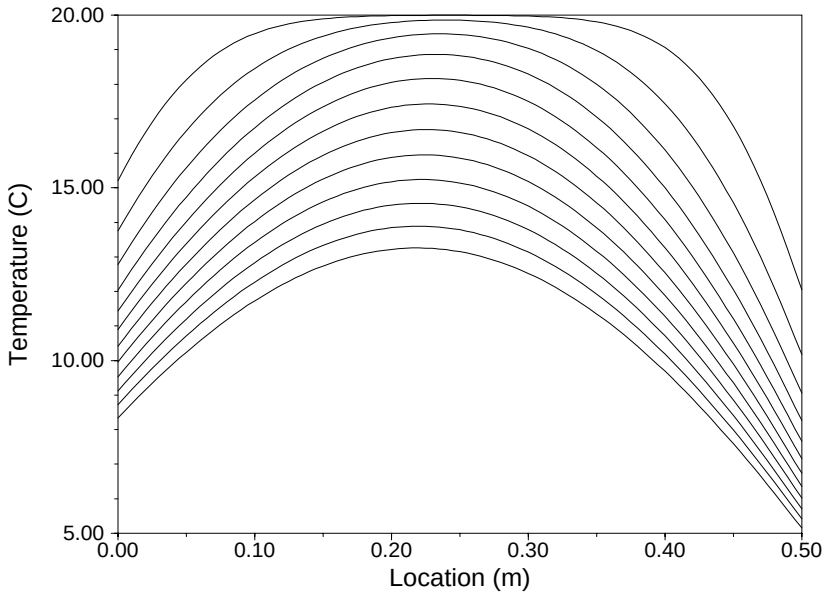

Figure 3.13 Dynamic characteristic length.

Similarly, a multi-layer wall is represented by a homogeneous wall whose thermal conductivity is equal to the lowest conductivity in the multi-layer wall. The necessity for this approach can be exemplified by assuming a three layer wall whose centre layer is the thinnest but which has relatively

high thermal resistance. For that slab, temperature variation is expected to occur even if the Biot rule is satisfied for the volume weighted average, or algebraic sum of thermal resistances.

After checking the validity of lumped formulation, different multi-layered construction lumping methods can be adopted. For example, the whole construction can be represented by one central node, two boundary nodes or both. In ESP-r the numerical lumped formulation is performed by replacing the multi-layer construction by a single layer which is then represented by the default ESP-r space discretisation algorithm. The boundary nodes are required to control the truncation error whereas the central node is required for compatibility with the other ESP-r facilities such as the control functions.

On the other hand, the thermophysical and geometrical properties of the construction are not altered by the ESP-r lumping approach as the three control volumes will have different thermophysical properties based on the original multi-layer construction. This is done by volume weighting the storage properties and algebraic summing of thermal resistances.

From the foregoing discussion, it is concluded that the simulation accuracy can be controlled via the employed gridding scheme. Furthermore, it was shown in Chapter 2 that there is a need for multi-dimensional heat conduction simulation which does not require high CPU effort. Such gridding scheme is presented in the coming section.

3.1.4 Multi-dimensional, variable resolution, error based building fabric modelling

There is no optimum grid generation technique for all purposes. Therefore, a study was carried out to select the best suitable grid generation technique for typical building energy simulation applications. However, the numerical method which will be used to solve the governing equations should be considered also since both the solution and gridding techniques are inter-dependent . Many numerical methods exist for solving transient heat conduction problems, of these the two major approaches include the finite difference method (FDM) and the finite element method (FEM) (Ozisik, 1993). The finite difference techniques are the most straight forward. However, it cannot be applied directly to irregular boundaries. Using the finite difference approach to solve a problem involving irregular boundaries usually requires interpolation between the boundaries and interior grids points. Such interpolations are expected to be a major source of error, especially if the boundary conditions are the driving force for heat flow, which is the case for most real problems. In general, the numerical solution of partial differential equations requires an accurate numerical representation of the boundary conditions.

Finite element techniques are suitable for domains of complex geometry. For that reason the technique is used by general purpose numerical computer programmes such as ANSYS (Swanson Analysis Systems, 1991). However, in comparing the finite element method and the finite difference method for transient problems, the finite elment method requires more memory capacity and computation time, and is more sensitive to numerical oscillation (Myers, 1971) than the finite difference

method. The mesh generation procedure cannot always be done automatically. Therefore, the finite element method was not employed.

Several approaches were developed in order to combine the advantages of both techniques, i.e. generally applicable for arbitrary bodies and with the simplicity of the finite difference method. These approaches can be classified into two categories: the boundary fitted curvilinear coordinate systems for the numerical solution of partial differential equations, and the generalised finite difference methods for nonuniform meshes. In order to define the most suitable approach, these approaches are summarised first. The theories employed by these approaches are detailed elsewhere (Arnone and Sestini, 1991; Fletcher, 1988; Thompson *et al*, 1985; Frey, 1977; MacNeal,1953).

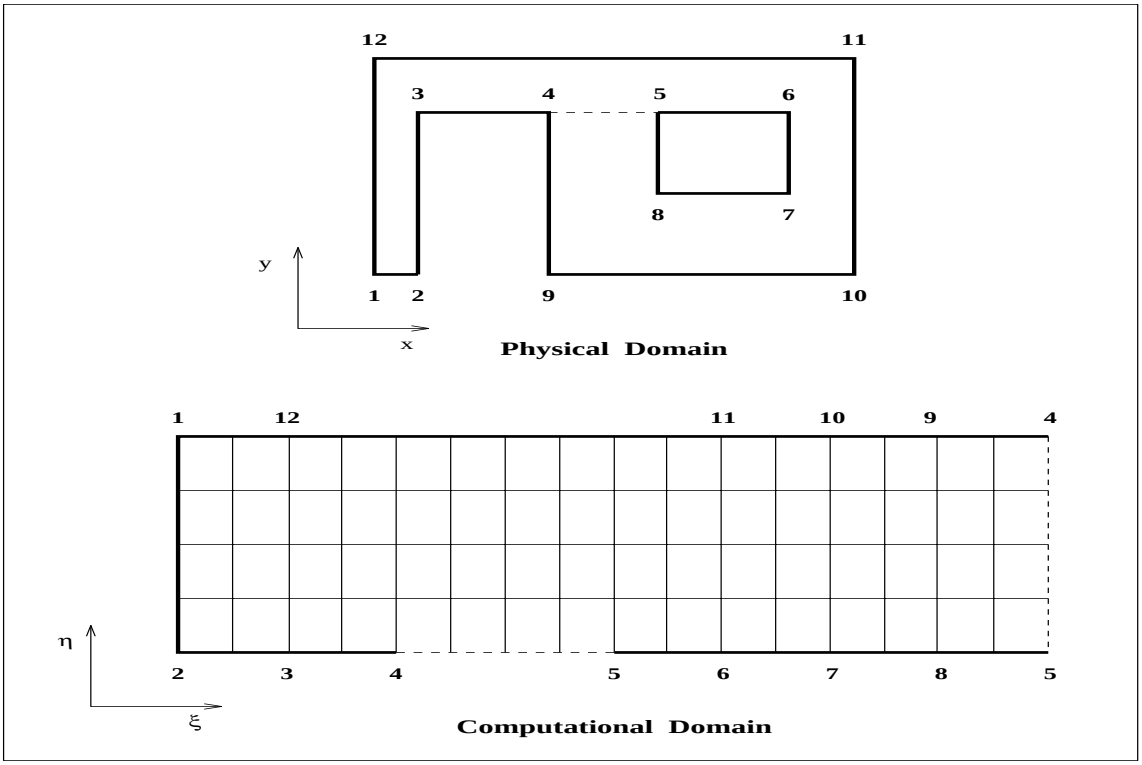

Figure 3.14 Solution domain transformation.

In the boundary fitted curvilinear coordinate systems approach, coordinate lines (or surfaces in 3-dimensional problems) conform with all boundaries. This ensures an accurate representation for the boundary conditions. With this approach a partial differential equation can be solved, after it had been transformed analytically to that curvilinear coordinate system, on a fixed rectangular field with standard finite difference techniques in the computational domain (Fletcher, 1988). While the domain is significantly simplified (see Figure 3.14), the equations resulting from transforming the partial differential equations to the curvilinear coordinates is of the same type as the original, but contains more

terms and variable coefficients. Of course, the boundary condition equations should also be transformed to the same curvilinear coordinates, resulting in a similar form to the original boundary condition equations, but with more variable coefficients. Generating curvilinear coordinate system procedures are of two general types: by solution of partial differential equations, and by algebraic transformations.

Although the use of boundary fitted coordinate system for a numerical solution of partial differential equations is a powerful technique, it was not chosen to be adapted to ESP-r due to reasons related to difficulties associated with creating a geometrically generic numerical grid generation source code, and because of the difficulties associated with transforming the governing equations.

Buildings are complex domains which are composed of multi-components linked together. This means that each component should be transformed in isolation taking into account the other linked components. This requires assuring the continuity of gridding lines at the interface of building components. In addition, building components such as walls can be geometrically complicated and so should be divided into sub-components. In the 3-dimensional problem, conformal or orthogonal coordinates are usually not possible. Therefore, the governing equations must be expressed in generalised curvilinear coordinates. This may involve second derivative transformation parameters which are usually difficult to evaluate accurately (Thompson *et al*, 1985).

On the other hand, there have been many attempts to develop a generalised finite difference method suitable for generally applicable source code. These attempts are mainly of two types. In the first type, the domain is represented by (or divided into) small finite stencils (or polyhedrons in 3-dimensional problems) which can have any shape (nonuniform mesh). Then for each node, its associated stencil is transformed separately into curvilinear coordinates where each stencil will be square. By using standard finite difference (volume) techniques, the partial differential equations are solved, after they have been transformed into the local curvilinear coordinates, for each stencil. It should be mentioned here that this technique is similar to the finite element technique, except after transforming the stencil (element) to its natural coordinates the standard finite difference techniques are used instead of creating the system (global) stiffness matrix (equations). Frey (1977) used a nine point isoparametric stencil, in which the geometric interpolation function and the temperature interpolation function are of the same type, for solving partial differential equations. Although this method sounds attractive, there is usually a limit for stencil nonuniformity (distortion). Furthermore, it requires a structured mesh. In building applications, an adaptive gridding should allow variable mesh density throughout the domain. This requires an un-structured mesh or multi-gridding technique (Arnone and Sestini, 1991). The former is usually preferred due to its simplicity.

In the second type of generalised finite difference method, the domain is represented by an asymmetrical finite difference network. A node is located at each network interaction. After that, a control volume is defined for each node. The control volume surfaces are perpendicular to the

network lines. An electrical analogy is usually used in order to determine the finite volume formulae for each node. MacNeal (1953) described a solution for second order boundary value problem by means of this method. In order to ensure correct mesh generation, he suggested that the network should not have an interior angle of more than 90 ^{o}. This approach is attractive because of its simplicity and conservation of energy. Accordingly, it was selected for developing the multi-dimensional gridding scheme. However, it requires some modifications to render it suitable for building gridding.

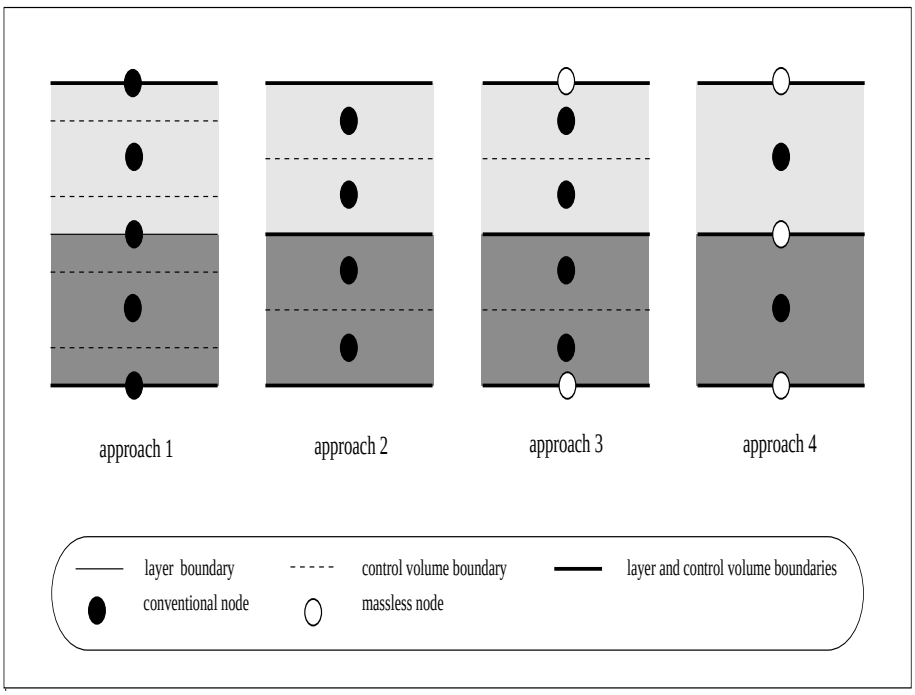

Figure 3.15 Control volume nodal schemes.

There are several possible schemes for the positioning of control volumes and their associated grid points (see Figure 3.15). For the multi-dimensional grid generation, approach 4 in Figure 3.15 was adopted. This gives continuity of heat capacity and density throughout the control volume, and continuity in the boundary conditions throughout each control volume surface. The grid points are located at the geometric centres of each control volume. This is expected to give the best representation of the average temperature over the control volume. In addition, massless nodes are located at the construction boundaries and layer interfaces in order to ensure continuity in the thermal conductivity between grid points and a better dynamic response to excitations at the construction boundaries.

The developed gridding technique is based on locating the control volumes first. This is done based on the mesh densities required. Then the conventional and massless nodes are positioned according to approach 4 in Figure 3.15. In order to allow flexible distribution of control volumes, the number of control volume sides are not restricted to a specific number. That is, a four sided control

volume can be connected to a ten sided one. Therefore, the number of connections per control volume is not fixed. It should be noted that the control volume sides can be co-linear. For example a square control volume may be ten sided. The main reason for using such a technique is to facilitate variable modelling resolution. This will also allow the importing of external building components such as from KOBRA.

3.2 Numerical model

By applying energy balance for a polyhedron control volume (refer to Chapter 2), the control volume formulation can be written as

$$V\ \rho\ c_p\ \frac{\partial \bar{T}}{\partial t} = -\sum_{i=1}^{N} A_i\ \vec{q}_i\ .\ \vec{n}_i + V\ \bar{g} \tag{3.25}$$

where N is a positive integer. Although this method ensures energy conservation, with no limitation at the gridding level, the accuracy of the simulation is strongly dependent on the generated mesh. For example, steep mesh spacing changes will magnify the local truncation (and hence the simulation) error as was shown in previous sub-sections.

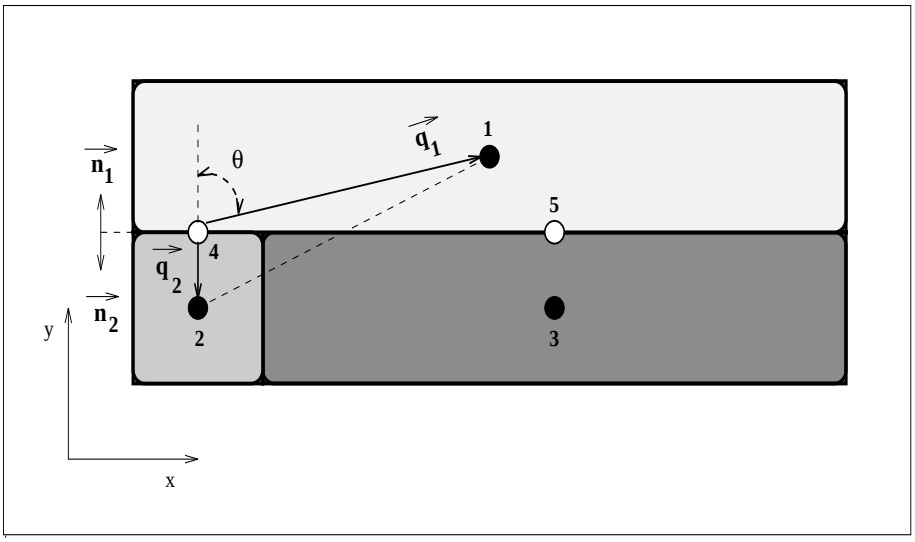

Figure 3.16 Unstructured 2-dimensional mesh.

Applying the control volume formulation (equation (3.25)) for the unstructured mesh shown in Figure 3.16, the heat flow between control volumes 1 and 2 cannot be estimated directly. This is because the temperature gradient ∇T cannot be defined due to geometrical difficulties and discontinuity in the transport property. This difficulty is overcome by employing massless nodes at the interface of these two control volumes. Therefore, using massless nodes not only ensure continuity in the

transport property but also allows the modelling of coarse unstructured meshes.

For a massless control volume (i.e. volume is zero), equation (3.25) reduces to

$$0 = \sum_{i=1}^{2} A\ \lambda\ (\ \nabla T_i\ .\ \vec{n}_i\ ) \tag{3.26}$$

where 2 is the number of surfaces, $A = A_{4,1} = A_{4,2}$, and

$$\nabla T_1\ .\ \vec{n}_1 = \frac{\Delta T_1}{\Delta r_1}\ \cos\theta = \frac{\Delta T_1}{\Delta r_1}\ \frac{\Delta y_1}{\Delta r_1}$$

$$\nabla T_2\ .\ \vec{n}_2 = \frac{\Delta T_2}{\Delta r_2}$$

On the other hand, there is a disadvantage to this type of grid flexibility - more storage is required for an unstructured mesh than for an equivalent structured one. In addition, the number of coefficients (connections) for each node is not constant, and there is a potential for some nodes to have a relatively large number of coefficients. Thus, convergence of the iterative solution methods is expected to be more difficult. Some relatively fast direct solution methods for structured grids (such as the Alternating Direction Implicit (ADI) or Explicit (ADE) methods (Ozisik, 1980)) are not applicable. It should be noted that even for structured meshes, the internal surface nodes are expected to have a relatively large number of coefficients due to internal longwave radiation flux. For the present implementation, storage and speed problems were reduced by introducing sparse storage and matrix solution techniques. However, solution times are still restrictive (although this problem should in time be reduced with increased computing power).

Based on the foregoing theory, a multi-dimensional, variable resolution, error based building fabric modelling technique is developed. In order to test the validity of this technique and make it available for building simulation practitioners, a building fabric modelling scheme was developed and integrated within a whole building simulation environment (ESP-r). The implementation of such technique is presented in the next section.

3.3 Implementation

3.3.1 Multi-dimensional building fabric gridding

Based on the foregoing discussion an adaptive multi-dimensional gridding module has been developed. The main feature of this module is that it allows localised multi-dimensional modelling. For example, a building can be modelled as a 1-dimensional problem except for one room which is 3-dimensional. Furthermore, within a zone, building components may be defined as 1-, 2- and 3-dimensional thermal models and then connected together to form a multi-dimensional zone.

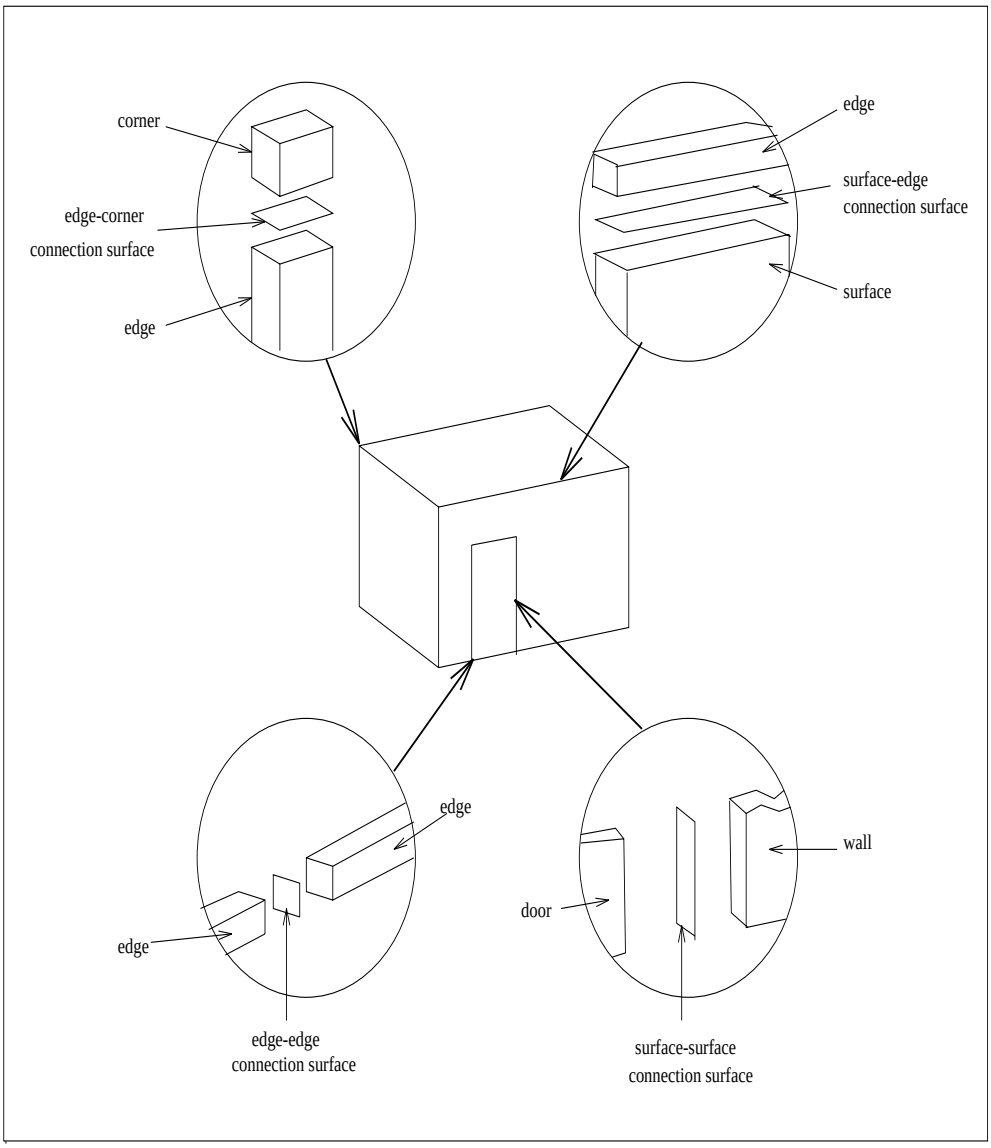

Figure 3.17 Connection surfaces types.

In order to allow such gridding flexibility, the building is divided into zones which are also divided into building components. The available building components are surface (wall, door, window), edge and corner. Each component can be defined as lumped or discretised. In addition, edges and corners can be ignored as in the default 1-dimensional case. These components can be connected to each other via connection surfaces as shown in Figure 3.17. Homogeneous (wall to wall) and heterogeneous (wall to edge) connections are possible. Therefore, four connection surfaces can be used: surface-to-surface, surface-to-edge, edge-to-edge and edge-to-corner. The connection surfaces are allowed to connect components at suitable gridding levels (not defined, lumped and discretised). In order to connect a wall to another component it should be defined as discretised. However, edges and

corners can be connected if they are lumped or discretised.

The multi-dimensional gridding scheme handles one zone at a time. In general, the existing 1-dimensional information is used as much as possible for the multi-dimensional gridding in order to prevent duplication in the data. From the geometry file, a wired mesh is created. Based on the construction thicknesses provided by the construction file, this wired mesh is transformed into solid model. However, this process requires information on the relative indentation for co-planner surfaces. Accordingly, the surfaces indentation from imaginary parallel surfaces (one imaginary surface for each set of co-planner surfaces) are stored. Finally, the boundary conditions for the zone are fed by the system configuration file.

In order to reduce the discretisation rounding errors, the definition of gridding details and gridding process are performed locally. That is, the global axes is transformed to the local axes of each building component or connection surface at times of definition and process of grids. The transformation of the global axes to local axes is performed by first translating the origin of the global axes to the origin of the local axes (refer to Appendix C). Then the translated global axis is rotated to match the local axes. Accordingly, the direction cosines of the local axes for all building components in the active zone must be estimated. This is done by first determining the local axes direction cosines for all surfaces. This may become laborious for general polygons. Therefore, a robust method was developed for the definition of the surfaces local axes. The definition of local axes for general polygons is demonstrated in Appendix C.

The local axes for other building components and connection surfaces are defined through their adjacent surfaces local axes. For edges, the x- and y-axes are defined from their associated surfaces, while the z-axis is defined from the first and last vertices defining them. Each edge is associated with only two surfaces, and edges having more than two surfaces are divided into edges of only two surfaces.

The thermophysical properties behind zone surfaces (constructions) are defined by the zone construction file. However, thermophysical properties for edges and corners are set by default to be concrete. This can be then changed by the user via a menu driven option or via a 3-dimensional configuration file which contains the complete description for the 3-dimensional zone. On the other hand, connection surfaces are massless and do not possess thermal properties.

When a zone is selected by the user for multi-dimensional gridding, the module will automatically create the default 3-dimensional description of the zone as shown in Figure 3.18. This is the most coarse 3-dimensional gridding acceptable. All the edges and corners are lumped, and the surfaces are discretised by using a least acceptable number of gridding lines as shown in Figure 3.19. The gridding lines are terminated at the intersection with the boundary lines (connection surfaces). This will prevent the creation of non-required control volumes. Additional gridding lines can be added to discretised building components. On the other hand, the connection surface details are

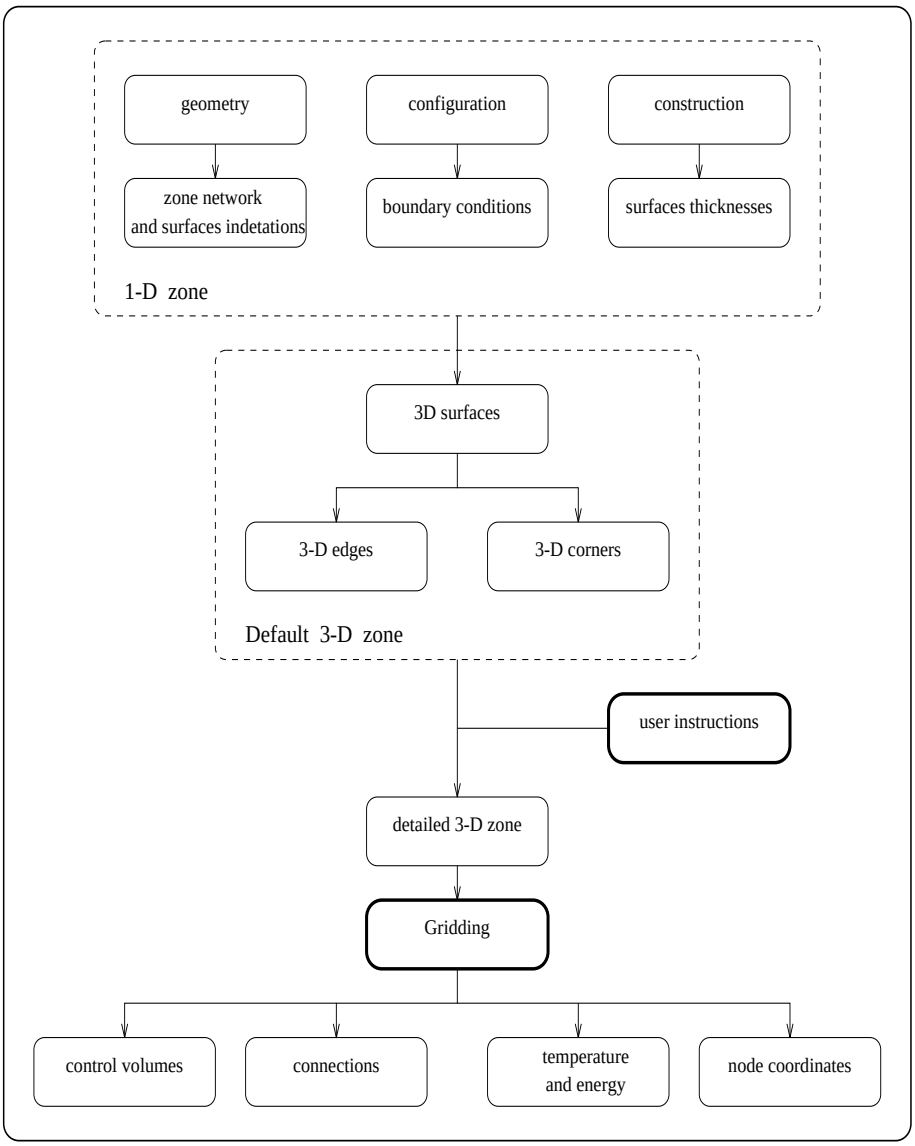

Figure 3.18 Flow chart for gridding process in grd module.

created by the module just before the gridding process. Only the activated connection surfaces are considered.

3.3.2 Ground modelling

Because of the generality of the multi-dimensional system matrix construction/solution, it can be used for modelling heat transfer through several domains beside building construction. This section describes 3-dimensional ground modelling via the multi-dimensional scheme. This is preceded by an introduction showing the importance of ground modelling for better simulation of heat flow

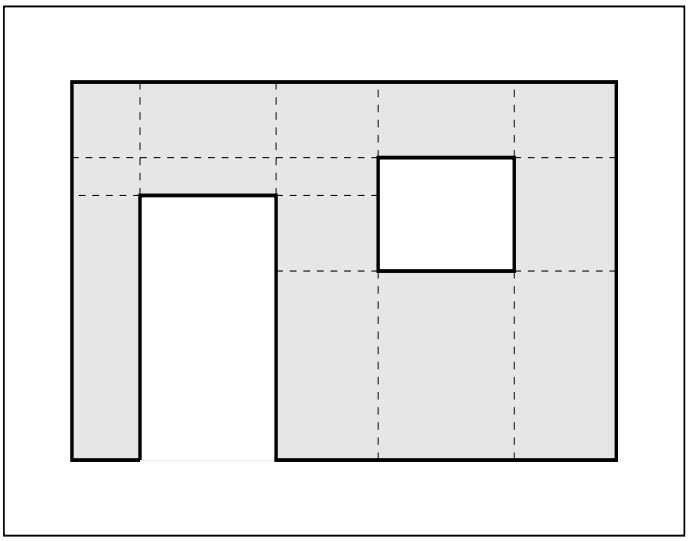

Figure 3.19 Default 3-dimensional surface gridding.

through building slab on the ground by providing more accurate boundary condition for the slab.

Several studies had been performed on heat flow between buildings and the ground of which most were steady state, 2-dimensional cases. Different study tools were adapted for these studies. These can be divided into experimental results, analytical formulae and numerical codes. Thomas and Lloyd (1994) monitored the thermal performance of the ground slab for a real occupied building. By implementing automatic data collection system, the full transient nature of the problem was captured. Claesson and Hagentoft (1991) used the method of superposition to generate a simplified analytical equation to describe the 3-dimensional transient heat flow through the ground with constant indoor temperature. They reduced the thermal process to three simpler processes: 3-dimensional steady state, 2-dimensional pure periodic outdoor temperature and 2-dimensional pure outdoor temperature step. The total heat flow is determined by the algebraic sum of the heat flows of the three separate solutions. Jones (1994) constructed a finite element computer program from the SERC's Finite Element Library. He used his 2-dimensional transient model to predict the temperature and heat flux in the floor slab and ground of industrial buildings.

For general building energy simulation codes, however, empirical and analytical formulae cannot be employed as they are only suitable for specific cases. Furthermore, Jones (1994) stated that there are significant differences between steady state and transient solutions for industrial buildings. In addition, Walton (1987) has reported that differences between 2- and 3-dimensional predictions of heat losses to the earth may be as large as 50 %. Accordingly, a discretised 3-dimensional transient numerical ground model should be developed and integrated within an environmental building performance code.

Heat flow through the slab on the ground is complex as it is a transient, 3-dimensional problem which depends on several factors. In order to select the most appropriate model for heat flow through such a slab, the factors which may need to be considered are:

- Heterogeneity of the building constructions and the ground. Usually, the ground consists of layers with different thermophysical properties. This can be easily considered in discretised ground models.
- Moisture transport through slab on the ground influences the energy flux. This effect can be neglected for relatively small moisture flows which is normally the case for ground floor slab.
- Ground water flow. This effect is usually neglected except for the rather extreme situations of shallow ground water table and very high ground water flows.
- Ground freezing. When fluids freeze, not only thermophysical properties of the domain are expected to change but also latent heat of freezing should be taken into account. Claesson and Hagentoft (1991) came to the conclusion that the effects of ground freezing are secondary and can be neglected in the simulation of heat flow between buildings and ground.
- Boundary conditions at adjacent ground surface. This is a compound factor which includes several items such as outdoor air temperature, wind velocity, direct and indirect solar insulation, ground surface cover (snow), and adjacent thermal zones.

Consequently, a discretised transient 3-dimensional ground module should be integrated with a general building energy simulation package which will provide the thermal ground model with the boundary conditions at adjacent ground surface. The thermal ground model can then provide the building energy package with information on slab heat flow. Davies *et al* (1994) came to similar conclusions.

The adapted 3-dimensional ground modelling scheme developed in the present work treats the ground as a multi-dimensional zone without an air node. That is, 3-dimensional ground modelling is performed as a special case of multi-dimensional zone modelling. This reduces the amount of coding required. Consequently, the developed 3-dimensional ground modelling scheme does not increase the size of the simulation executable significantly. In addition, unstructured meshes can be used. In principle, adaptive ground modelling requires unstructure meshes as the temperature variation differs dramatically over the domain.

Usually, 1-dimensional ground models connect the heat flow through the ground slab to the deep ground temperature. One of the main disadvantages of such an approach is associated with the uncertainties in the correct values for the deep ground temperature. On the other hand, 3-dimensional discretised ground modelling can connect the heat flow through the slab to the outside air.

On the discretisation side, no boundary massless control volumes are used in the ground grid. This is because adiabatic boundary conditions are very common for ground modelling, and massless

nodes at adiabatic boundary are not expected to perform well. This can be clarified by applying an adiabatic boundary to the characteristic equation for a massless node. That is

$$a_{i+1}^{n+1}\ T_i^{n+1} - a_{i+1}^{n+1}\ T_{i+1}^{n+1} = -\ a_{i+1}^{n}\ T_i^{n} + a_{i+1}^{n}\ T_{i+1}^{n} \quad .$$

Assuming uniform initial temperature distribution, which is acceptable for general building simulation packages, gives $T_i^{n+1} = T_{i+1}^{n+1}$. This is usually acceptable, but does not include all possible adiabatic cases as not all adiabatic boundaries have uniform temperature near it. In other words, massless nodes will increase computation time without any advantage for adiabatic boundaries.

The start up period for the ground is usually very long and can be equal to several years as was demonstrated by Jones (1994). Beside that, it is dependent on the defined boundary conditions. Therefore, numerical investigation is usually required to determine the start up period for the domain. However, this is expected to be time consuming by it self. Therefore, an approximate analytical method is used to determine the time constant of the ground assuming 1-dimensional heat flow from the deepest point to the surface. The time constant τ is defined as the product of the thermal resistance and thermal capacitance

$$\tau = (R / A) (\rho c_p V)$$

where R is the maximum 1-dimensional total resistance from the bottom of the domain to its upper surface. In order to reduce the computation time, temperatures from previous runs can be used for initialisation. In addition, within the ground-only start up period, all multi-dimensional zones are temporarily set to their equivalent 1-dimensional models.

The 3-dimensional ground matrix is constructed and solved with the same multi-dimensional zone routines. The supported implicitness degree is from 0.1 to 1.0 inclusive. However for 3-dimensional ground modelling, an explicit ($\gamma = 0$) scheme can be used for some cases as the thermal diffusivity for the ground is small, thermal storage is very high and the space steps are usually relatively large (i.e. low temperature variation). This combination produces a low Fourier number which is required by the stability limits. In addition, no control actuator is expected to be located in the ground. Therefore, the solver can be very compact and easy to develop. However, this was not done because the stability limits for 3-dimensional modelling is lower than that for 1-dimensional modelling, and the stability limits for boundary conditions higher than the first kind are not known and may be problem dependent. In addition, using unstructured meshes will increase the uncertainty of stability limits.

The 3-dimensional ground model can be linked to 1- and multi-dimensional zones. This should be done from both sides. That is a 3-dimensional ground should be linked to 1- and/or multi-dimensional zones via its associated 3-dimensional files, and vice versa (refer to Chapter 7).

3.4 Solution method

The integration of multi-dimensional conduction modelling into ESP-r is shown in Figure 3.20. The multi-dimensional conduction modelling is divided into two parts: gridding, and system matrix construction/solution. The segregation of multi-dimensional modelling into two parts allows other packages to be employed for the gridding process. This usually requires a small adaptor routine which can provide the multi-dimensional files with the required format.

The gridding module creates four files: control volumes, connections, node coordinates, and node temperatures. The control volumes file saves the associated node number, volume, the multiple of density and heat capacity, and two miscellaneous data items defining the associated component as shown in Table 3.2. More than one control volume can be assigned to a single node. The connections file contains the node number, perpendicular distance (only for inter-constructional connection), connection area, thermal conductivity, connection type, and two miscellaneous data associated with the connection type as shown in Table 3.3. The nodes coordinates file contains the global 3-dimensional cartesian coordinates of nodes. And the nodes temperature file contain the initial node temperatures and plant flux.

Table 3.2 Control volume location.

misc. data (1)	misc. data (2)	Description
IS > 0	IN	within surface IS, and associated with 1-D node IN.
-2	IEG	within edge IEG.
-3	ICR	within corner ICR.
-4	ISS	within surface-surface connection surface ISS.
-5	ISE	within surface-edge connection surface ISE.
-6	IEE	within edge-edge connection surface IEE.
-7	IEC	within edge-corner connection surface IEC.

While the first three files are static, the nodes temperature file saves the latest present and future values. On the other hand, all the files are used by the Simulator except the nodes coordinates file which is created for future adoption in 4-dimensional (temperature and 3 space coordinates) graphical tools for 3-dimensional result analysis. The current version of the Simulator fills the 1-dimensional variables based on volume weighting.

All the 3-dimensional files are binary files. An ASCII version of the 3-dimensional files can be created via the support facilities of the multi-dimensional gridding scheme. Similarly, binary versions can be created from the ASCII ones. This allows the creation or modification of the 3-dimensional

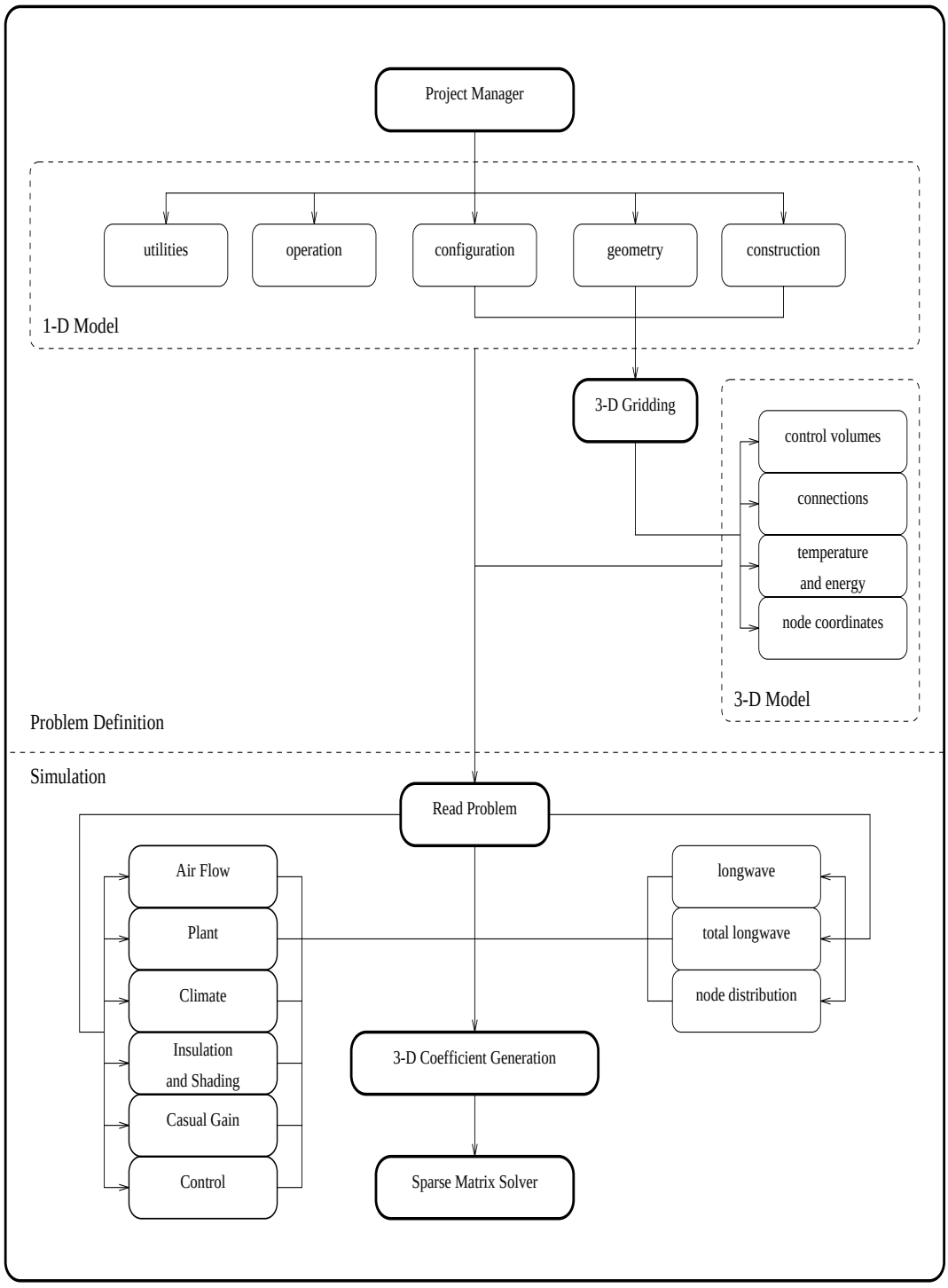

Figure 3.20 Integration of multi-dimensional conduction modelling into ESP-r.

files directly by the user. For example, a heat pipe can be simply modelled by defining a new connection between the required two nodes.

Table 3.3 Thermal connection type.

type	misc. data (1)	misc. data (2)	Description
11	IZ	IN	connection with another 3-D node IN in zone IZ.
21	IZ	IS	convective and radiative boundary similar to exterior boundary for surface IS in zone IZ.
22	IZ	IS	convective only boundary similar to exterior boundary for surface IS in zone IZ.
31	IZ	IS	convective and radiative boundary similar to interior boundary for surface IS in zone IZ.
32	IZ	IS	convective only boundary similar to interior boundary for surface IS in zone IZ.
IT > 100	IS	IN	connection with 1-D node IN of surface IS in zone number (IT-100).

The developed multi-dimensional conduction modelling scheme is based on the control volume technique which is established according to the energy conservation law. For building energy simulation the energy conservation law should be combined with the Fourier law of heat conduction in solids, the Newton law for convection between the internal and external air and the wall, and the Stefan-Boltzmann law for heat exchange by radiation between wall surfaces and the surrounding surfaces. In addition, several heat generation (source and sink) modes such as plant interaction and radiation absorption should be coupled.

Accordingly, in order to allow multi-dimensional conduction modelling, the other inter-related processes should also be modified to provide the proper boundary conditions. For example, in ESP-r, internal longwave radiation is estimated by

$$(q_r)^n_{2\to1} = \frac{\varepsilon_1\ \varepsilon_2\ \sigma\ (\ A_2\ f_{2\to1}\ (T_2^n)^4 - A_1\ f_{1\to2}\ (T_1^n)^4\ )}{1-(\ 1-\varepsilon_1\ )\ (\ 1-\varepsilon_2\ )\ f_{1\to2}\ f_{2\to1}} +$$

$$\sum_{i=1}^{N} \frac{\varepsilon_1\ \varepsilon_2\ (\ 1-\varepsilon_i\ )\ \sigma\ A_2\ f_{2\to i}\ f_{i\to1}\ (T_2^n)^4}{1-(\ 1-\varepsilon_1\ )\ (\ 1-\varepsilon_2\ )\ (\ 1-\varepsilon_i\ )\ f_{1\to2}\ f_{2\to i}\ f_{i\to1}} -$$

$$\sum_{i=1}^{N} \frac{\varepsilon_1\ \varepsilon_2\ (\ 1-\varepsilon_i\ )\ \sigma\ A_1\ f_{1\to i}\ f_{i\to2}\ (T_1^n)^4}{1-(\ 1-\varepsilon_1\ )\ (\ 1-\varepsilon_2\ )\ (\ 1-\varepsilon_i\ )\ f_{2\to1}\ f_{1\to i}\ f_{i\to2}}$$

where $f_{1\to2}$ is the geometric view factor between surface nodes 1 and 2, and N is the total number of internal surface nodes. Therefore, internal longwave radiation terms are based on the area of associated control volume surfaces. For 1-dimensional conduction modelling, the area of an internal surface nodes is equal to the area of the construction it represents, as the number of internal surface nodes per construction is one. However, for multi-dimensional modelling , an internal surface is expected to be represented by more than one node. In order to maintain the size of the executable code, the internal longwave data is saved in two files. One contains the newest future values for longwave radiation between each two internal surface nodes, the other contains the newest present and future total energy gained by internal longwave for each internal surface node. These files are temporary files which are removed at the end of the simulation.

Accordingly, the current version of the gridding module supports two levels of boundary nodes modelling. In the first level, all boundary nodes have convective and radiative boundary conditions. In the second level, only the surfaces boundary nodes have radiative and convective boundary conditions, while the other boundary nodes have convective only boundary conditions. This allows control of the accuracy and speed of a simulation. For example, some internal boundary nodes can be created due to differences in the co-planner surfaces thicknesses and/or indentations. If these nodes are defined as convective and radiative (i.e. the first level), not only will the longwave calculations be expanded but also the system matrix solution process will be much slower since more coefficients are considered.

On the other hand, another temporary file created by the multi-dimensional conduction modelling scheme is the node distribution file. This file is used to fill up the associated 1-dimensional variables for a multi-dimensional simulation. The 1-dimensional variable value is estimated by volume weighting (or surface weighting for massless nodes) its associated multi-dimensional nodes. This process links the 1-dimensional scheme with the multi-dimensional scheme.

In general, a zone matrix consists of four type of coefficients (refer to Appendix A):

- one future self coupling coefficient for each node.
- one future cross coupling coefficient for each connection. This can be for conduction, convection or internal longwave radiation.
- one future source coefficient for each node.
- one coefficient for present and known coefficients. This includes also the present source coefficient.

Based on the above system matrix coefficients category, an adaptive matrix construction scheme was developed. At each time step, all the matrix coefficients are set to zero. Then, based on the available connections, some coefficients are estimated partially or fully. For example, the future cross coupling coefficient is usually calculated fully for each connection. However, the same connection will

add a term to the present and future self coupling coefficients. After scanning the connection file, the control volume file is read and accordingly the heat storage term of the self coupling coefficients are defined. The future source term coefficients are created based on the control actuator location(s).

A zone matrix arising for building energy simulation is very sparse §, as the average number of connections per node to the total number of nodes is very small. Accordingly, an adaptive scheme should be provided with a sparse storage method. There are mainly two types of sparse storages: static and dynamic. In a static storage method, the storage space is fixed and at least should be able to include all non-zero and fill-in elements. However, in a dynamic storage method, the storage space changes as the number of non-zero elements changes. In fact, in some dynamic methods the spaces which become available due to the elimination process are used to store new fill-in elements. The dynamic method was selected as the number of fill-ins is related to the simulation degree (i.e. number of coefficients per node).

Sparse matrices can be stored in linked or unlinked lists. The unlinked list technique requires less storage capacity than the linked list technique. However, the fill-in elements created during the matrix solution steps can be introduced only by relocating the complete storage list. Based on numerical investigation, the linked list technique was preferred. This is mainly because the expected number of fill-ins (storage list relocation), for a typical multi-dimensional problem, is relatively high.

The total storage required by the employed linked list consists of two parts: beginning of row address (BR), and storage for items (IS). BR requires n (number of rows or nodes)storage locations. However, IS requires 3 E (E: number of nonzero elements; and 3: value of element, column index, and address for the next element) storage locations. One more storage location is required for the index of the first available location.

On the other hand, in attempting to find the most suitable system matrix solution method, a theoretical study was performed. There are two main methods for the simultaneous solution of linear equations: direct and iterative. Although iterative methods preserve the sparseness of the matrix and produce less accumulative round off errors§, direct methods are preferred for building energy simulation because:

- the number of solution operations in the direct solution methods is known, whereas, in iterative methods it is dependent on the ratio of storage properties to transport property values (i.e. the degree of diagonal dominance). That is, the solution time will be dependent on the problem simulated.
- the self coupling coefficient, in the massless nodes equations, is not greater than the summation of the cross coupling coefficients. This will slow down the convergence.

§ A sparse matrix is a matrix which has only a small percentage of non-zero elements.

§ For iterative solution method, unlinked (ordered) list static storage technique is recommended.

- the complete set of operations associated with the control algorithm should be included in the iteration loop, whereas, in direct methods they can usually be called once after the forward elimination process.
- the employment of some control equations, which are not continuous, may cause convergence instabilities or divergence of the solution.
- the convergence speed of the system matrix is strongly dependent on the number of coefficients per node. This means that internal surface nodes, which may have more than one hundred coefficients, will slow down the convergence.

The Gaussian elimination method (Smith, 1985) is used for the solution of the systems of linear equations as it is one of the best known direct methods for that purpose. When sparse storage techniques are used, the coding can become more complicated. The coding employed is adaptive for the dynamic and linked storage technique used. For example, each time an element is called from the storage its previous item index is also determined. This is required for the elimination of that element as the previous item should be linked to the item the eliminated element was linked to. Furthermore, the core calculations in the solution process are performed with double precision arithmetic as there is a high potential for rounding off errors. This is because the magnitudes of the elements of the system matrix are expected to vary greatly in size.

In an attempt to reduce computation time, the Simulator can perform node number reordering and the control algorithm is implemented within the matrix solution process (Clarke, 1985). The node number reordering option numbers the nodes based on the number of their coefficients in the matrix (number of connections). Accordingly, all 3-dimensional files are updated if this option was invoked by the user. On the other hand, the implementation of control algorithm within the matrix solution process is done by preserving the coefficients in the column number equal to the actuator location node number. This will ensure that the modified future source coefficient for that node is available at the end of the forward reduction process. At that stage, the air node (maximum node number) equation should contain a maximum of three terms (for the one actuator point case): the future self coupling term, the future source term, and the known term which may equal zero. This equation, which contains two unknowns, is solved simultaneously with the control equation(s) which has the same two unknowns. Accordingly, the air node (or sensor node) temperature and actuator node energy are calculated. After that, the backward substitution is performed in order to determine the future temperature for the remaining nodes. The current structure of the solution routine facilitates future developments of the multi-actuator control algorithms.

The system matrix is usually diagonally dominant. For such matrices, pivoting is not required (Smith, 1985). However, the selection of a pivot element is modified in order to allow flexibility in the actuator location. That is, the pivot element is the one with maximum magnitude (usually the diagonal) unless its column number is associated with an actuator location.

On the other hand, pivoting can be used to reduce the fill-ins which will reduce the storage space and computation time. This itself can be time consuming. Therefore, another technique is used in the multi-dimensional module for reducing the fill-ins. It is based on renumbering the problem nodes in such away that nodes with fewer coefficients are assigned lower numbers. The number of coefficients per node can be determined by scanning the connection file. This process is performed once at the initialisation stage. If node re-numbering is performed, the associated multi-dimensional files are rearranged to cope with it.

3.5 Conclusions

Due to the complexity of the building domain, the stability error is expected not to be uniform throughout the domain. This can be dealt with by employing different implicitness degrees. However, this will produce an unconservative numerical model. For example, the air node, whose equation has a fixed implicitness degree, will be connected to inside surface node with different implicitness degrees. Hence, the heat flow terms in the air node characteristic equation are not similar to their equivalent terms in the surfaces node equations.

When detailed simulations of whole building performance is required, it is sometimes necessary to take 2- and 3-dimensional effects into account. The method, and limitations, adopted in two recent international projects has been outlined. An attempt has now been made to provide a more fundamental treatment of 3-dimensional conduction within the dynamic thermal simulation program ESP-r. Results from some validation exercises applied to the new code show that 3-dimensional conduction can now be successfully applied, although further improvements in solution speed (or computing power) and ease of problem specification is required before it can be routinely applied.

Although a coarse ground discretised numerical model may not accurately represent the dynamic thermal behaviour of the ground, it can be used to improve the prediction of heat flow through building ground slabs. This model is more flexible and generic than other analytical and empirical based models. However, it requires a very long start up period which is due to the nature of the outside temperature. The outside temperature can be approximated by two sinusoidal equation: daily and yearly. The daily oscillations damp out faster than the yearly and so the effect of the yearly oscillation affects deeper locations than the daily one. In order to account for the yearly fluctuation in the outside temperature, the start up period should be measured in years. This can be overcome by using temperature distributions from previous simulations. In this case the start up period should be set according to daily temperature fluctuations. This depends on the number of days between the last run’s end date and the current run’s start date.

References

Aasem, E O1993. , *Personal communication*.

Alvarez, S., J.L. Molina, and J.M. Cejudo 1993. ‘‘Numerical solution of transient 1-D heat conduction equation: Analysis of the C.E.N. method and ways for improvement,’’ PASCOOL Programme, Model Validation Subgroup.

Arnone, A and A Sestini 1991. ‘‘Multi-grid heat transfer calculations using different iterative schemes,’’ *Numerical Heat Transfer. Part B*, vol. 19, pp. 1-11.

Bickley and Thompson1964. , *Matrices, Their Meaning and Manipulation*, London.

Claesson, J and C Hagentoft 1991. ‘‘Heat Loss to the Ground from a Building - I: General Theory,’’ *Building and Environment*, vol. 26, no. 2, pp. 195-208, Pergamon Press, UK.

Crandall, S. H. 1955. ‘‘An Optimum Implicit Recurrence Formula for the Heat Conduction Equation,’’ *Quarterly of Applied Mathematics*, vol. 13, pp. 318-320.

Davies, M, A Tindale, and J Littler 1994. ‘‘The Addition of a 3-D Heat Flow Module to APACHE,’’ *Building Environmental Performance: Facing the Future*, pp. 21-26, York.

Fletcher, C A J 1988. *Computational Techniques for Fluid Dynamics. Volume I and II*, Springer-Verlag.

Frey, W. 1977. ‘‘Flexible finite difference stencils from isoparametric finite element,’’ *international journal for numerical methods in engineering*, vol. 11.

Hensen, J.L.M. and A.E. Nakhi 1994. ‘‘Fourier and Biot Numbers and the Accuracy of Conduction Modelling,’’ in *Proceedings of Building Environmental Performance*, pp. 247-256.

Holman, J P 1989. *Heat Transfer*, McGraw-Hill Book Company.

Jones, P J 1994. ‘‘Thermal Performance of Solid Ground Floor Slabs,’’ *Building Environmental Performance: Facing the Future*, pp. 27-34, York.

MacNeal, R. 1953. ‘‘An asymmetrical finite difference network,’’ *quarterly of applied mathematics*, vol. 11, no. 3, pp. 295-310.

Myers, G E 1971. in *Analytical Methods in Conduction Heat Transfer*, McGraw-Hill Book Company, USA.

Ozisik, M.N. 1993. *Heat Conduction*, John Wiley, USA.

Smith, G. D. 1985. *Numerical Solution of Partial Differential Equations: Finite Difference Methods*, Clarendon Press, Oxford.

Thomas, H R and R M Lloyd 1994. ‘‘The Thermal Performance of an Uninsulated Ground Floor Slab in A Real, occupied Building - A Long Term Monitoring Programme.,’’ *Building Environmental*

Performance: Facing the Future, pp. 35-41, York.

Thompson, J A, Z U A Warsi, and C W Mastin 1985. *Numerical Grid Generation Foundations and Applications*, North-Holland.

Walton, G N 1987. ‘‘Estimating 3-D heat loss from rectangular basement and slabs using 2-D calculations,’’ *ASHRAE Transactions*, vol. 93, no. 1.

Waters, J. R. and A. J. Wright 1985. ‘‘Criteria for the Distribution of Nodes in Multilayer Wall in Finite-difference Thermal Modelling,’’ *Building and Environment*, vol. 20, no. 3, pp. 151-162.

CHAPTER 4

Variable Thermophysical Properties

In this chapter the development of a scheme for simulation variable thermophysical properties is presented. The mathematical approach for heat conduction with variable transport and storage properties is shown first. After that, the problem is described in by numerical formulation. The implementation of the numerical model in an environmental building performance program is discussed and the employed solution method is presented. Finally, conclusions are given.

4.1 Mathematical model

The governing equation of heat conduction for a stationary homogeneous isotropic solid with constant thermophysical properties is given by equation (2.8). If the thermophysical properties are functions of space only, equation (2.8) becomes a linear differential equation with variable coefficients. However, equation (2.8) becomes nonlinear if one or more of the thermophysical properties is dependent on temperature. For variable thermophysical properties equation (2.7) becomes

$$\frac{\partial}{\partial t}\,\rho\,(\,T\,)\,\mathbf{h}\,(\,T\,) = \nabla\,.\,[\,\lambda\,(\,T\,)\,\nabla T(\vec{r},t)\,] + g(\vec{r},t) \tag{4.1a}$$

when $\partial\rho/\partial t \approx 0$, equation (4.1a) becomes

$$\rho\,(\,T\,)\,c_p\,(\,T\,)\,\frac{\partial T(\vec{r},t)}{\partial t} = \nabla\,.\,[\,\lambda\,(\,T\,)\,\nabla T(\vec{r},t)\,] + g(\vec{r},t) \tag{4.1b}$$

where,

$$\frac{\partial \mathbf{h}}{\partial t} = \frac{\partial \mathbf{h}}{\partial T}\,\frac{\partial T}{\partial t} = c_p\,(\,T\,)\,\frac{\partial T}{\partial t}$$

While the superposition principles of linear theory of mathematics can be used to solve a linear heat conduction problem, no general theory exists for the solution of nonlinear heat conduction problems. The analytical solution of such problems are usually not possible, or are complicated. For the cases which do have analytical solutions, these solutions are commonly based on approximated

methods and applicable only to the specific case.

For the nonlinear problem defined by equation (4.1b), a Kirchhoff transformation (Ozisik, 1980) can be used to remove the thermal conductivity, λ, outside the differential operator by defining a new dependent variable, Γ, which is defined by

$$\Gamma = \int_{T_r}^{T} \frac{\lambda\,(T)}{\lambda_r}\, dT \tag{4.2}$$

Where T_r is the reference temperature and λ_r is the value of thermal conductivity at the reference temperature. Accordingly, equation (4.2) can be rearranged as

$$\rho(T)\, c_p(T)\, \frac{\partial T}{\partial \Gamma}\, \frac{\partial \Gamma}{\partial t} = \nabla \cdot \left[\lambda(T)\, \frac{\partial T}{\partial \Gamma}\, \nabla \Gamma \right] + g(\vec{r}, t) \tag{4.3a}$$

or

$$\frac{1}{\alpha(T)}\, \frac{\partial \Gamma(\vec{r}, t)}{\partial t} = \nabla^2 \Gamma(\vec{r}, t) + \frac{1}{\lambda_r}\, g(\vec{r}, t) \tag{4.3b}$$

Where,

$$\frac{\partial T}{\partial \Gamma} = \frac{\lambda_r}{\lambda(T)}$$

$$\alpha\,(T) = \frac{\lambda\,(T)}{\rho\,(T)\, c_p\,(T)}$$

Although equation (4.3) is nonlinear, it is in a more suitable form for analytical analysis than equation (4.1). Equation (4.3) becomes linear if the changes in $\alpha\,(T)$ is assumed constant. This is a function of the combined effect of the thermophysical properties' temperature dependences. For many solids, the temperature dependence of thermal diffusivity can be ignored compared to that of thermal conductivity. In order to show how the Kirchhoff transformation can be used to solve a heat conduction problem defined by equation (4.3), the boundary and initial conditions, and the temperature dependence of the thermophysical properties must be defined. Assuming a 1D conduction through a slab ($0 \le x \le d$) whose boundaries and initial conditions are defined by

$$\frac{\partial T}{\partial x} = 0 \quad , \qquad x = 0, \quad t > 0$$

$$T = T_d \quad , \qquad x = d, \quad t > 0$$

$$T = T_o \quad , \qquad 0 \le x \le d, \quad t = 0$$

In order to simplify the analytical solution, linear temperature dependence for thermal conductivity is assumed defined by

$$\lambda\ (\ T\ ) = \lambda_r\ (\ 1 + a\ T\ )$$

The boundary conditions can be transformed by Kirchhoff transformation:

$$\frac{\partial \Gamma}{\partial x} = 0\ ,\qquad x = 0 \tag{4.3c}$$

Where,

$$\frac{\partial T}{\partial x} = \frac{\partial T}{\partial \Gamma}\ \frac{\partial \Gamma}{\partial x} = \frac{\lambda_r}{\lambda\ (\ T\ )}\ \frac{\partial \Gamma}{\partial x}$$

And,

$$\Gamma = \Gamma_d\ ,\qquad x = d,\quad t > 0 \tag{4.3d}$$

Where,

$$\Gamma_d = \int_{T_r}^{T_d} \frac{\lambda\ (\ T\ )}{\lambda_r}\ dT = \int_{T_r}^{T_d} (\ 1 + a\ T\ )\ dT = (\ T_d - T_r\ ) + \frac{a}{2}\ (\ T_d^2 - T_r^2\ ) \tag{4.3e}$$

The analytical solution will be much simplified if the reference temperature, T_r, and the boundary temperature at x=d, T_d, are assumed to be zero. Accordingly, equation (4.3d) reduces to

$$\Gamma = 0\ ,\qquad x = d,\quad t > 0 \tag{4.3f}$$

Clearly, the boundary condition kinds did not change by the Kirchhoff transformation. This is the case for all boundary conditions of the first and second kind (refer to Chapter 2). However, the Kirchhoff transformation of the third kind boundary condition is usually not possible except under certain constraints on the convective heat transfer coefficient (Ozisik, 1980). Problems involving such boundary conditions are usually solved numerically (Kakac and Yener, 1993). The initial condition is transformed by Kirchhoff transformation to

$$\Gamma = T_o + \frac{a\ T_o^2}{2} = \Gamma_o\ ,\qquad 0 \le x \le d,\quad t = 0 \tag{4.3g}$$

Equation (4.3) is linear as $\alpha\ (\ T\ )$ is assumed to be constant. Thus, the superposition principles of linear theory of mathematics can be used to solve it. The solution procedure is shown in the Appendix B. The solution is given by

$$\Gamma(x,t) = \frac{2\,\Gamma_o}{d} \sum_{m=1}^{\infty} \frac{e^{-\alpha\,\omega_m^2\,t}\,\cos(\omega_m\,x)\,\sin(\omega_m\,d)}{\omega_m} \tag{4.4}$$

Where ω_m are the roots of the following equation

$$\cos(\omega_m\,d) = 0$$

or

$$\omega_m = \frac{(2m-1)\,\pi}{2\,d}$$

Knowing the Γ distribution from equation (4.4), the temperature distribution can be determined from equation (4.3e) as T is the physically acceptable roots for equation (4.3e). Substituting the value of the reference temperature into equation (4.3e), Γ reduces to

$$\Gamma = T + \frac{a}{2}\,T^2 \tag{4.5a}$$

or,

$$\frac{a}{2}\,T^2 + T - \Gamma = 0 \tag{4.5b}$$

For which the physically acceptable root (T and Γ have the same sign) is

$$T(x,t) = \frac{-1 + \sqrt{1 + 2\,a\,\Gamma(x,t)}}{a} \tag{4.6}$$

In reality, heat conduction is more complicated than described here (refer to Chapter 2). For example some building materials are isotropic. In addition, the thermal contact resistance should be considered for multi-layered constructions. While these two parameters are analytically and experimentally complex, their numerical implementation is simple. However, they were not adopted in ESP-r due to lack of associated data, and extensive storage requirements.

4.2 Numerical model

For variable thermophysical properties, equation (2.12) becomes

$$\rho(\bar{T})\,c_p(\bar{T})\,V(\bar{T})\,\frac{\partial \bar{T}}{\partial t} = -\sum_{s=1}^{N} A_s\,\vec{q}_s\,.\,\vec{n}_s + V(\bar{T})\,\bar{g} \tag{4.7}$$

where $\bar{T}$ and $\bar{g}$ are the average temperature and heat generation rate over the control volume respectively. In finite difference approximation, $\bar{T}$ is equal to a node temperature. For a domain with conduction only heat transfer, equation (4.7) becomes

$$\rho\,(\,\bar{T}\,)\,c_p\,(\,\bar{T}\,)\,V\,(\,\bar{T}\,)\,\frac{\partial \bar{T}}{\partial t} = -\,\lambda_s\,(\,T\,)\,\frac{\partial T}{\partial n_s} + V\,(\,\bar{T}\,)\,\bar{g} \tag{4.8}$$

where $\vec{n}_s$ is the outward drawn normal unit vector and ($\partial/\partial n_s$) is the derivative along the $\vec{n}_s$ direction.

It should be noted that the derivative of temperature with respect to space ($\partial/\partial n_s$) is at the control volume surface. However, in finite difference representation that derivative is replaced by a numerical derivative of temperature between grid points. This effect is more obvious for transient conduction than the steady state. The effect of this approximation vanishes as the actual temperature contour between grid points approaches linear profile.

By employing the two point finite difference formulae, equation (4.8) becomes

$$a_i^{n+1}\,T_i^{n+1} + \sum_j a_j^{n+1}\,T_j^{n+1} - \gamma\,G_i^{n+1}\,\Delta t = a_i^n\,T_i^n + \sum_j a_j^n\,T_j^n - (\,1-\gamma\,)\,G_i^n\,\Delta t \tag{4.9}$$

Where,

$$a_j^{n+1} = \frac{-\,\gamma\,A\,\lambda_{j\to i}^{n+1}\,\Delta t}{\Delta X_{j\to i}}$$

$$a_j^{n} = \frac{(\,1-\gamma\,)\,A\,\lambda_{j\to i}^{n}\,\Delta t}{\Delta X_{j\to i}}$$

$$a_i^k = \rho_o\,c_p\,V - \sum_j a_j^k$$

$$G^k = V\,g^k$$

4.3 Implementation

In order to integrate the variable thermophysical properties scheme in the environmental building performance program ESP-r, equation (4.9) should be written in the ESP-r format. This is achieved by dividing equation (4.9) by the thermal storage term ($\rho_o\,c_p\,V$), which produces

$$a_i^{n+1}\,T_i^{n+1} + \sum_j a_j^{n+1}\,T_j^{n+1} - \frac{\gamma\,g_i^{n+1}\,\Delta t}{\rho_o\,c_p} = a_i^n\,T_i^n + \sum_j a_j^n\,T_j^n - \frac{(\,1-\gamma\,)\,g_i^n\,\Delta t}{\rho_o\,c_p} \tag{4.10}$$

Where,

$$a_j^{n+1} = \frac{-\,\gamma\,A\,\lambda_{j\to i}^{n+1}\,\Delta t}{\Delta X_{j\to i}\,\rho_o\,c_p\,V}$$

$$a_j^{n} = \frac{(\,1-\gamma\,)\,A\,\lambda_{j\to i}^{n}\,\Delta t}{\Delta X_{j\to i}\,\rho_o\,c_p\,V}$$

$$a_i^k = 1.0 - \sum_j a_j^k$$

Variable thermophysical properties simulation requires that the storage and transfer properties values are estimated at each time step. This requires the knowledge of moisture distribution if its dependence is to be considered. This should be an easy task if the moisture discretisation is similar to the heat discretisation. However, this is not the case as shown in Chapter 5. This is due to the expected different dynamic behaviour for moisture transport from that for heat flow. Figure 4.1 shows the discretisation for combined heat and moisture transport. If the moisture content for each moisture grid point is assumed to be constant throughout the control volume, then the moisture content for each heat grid point is equal to the algebraic sum of the moisture contents of the moisture grid points within the heat control volume, with volume weighting used for partially included moisture control volumes. For example, the moisture content for the heat node shown in Figure 4.1 is given by

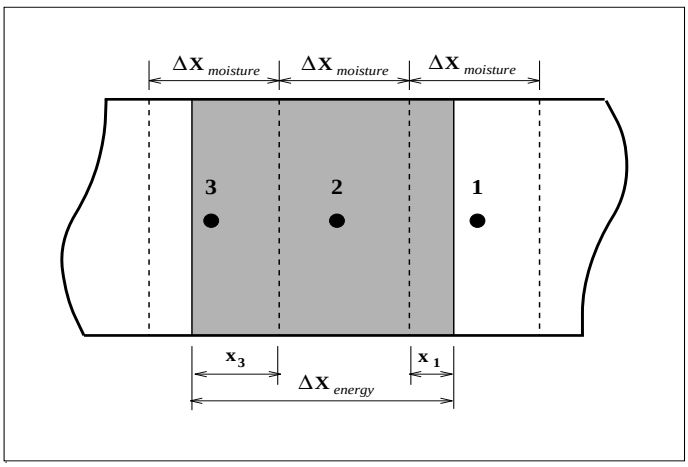

Figure 4.1 Combined moisture and heat discretisation.

$$u = u_1 \frac{x_1}{\Delta X_{moiture}} + u_2 + u_3 \frac{x_3}{\Delta X_{moiture}}$$

In addition to the moisture distribution, the temperature distribution is required for determining the variable properties values. The storage properties can be estimated directly from the grid points temperatures. This is because they are a function of the average control volume temperature which is assumed to be the grid point temperature. However, the value of thermal conductivity is supposed to be determined at the control volume surfaces. To do that, the temperature profile assumption(s) should be used.

The profile assumptions for all thermophysical properties are required. These profiles are required for modelling heat conduction with constant and variable thermophysical properties. Not

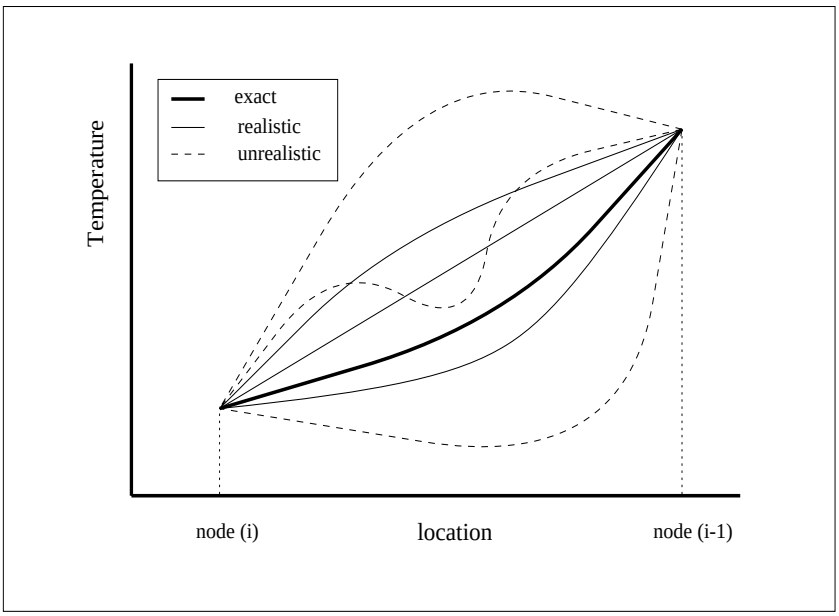

Figure 4.2 Profiles behaviour for heat conduction without heat generation.

only can different profiles be used for different variables, but also for a given variable different profiles can be used to estimate its different terms. The number of profiles can be reduced by assuming similar profile assumptions for all control volumes, and by relating the quantities to the dependent variable (i.e. temperature) profile. For example, instead of defining the profile for each thermophysical property, the temperature profile can be used to define the temperature distribution and thereby the thermophysical properties can be estimated.

The governing principles for adopting a profile are physically realistic behaviour and overall balance. The behaviour of a realistic profile assumption should have a similar qualitative trend as the exact profile. For example, for one dimensional heat conduction without interstitial heat sources or sinks, the temperature profile between each two successive grid points must be within the temperature range bounded by those two grid point's temperatures, with a fixed direction for the temperature slope as shown in Figure 4.2. Overall balance requires that the flux cross any two adjacent control volumes should be represented by the same expression in their associated discretisation equations. However, this does not necessarily mean that the system matrix should be symmetric.

As shown in equation (4.8), for a homogeneous control volume, the density and heat capacity values must be determined based on the average temperature over the control volume. In principle, the temperature at the grid point is assumed to be a good representative for the average temperature. Therefore, for a homogeneous control volume, the values for the density and heat capacity can be determined directly from the temperature of the associated grid point. Whereas, for a heterogeneous

control volume the storage properties can be estimated by dividing it into sub-control volumes of homogeneous storage properties. For 1D heat conduction through building multi-layered constructions, a heterogeneous control volume consists of two materials only. In addition, the adopted space discretisation approach assures positioning a grid point at the interface of these materials (i.e. layers). This allows the control volume to be divided into two homogeneous control volumes as shown in Figure 4.3. Clearly, their grid point temperatures should be equal since the thermal contact resistance is not considered. Here, the disadvantage of this space discretisation approach is exposed as the grid point temperatures are not expected to be the best representation for the average temperatures. Nevertheless, it is usually a good representation for the average temperature if adequate discretisation is employed. The equation for the heterogeneous control volume is established by summing up the equations for the two homogeneous sub-control volumes. That is

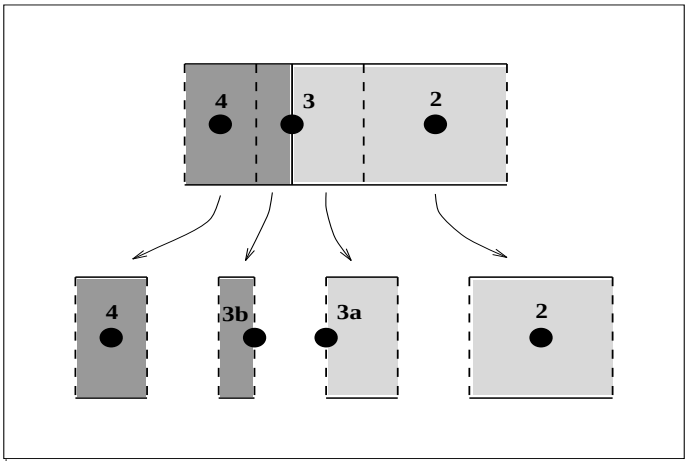

Figure 4.3 Discretisation of heterogeneous control volume.

$$\left[\ \rho_{3a}\ c_{3a}\ V_{3a} + a_2^{n+1} + a_{3b}^{n+1}\ \right] T_{3a}^{n+1} - a_2^{n+1}\ T_2^{n+1} - a_{3b}^{n+1}\ T_{3b}^{n+1} - \gamma\ G_{3a}^{n+1}\ \Delta t =$$

$$\left[\ \rho_{3a}\ c_{3a}\ V_{3a} - a_2^{n} - a_{3b}^{n}\ \right] T_{3a}^{n} + a_2^{n}\ T_2^{n} + a_{3b}^{n}\ T_{3b}^{n} + (\ 1 - \gamma\ )\ G_{3a}^{n}\ \Delta t \qquad (4.11a)$$

$$\left[\ \rho_{3b}\ c_{3b}\ V_{3b} + a_{3a}^{n+1} + a_4^{n+1}\ \right] T_{3b}^{n+1} - a_{3a}^{n+1}\ T_{3a}^{n+1} - a_4^{n+1}\ T_4^{n+1} - \gamma\ G_{3b}^{n+1}\ \Delta t =$$

$$\left[\ \rho_{3b}\ c_{3b}\ V_{3b} - a_{3a}^{n} - a_4^{n}\ \right] T_{3b}^{n} + a_{3a}^{n}\ T_{3a}^{n} + a_4^{n}\ T_4^{n} + (\ 1 - \gamma\ )\ G_{3b}^{n}\ \Delta t \qquad (4.11b)$$

Knowing that $T_{3a} = T_{3b} = T_3$, equations (4.11a) and (4.11b) reduce to

$$\left[\rho_{3a}\, c_{3a}\, V_{3a} + a_2^{n+1} \right] T_3^{n+1} - a_2^{n+1}\, T_2^{n+1} - \gamma\, G_{3a}^{n+1}\, \Delta t =$$

$$\left[\rho_{3a}\, c_{3a}\, V_{3a} - a_2^{n} \right] T_3^{n} + a_2^{n}\, T_2^{n} + (1 - \gamma)\, G_{3a}^{n}\, \Delta t \tag{4.11c}$$

$$\left[\rho_{3b}\, c_{3b}\, V_{3b} + a_4^{n+1} \right] T_3^{n+1} - a_4^{n+1}\, T_4^{n+1} - \gamma\, G_{3b}^{n+1}\, \Delta t =$$

$$\left[\rho_{3b}\, c_{3b}\, V_{3b} - a_4^{n} \right] T_3^{n} + a_4^{n}\, T_4^{n} + (1 - \gamma)\, G_{3b}^{n}\, \Delta t \tag{4.11d}$$

Summing up equations (4.11c) and (4.11d), we get

$$\left[\rho_{3a}\, c_{3a}\, V_{3a} + \rho_{3b}\, c_{3b}\, V_{3b} + a_2^{n+1} + a_4^{n+1} \right] T_3^{n+1} - a_2^{n+1}\, T_2^{n+1} - a_4^{n+1}\, T_4^{n+1} -$$

$$\gamma\, (G_{3a}^{n+1} + G_{3b}^{n+1})\, \Delta t = \left[\rho_{3a}\, c_{3a}\, V_{3a} + \rho_{3b}\, c_{3b}\, V_{3b} - a_2^{n} - a_4^{n} \right] T_3^{n} +$$

$$a_2^{n}\, T_2^{n} + a_4^{n}\, T_4^{n} + (1 - \gamma)\, (G_{3a}^{n} + G_{3b}^{n})\, \Delta t \tag{4.11e}$$

The coefficients for the heterogeneous control volume are defined by comparing equation (3.14) with equation (4.11e). Clearly, the heat storage and generation coefficients are the algebraic sum of the sub-control volumes heat storage and generation coefficients. Therefore, the storage properties for a heterogeneous control volume is equal to the volume weighted average of the storage properties for the homogeneous sub-control volumes. That is

$$\rho\, c_p = \frac{\sum_{i=1}^{m} (\rho_o\, c_p\, V)_i}{\sum_{i=1}^{m} V_i} \tag{4.11f}$$

The thermal conductivity profile assumption is more troublesome than that for the density and heat capacity. For the thermal conductivity (the most straight forward assumption, which maintains the two profile assumption conditions mentioned above) is the linear variation in the space dimension between each two nodes. However, a more practical formulation is the stepwise profile in which the thermal conductivity is assumed to be constant between each two nodes and its magnitude is determined with respect to the algebraic average of these two nodes temperatures. It should be noted here that this formulation is different from the other stepwise profile in which the thermal conductivity value is assumed to be constant over the control volume (i.e. dT/dx is not defined at the control volume faces). The proposed stepwise profile has many advantages over the linear profile, such as:

- The value of the thermal conductivity is determined more directly. After estimating the average of the temperature of the two adjacent nodes, it is substituted in the equations

describing the dependence of the thermal conductivity on temperature. Whereas, in the linear profile case, thermal conductivity should be calculated at both adjacent nodes and then their space averages should be estimated as the interface thermal conductivity value.

- It is easier and faster to adapt polynomial equations of order n (as a function of temperature), to describe the thermal conductivity dependence on temperature in case of a stepwise profile than in the case of a linear profile.
- With the stepwise profile it is easier to include a control logic which decides which equation, if any, should be used to estimate the thermal conductivity value according to the averaged (interface) temperature.

The profile assumption is usually associated with the employed space discretisation. For example, the thermal conductivity profile adopted here is not necessarily acceptable for the second space discretisation practice.

4.4 Solution method

The numerical formulation for the nonlinear heat conduction equation (4.10) is nonlinear. Therefore, direct solution methods are not directly applicable. In addition, convergence instabilities and divergence are expected to occur with iterative solution methods (depending on the nonlinearity type and degree). Linearisation schemes can be used to simplify the iterative solution methods and allow direct solution methods. Several linearisation schemes are available of which the following can be easily applied to existing simulation codes such ESP-r: algebraic linearisation procedures, one time step in arrear, and extrapolation.

The algebraic linearisation procedures are usually used for linearisation of the heat source terms. This is done by transforming the nonlinear source term to an equivalent linear source term defined by

$$g = a + b\,T \tag{4.12}$$

For example, longwave radiation between two surfaces i and j is a function of $(T_i^4 - T_j^4)$. Algebraic linearisation procedures can be used to transform the nonlinear longwave equation to a linear one by using the following expansion formula

$$(T_i^4 - T_j^4) = (T_i - T_j)^{n+1} \left[T_i^3 + T_i^2\, T_j + T_i\, T_j^2 + T_j^3 \right]^n$$

Where the global superscripts n and n+1 denote present and future time-row values respectively. However, a different procedure is implemented in ESP-r for the algebraic linearisation of internal longwave radiation as it is based on three-surface interaction (i.e. indirect longwave radiation is also considered). In ESP-r, the net longwave radiation gained by surface 1 from surface 2 is estimated by

$$(\vec{q}_l)^{n+1}_{2\to1} = (h_r)^n_{2\to1}\ A_1\ (\ T_2^{n+1} - T_1^{n+1}\ )$$

Where, the linearised longwave term, $\vec{q}_l$, is a function of the radiative heat transfer coefficient, h_r, which is defined by

$$(h_r)^n_{2\to1} = \frac{(\vec{q}_l)^n_{2\to1}}{A_1\ (\ T_2^n - T_1^n\ )}$$

Comparing this equation with equation (4.12), it can concluded that coefficient (a) is set to zero. However, if this scheme is used for linearising thermophysical properties the coefficient (b) should always be zero as the thermophysical properties are already multiplied by the temperature (i.e. dependent variable). Thus, instead of linearising the term, it is converted into a constant term.

The one time step in arrear method (Clarke, 1985) is based on estimating the current step present and future values for the thermophysical properties based on the present and future temperature distribution at the previous time step. However, this does not require saving the temperature at three levels if the temperature is updated after determining the coefficients values (i.e. just before calculating the new future values), or by simply equating the current present thermophysical values to the previous future values and estimating the current future thermophysical values based on the current present temperatures. The matrix representation for the one time step in arrear method is

$$\mathbf{A}^n\ \mathbf{T}^{n+1} + \mathbf{B}^n = \mathbf{A}^{n-1}\ \mathbf{T}^n + \mathbf{B}^{n-1} \tag{4.13a}$$

or

$$\mathbf{A}^n\ \mathbf{T}^{n+1} = \mathbf{C} \tag{4.13b}$$

where,

$$\mathbf{C} = \mathbf{A}^{n-1}\ \mathbf{T}^n + \mathbf{B}^{n-1} - \ \mathbf{B}^n$$

Clearly, the set of equations defined by (4.13) are linear as the coefficients matrices, **A**, and the boundary matrices, **B**, are known and constant for each time step.

The extrapolation scheme is based on predicting the future variable values by knowing the variable values history. Three different approaches are presented here. the first method extrapolates the temperature distribution from which the future thermophysical properties are estimated. That is

$$T_i^{n+1} = T_i^n + \left(\frac{dT_i}{dt}\right)^{n-\frac{1}{2}} \Delta t$$

and

$$\left(\frac{dT_i}{dt}\right)^{n-\frac{1}{2}} \approx \frac{T_i^n - T_i^{n-1}}{\Delta t}$$

Therefore,

$$T_i^{n+1} = 2\ T_i^n - T_i^{n-1}$$

In the second scheme, thermophysical properties are extrapolated directly by

$$\Lambda^{n+1} = \Lambda^n + \left(\frac{d\Lambda}{dt}\right)^n \Delta t$$

$$\Lambda^{n+1} = \Lambda^n + \left(\frac{d\Lambda}{dT}\right)^n \left(\frac{dT}{dt}\right)^n \Delta t$$

Assuming

$$\left(\frac{dT}{dt}\right)^n = \left(\frac{dT}{dt}\right)^{n-\frac{1}{2}}$$

$$\Lambda^{n+1} = \Lambda^n + \left(\frac{d\Lambda}{dT}\right)^n \left(\ T^n - T^{n-1}\ \right)$$

And $(d\Lambda/dT)^n$ can be determined analytically. The third scheme is a mixed direct/iterative solution method with only two iterations. In the first iteration the one time step in arrear is adopted for solving the system matrix directly. Then the future temperatures determined from the first iteration are used as the expected future temperature distribution for calculating the future thermophysical properties at the current time step.

The one time step in arrear scheme with possible iteration is used in ESP-r due to its simplicity as no one scheme is expected to give the most accurate prediction for all cases involved in building energy simulation. Even the third extrapolation scheme may give less accurate predictions than that by the one time step in arrear despite the additional coding and CPU effort required. That is because the temperature slope within a building construction may change its sign throughout the simulation as most of the building processes are expected to vary (e.g. climate, plant and occupant).

In ESP-r, the system matrix is generated in two stages: static and dynamic. At the static level the static part (e.g. space steps) of each coefficient are calculated. Usually, this is done only once for each problem regardless of the number of simulations invoked. At the dynamic level the static coefficients are modified to account for the dynamic part (e.g. heat transfer coefficient). In order to maintain that advantage for constant thermophysical properties simulation the correction factor is introduced as the ratio between the actual thermophysical properties and their reference (constant) values. Two correction factors are assigned for each thermophysical property in order to allow mixed explicit/implicit formulations. This factor is calculated at each time step and applied to the dynamic coefficients within the system matrix creation process. For constant thermophysical properties

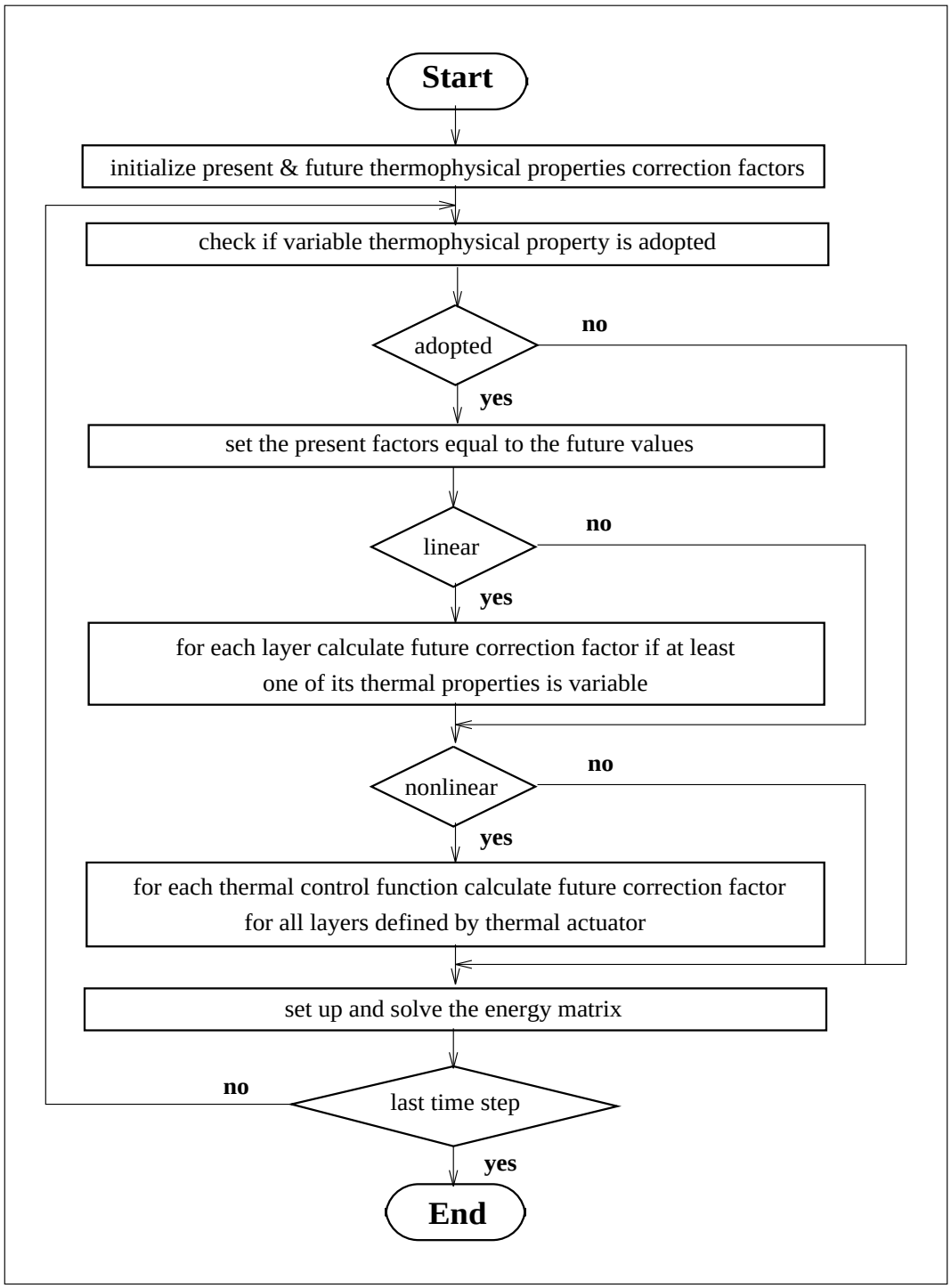

Figure 4.4 Solution method flow chart.

simulation, the correction factors are initialised as one and remain unchanged throughout the simulation. Therefore, there is almost no increase in the CPU due to the integration of the variable thermophysical properties scheme if it is not invoked. The integration of the variable thermophysical

properties scheme into ESP-r is shown in Figure 4.4.

4.5 Conclusion

Heat conduction through porous building materials is a complex physical process. Macroscopically equivalent thermophysical properties are used in order to simplify the microscopically complex thermal process. These properties are expected to vary with temperature and/or moisture content variations. This is because the thermal properties are functions of these variables at the microscopic level, and the equivalent properties represent the compound effect of complex microscopically process which are expected to respond differently to the variables' changes. Therefore, environmental building performance evaluation packages should allow variable thermophysical properties simulation. The default case for a simulation should be variable thermophysical properties. Constant thermophysical properties simulation can be employed when the dependence data are not available, when the impact is known to be very minor for a specific simulation, or when high simulation accuracy is not required.

The impact of adopting variable storage and transport properties and their interaction on the thermal behaviour can be seen from the physical numerical, and mathematical points of view. From the physical viewpoint, changes in thermal conductivity causes changes in the heat flux and accordingly changes in the temperature distribution. This is entirely appropriate for the steady state case with no heat generation. However, for the transient case, greater heat storage require greater changes in flux in order to cause the same dynamic change in temperature distribution. Therefore, for the dynamic case, the impact of varying thermal conductivity is linked with the storage term magnitude. That is, for the same change in thermal conductivity, higher dynamic changes in temperature distribution is expected for the storage term materials than that with larger storage term ones.

From the numerical point of view, the system coefficient matrix equation contains self- and cross-coupling coefficients. Greater cross coupling coefficients are expected to produce greater temperature variation in the time dimension. Greater self coupling coefficients are expected to produce smaller temperature variations in the time dimension. In fact the self coupling coefficient acts as a damper for temperature variations with time. And this is the principle behind the inertia (i.e. false time step) relaxation factor which can be used with iterative solution methods. From equation (4.9) it is clear that the cross coupling coefficient contains the transport property, and the self coupling coefficient contains the storage properties. Therefore, the dynamic temperature distribution is related to the change in thermal diffusivity magnitude.

This can be seen from the mathematical point of view too. The heat conduction equation (4.3b) resulting from applying the Kirchhoff transformation, combines the storage and transport properties into thermal diffusivity. This implies that the changes in the thermal diffusivity is the driving property for changing dynamic temperature distribution and not each thermal property in insolation.

The impact of adopting variable thermophysical properties during building performance evaluation is dependent on the following factors:

- the range of temperature and moisture content (i.e. simulation dependent variables) differences during the required simulation period.
- the type and degree of temperature and moisture content dependences for the thermophysical properties of construction materials.
- the relative change in the magnitude of thermal diffusivity.

Finally, it is clear that simulation of moisture transport within porous building materials is required in order to allow simulation of moisture content dependence for the thermophysical properties. This is considered in the next chapter.

References

Clarke, J. A. 1985. *Energy simulation in building design,* Adam Hilger Ltd, Bristol,UK.

Kakac, S and Y Yener 1993. *Heat Conduction,* Taylor and Francis, USA.

Ozisik, M.N. 1980. *Heat Conduction,* John Wiley, USA.

Ozisik, M.N. 1993. *Heat Conduction,* John Wiley, USA.

Patankar, S V 1980. *Numerical Heat Transfer and Fluid Flow,* Hemisphere Publishing Corporation, USA.

CHAPTER 5

Combined Heat and Moisture Transfer

Chapter 2 presented the fundamental equations for combined heat and moisture transport. These equations are used in this chapter to develop a dynamic 1-dimensional model for combined heat and moisture transport within an environmental building performance program. For the required physical model, the governing equations are developed from those presented in Chapter 2. Then, the numerical representation of the developed mathematical model is shown. After that, the implementation of the numerical model in a building energy simulation program ESP-r is presented. This is followed by a discussion on the adopted solution method. Finally, conclusions are given.

5.1 Mathematical model

Recalling the governing equations for combined heat and moisture transport from Chapter 2, we get

$$\rho_o \frac{\partial u_i}{\partial t} = -\nabla \cdot \vec{J}_i + I_i + s_i \qquad i = 1, 2 \tag{5.1}$$

$$\sum_{i=0}^{2} \left(\rho_i \frac{\partial \mathbf{h}_i}{\partial t} + \mathbf{h}_i \frac{\partial \rho_i}{\partial t} \right) = -\nabla \cdot \vec{q} - \sum_{i=1}^{2} \nabla \cdot \mathbf{h}_i \vec{J}_i + g \tag{5.2}$$

According to Galbraith (1992) and Laan (1994) filtration flow due to total pressure difference between inside and outside boundaries is negligible, except when severe winds occur. Therefore, vapour and liquid transport by the filtration mechanism is not considered. Accordingly, equation (5.1) becomes

$$\rho_o \frac{\partial u_{tot}}{\partial t} = \frac{\partial}{\partial x} \left(\delta_P^T \frac{\partial P}{\partial x} + D_T^P \frac{\partial T}{\partial x} \right) + s \tag{5.3a}$$

where

$$u_{tot} = u_1 + u_2$$

$$-\nabla \cdot \vec{J}_1 - \nabla \cdot \vec{J}_2 = \frac{\partial}{\partial x}\left(\delta_P^T \frac{\partial P}{\partial x} + D_T^P \frac{\partial T}{\partial x} \right)$$

$$\sum_{i=1}^{2} I_i = 0$$

$$s = s_1 + s_2$$

In order to solve the energy governing equation the rate of mass flow and phase conversion of individual phases (i.e. vapour and liquid) should be defined. Because of the unavailability of sufficient data, the enthalpy of diffused moisture is estimated based on vapour specific enthalpy. In addition, heat absorption or dissipation due to moisture phase change is assumed to occur at saturation. It should be noted that these two assumptions are used in the energy equation only. That is liquid flow and capillary condensation are considered in the moisture equation, however their associated enthalpies are approximated by the above assumptions. The validity of these assumptions for building applications is shown in Chapter 7. Accordingly, equation (5.3a) can be rewritten as

$$\rho_o \frac{\partial u_v}{\partial t} + \rho_o \frac{\partial u_l}{\partial t} = \frac{\partial}{\partial x}\left(\delta_P^T \frac{\partial P}{\partial x} + D_T^P \frac{\partial T}{\partial x} \right) + s \qquad (5.3b)$$

Where, u_v is the moisture content with vapour enthalpy and u_l is the moisture content with liquid enthalpy. That is

$$u_v = \begin{cases} u_{tot} & when \quad u_{tot} \le u_{\max} \\ u_{\max} & when \quad u_{tot} > u_{\max} \end{cases}$$

$$u_l = u_{tot} - u_v$$

where

$$u_{\max} = u\ (\ \phi_{\max}\ )$$

In order to reduce the number of dependent variables in equation (5.3b) by one (i.e. cancelling u_v), the moisture storage term should rewritten as

$$\rho_o \frac{\partial u_v}{\partial t} = \rho_o \frac{\partial u_v}{\partial \phi} \frac{\partial \phi}{\partial t} = \rho_o \, \xi \, \frac{\partial (P/P_s)}{\partial t}$$

Therefore, equation (5.3b) becomes

$$\rho_o \, \xi \, \frac{\partial (P/P_s)}{\partial t} + \frac{d \rho_l}{dt} = \frac{\partial}{\partial x}\left(\delta_P^T \frac{\partial P}{\partial x} + D_T^P \frac{\partial T}{\partial x} \right) + s \qquad (5.3c)$$

Similarly, for 1D analysis, the energy equation (5.2) can be rewritten as

$$[\ \rho_o\ (\ c_o + c_v\ u_v\ ) + c_l\ \rho_l\ ]\ \frac{\partial T}{\partial t} + \mathbf{h}_v\ \frac{\partial \rho_v}{\partial t} + \mathbf{h}_l\ \frac{\partial \rho_l}{\partial t} = \frac{\partial}{\partial x}\left(\ \lambda\ \frac{\partial T}{\partial x}\ \right) - \frac{\partial\ \mathbf{h}_s J_v}{\partial x} + g \qquad (5.4)$$

where $\mathbf{h}_s$ is the enthalpy at the source of moisture flux. It is positive if the moisture is entering the control volume, otherwise it is negative. The governing equations for combined heat and moisture transport (equations (5.3c) and (5.4)) contain 3 dependent variables (P, T and ρ_l). Therefore, one more equation is needed to solve these equations. The third equation is the condensation/evaporation control equation. Based on the assumptions mentioned above, the control equation is a function of the saturation pressure only. The control algorithm should be modified to account for capillary condensation on the energy equation.

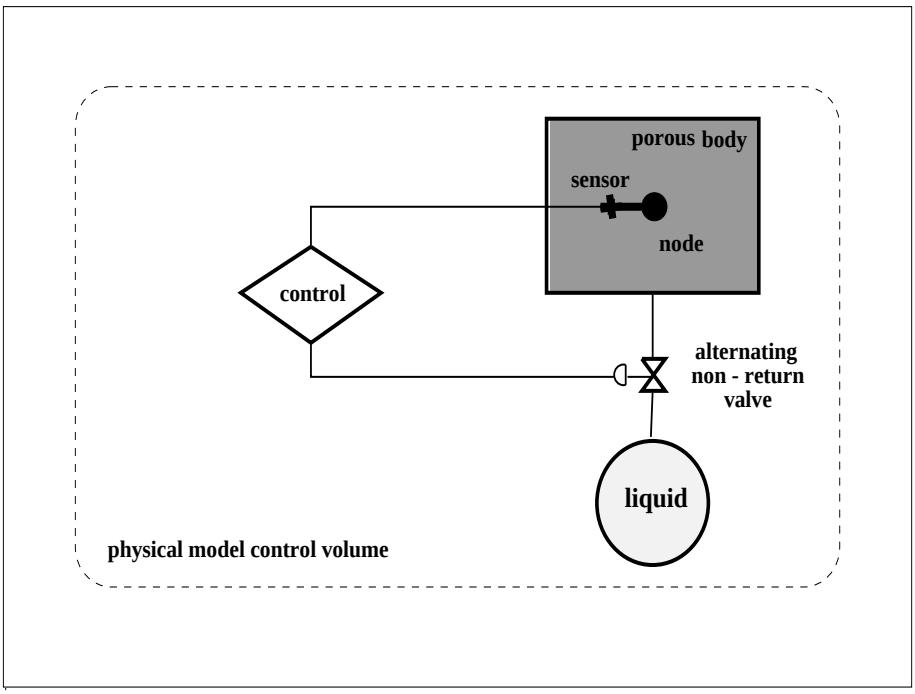

Figure 5.1 Condensation/evaporation control algorithm.

The interaction between the vapour (i.e. moisture with vapour enthalpy) and liquid within a control volume is shown in Figure 5.1. The valve shown is an alternating one way liquid valve. The valve is activated by the controlling device which senses the relative humidity in the control volume. If the relative humidity reaches its maximum value, vapour condensation will start and the valve will only allow the flow of condensed moisture from the solid body to an imaginary liquid tank. When the relative humidity falls below its maximum value the valve will only allow the flow of liquid from the tank to the solid body. This liquid will evaporate as it enters the body. Therefore, this flow will stop

as soon as the maximum relative humidity is reached.

5.2 Numerical model

By applying the two point finite difference formulae to both the moisture and heat equations (5.3c) and (5.4) respectively, the following finite difference approximations are derived

$$a_i^{n+1}\ P_i^{n+1} + \sum_{j=1}^{2} a_j^{n+1}\ P_j^{n+1} + (m_l)_i^{n+1} - \gamma\ \Delta t\ S_i^{n+1} = a_i^n\ P_i^n + \sum_{j=1}^{2} a_j^n\ P_j^n +$$

$$(m_l)_i^n + (\ 1-\gamma\ )\ \Delta t\ S_i^n + \sum_{j=1}^{2} b_j^n\ (\ T_j^n - T_i^n\ ) + \sum_{j=1}^{2} b_j^{n+1}\ (\ T_j^{n+1} - T_i^{n+1}\ ) \qquad (5.5)$$

where,

$$a_j^{n+1} = -\frac{\gamma\ (\ \delta_P^T\ )_{j\to i}^{n+1}\ A\ \Delta t}{\Delta X_{j\to i}}$$

$$a_j^n = \frac{(\ 1-\gamma\ )\ (\ \delta_P^T\ )_{j\to i}^{n}\ A\ \Delta t}{\Delta X_{j\to i}}$$

$$a_i^k = \left[\frac{\rho_o\ \xi_i\ V}{(P_s)_i^k} - a_{i-1}^k - a_{i+1}^k\right]$$

$$b_j^{n+1} = \frac{-\gamma\ (\ D_T^P\ )_{j\to i}^{n+1}\ A\ \Delta t}{\Delta X_{j\to i}}$$

$$b_j^n = \frac{(\ 1-\gamma\ )\ (\ D_T^P\ )_{j\to i}^{n}\ A\ \Delta t}{\Delta X_{j\to i}}$$

$$m_l^k = V\ \rho_l^k \quad (kg_{moisture})$$

$$S_i^k = V\ s_i^k \quad \left(\frac{kg_{moisture}}{sec}\right).$$

and

$$a_i^{n+1}\ T_i^{n+1} + \sum_{j=1}^{2} a_j^{n+1}\ T_j^{n+1} - \gamma\ G_i^{n+1}\ \Delta t - \gamma\ (\ \mathbf{h}_s\ \dot{m}_v\ )^{n+1}\ \Delta t = a_i^n\ T_i^n + \sum_{j=1}^{2} a_j^n\ T_j^n + (\ 1-\gamma\ )\ G_i^n\ \Delta t +$$

$$(\ 1-\gamma\ )\ (\ \mathbf{h}_s\ \dot{m}_v\ )^n\ \Delta t - (\mathbf{h}_l)_i^{n+1}\ [\ (m_l)_i^{n+1} - (m_l)_i^n\ ] - (\mathbf{h}_v)_i^{n+1}\ [\ (m_v)_i^{n+1} - (m_v)_i^n\ ] \qquad (5.6)$$

where,

$$a_j^{n+1} = -\frac{\gamma\ A\ \lambda_{j\to i}^{n+1}\ \Delta t}{\Delta X_{j\to i}}$$

$$a_j^{n} = \frac{(\ 1-\gamma\ )\ A\ \lambda_{j\to i}^{n}\ \Delta t}{\Delta X_{j\to i}}$$

$$a_i^k = \left[\ \rho_o\ V\ (\ c_o + c_v\ u_v\ ) + c_l\ m_l - \sum_{j=1}^{2} a_j^k\ \right]$$

$\dot{m}_v$: *moisture mass flow rate* [kg_v/s]

In equation (5.6), the heat flux term due to moisture transfer, $\mathbf{h}_s\ \dot{m}_v$, is treated as source term. This is because of the difficulties associated with its dependence on the moisture flow direction. If moisture is flowing into the control volume *i* the enthalpy's value is associated with the other node's *j* temperature, while if moisture flow is outward its enthalpy value is dependent on the current node's *i* temperature. This treatment is also required for different heat and moisture gridding as well be shown later.

In order to solve the moisture and heat transfer equations simultaneously and with acceptable accuracy, similar time and space discretisations are not acceptable because of the following

- Based on the units employed, the variable gradient for the heat transfer equation (i.e. temperature gradient) is usually much less than that for the moisture transfer equation (i.e. vapour pressure gradient). This is true in both the time and space dimensions. Therefore, for the same time and space discretisation, the truncation error in the moisture transfer equation will be much higher than that for the heat transfer equation.

- If the same time and space discretisation is employed then the heat transfer Fourier number will be considerably higher than that for moisture transfer. This means that different error propagation (stability error) behaviour will result although an implicitness degrees equal to or greater than 0.5 (e.g. Crank - Nicolson) can be used to ensure stability. The error propagation factors for these two equations will be different. So the accuracy of the whole simulation will be related to the less accurate equation.

- The vapour diffusivity is much less than the thermal diffusivity. Thus, the penetration depth for moisture transport is expected to be smaller than the heat transfer penetration depth. In order to maintain the simulation accuracy within an acceptable range, at least one control volume should be included within the effective penetration depth (refer to Chapter 3). While the effective penetration depth can usually be estimated from the domain's boundary, in building applications this is not always true because the effective penetration depth should be calculated on the basis of the excitation characteristics and location. In building applications several excitation types and locations are possible. Therefore, from the penetration depth point

of view, a finer discretisation is required for moisture transport throughout the domain.

In building simulation a one hour time step is often used. This is usually acceptable from both a numerical accuracy and the weather data availability point of view. In addition, reducing the energy equation time step will significantly increase the CPU time. This is because the energy equation is usually at the core of building simulation packages. Therefore, different space discretisation or gridding should be employed as shown in Figure 5.2. The moisture gridding is finer than that for energy because of the stability and truncation errors as mentioned above. Furthermore, the energy control volume boundaries overlap the moisture control volume boundaries. This is necessary for estimating the amount of energy transferred between adjacent energy control volumes due to moisture transfer. Clearly, if moisture flow is inward the amount of energy convected by moisture flow will be dependent on the first adjacent **moisture** node. Treating this convective energy as a source term simplifies the analysis.

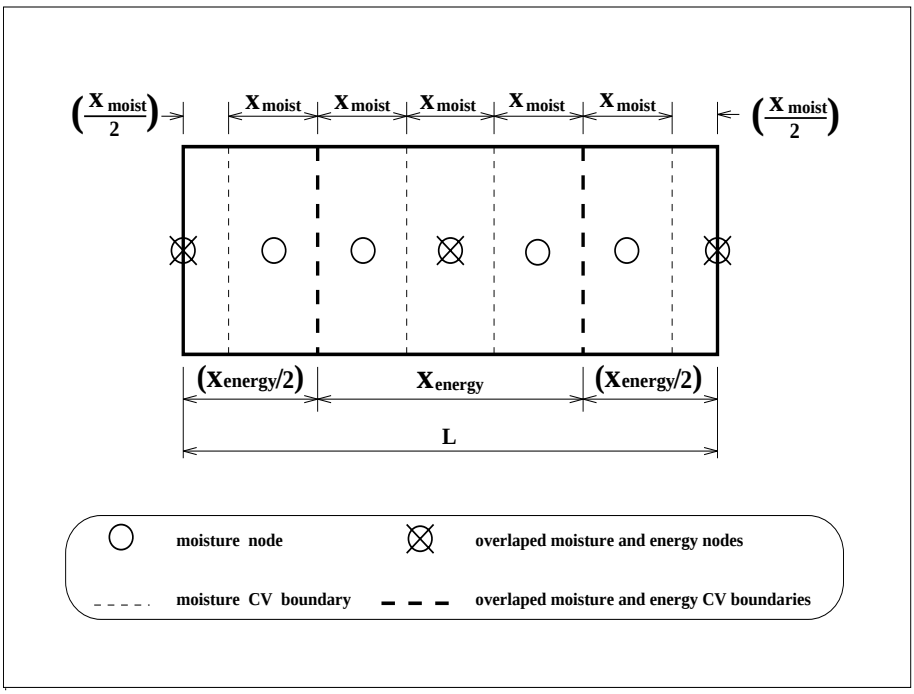

Figure 5.2 Combined moisture and heat domain gridding.

As was mentioned in Chapter 2, space gridding can be performed by two main approaches. In the first, the control volumes are placed before the nodes are positioned at the centres of the control volumes. In the second approach the nodes are placed first then the control volume faces are defined mid-way between the nodes. The main advantage of the first approach is that the node's variable value is a better representation for the control volume variable value. Although, this is not always true for the second approach, this can be overcomed by allowing a variable number of nodes per layer as

the problem mainly occurs at the layer interfaces. On the other hand, for multi-layered constructions, the second approach requires less effort and storage space. Accordingly, the second approach with, variable number of nodes per layer was selected.

5.3 Implementation

The numerical model described above cannot be directly implemented into ESP-r since the format of the energy equation is not compatible with the existing one in ESP-r. Therefore, equation (5.6) is multiplied by the inverse of the thermal storage term $\Theta\ (\ 1\ /\ [\ \rho_i\ V\ (\ c_o + c_v\ u_v\ ) + c_l\ m_l\ ]\ )$ producing

$$a_i^{n+1}\ T_i^{n+1} + \sum_{j=1}^{2} a_j^{n+1}\ T_j^{n+1} - \gamma\ G_i^{n+1}\ \Delta t\ \Theta - \gamma\ (\ \mathbf{h}_s\ \dot{m}_v\ )^{n+1}\ \Delta t\ \Theta = a_i^n\ T_i^n + \sum_{j=1}^{2} a_j^n\ T_j^n + (\ 1-\gamma\ )\ G_i^n\ \Delta t\ \Theta +$$

$$(\ 1-\gamma\ )\ (\ \mathbf{h}_s\ \dot{m}_v\ )^n\ \Delta t\ \Theta - (\mathbf{h}_l)_i^{n+1}\ \Theta\ [\ (m_l)_i^{n+1} - (m_l)_i^n\ ] - (\mathbf{h}_v)_i^{n+1}\ \Theta\ [\ (m_v)_i^{n+1} - (m_v)_i^n\ ] \quad (5.7)$$

where,

$$a_j^{n+1} = -\ \frac{\gamma\ A\ \lambda_{j\to i}^{n+1}\ \Delta t\ \Theta}{\Delta X_{j\to i}}$$

$$a_j^n = \frac{(\ 1-\gamma\ )\ A\ \lambda_{j\to i}^{n}\ \Delta t\ \Theta}{\Delta X_{j\to i}}$$

$$a_i^k = \left[\ 1.0 - \sum_{j=1}^{2} a_j^k\ \right]$$

The flow paths considered within the developed moisture transport model and their interaction with the existing ESP-r models are shown in Figure 5.3. The developed model simulates moisture flow through building constructions. The other flow paths shown in Figure 5.3 are estimated by the existing ESP-r modules and provided as moisture source term to the moisture transport model. On the other hand, the moisture transport model provides the existing ESP-r modules with the indoor moisture content. As shown in Figure 5.3, the developed model accounts for the interaction with plant and equipment, occupants, ventilation and infiltration and inter-zone air flow. Although Figure 5.3 shows the interaction of different models via the air node, it is possible to define other locations (i.e. moisture nodes) for the interaction.

The vapour transport and storage coefficients are available in several forms. For this, the moisture flow coefficients are supplied to the ESP-r simulator with one extra variable for each moisture transfer and storage coefficient for each layer. This additional variable is used to define the specific function to be invoked. However, for each moisture coefficient only one formula is supported within

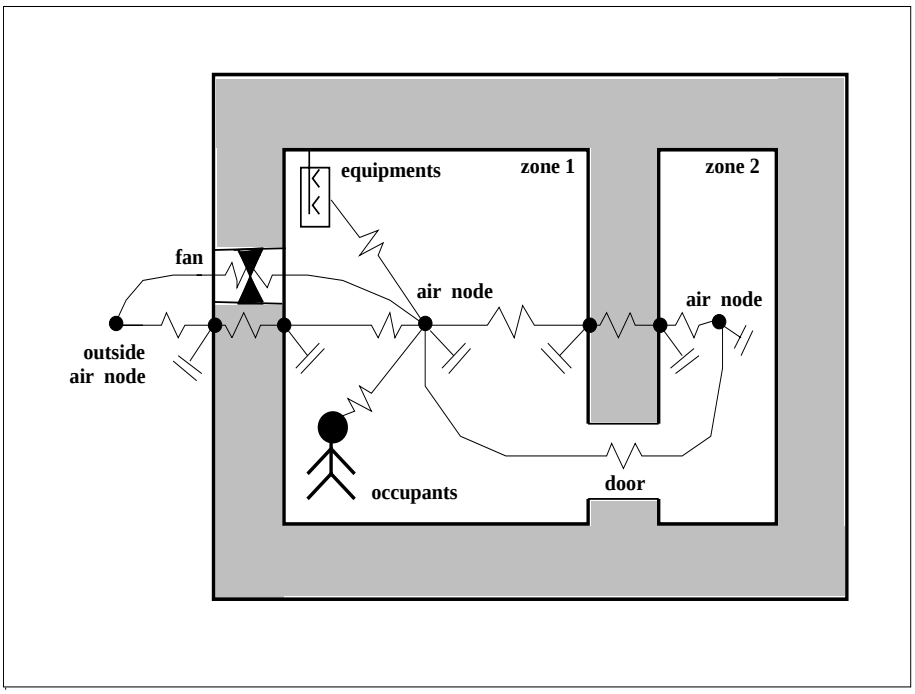

Figure 5.3 Integration of moisture transport model with ESP-r.

the ESP-r simulator. The sorption isotherm (which describes the relationship between relative humidity and equilibrium moisture content) can be described by various formulae such as

$$w = \frac{\phi}{A_1\,\phi^2 + A_2\,\phi + A_3} \qquad 0 \le \phi \le 1 \tag{5.8}$$

$$u = u_h \left(1.0 - \frac{\ln \phi}{A} \right)^{-\frac{1.0}{n}} \qquad 0 \le \phi \le 1 \tag{5.9}$$

Equation (5.8) is provided by the IEA Annex XIV catalogue of material properties (1991) and is called the BET-function. The moisture content, w, is expressed as mass per unit volume. Equation (5.9) is provided by Hansen (1986) through his catalogue of sorption isotherms which covers a wide range of building materials. In addition, the measured adsorption and desorption data are presented in graphical, tabular and curve fitted forms. Furthermore, Hansen's formula was introduced in the upgraded version of the IEA Annex 14 catalogue of material properties (1994). Accordingly, the second function was employed in ESP-r. Knowing the moisture content, the sorption isotherm function can be directly created by

$$\xi = \frac{\partial u}{\partial \phi} = \frac{u_h}{n\,A\,\phi} \left(1.0 - \frac{\ln \phi}{A} \right)^{-\frac{n+1}{n}} \qquad 0 \le \phi \le 1 \tag{5.10}$$

In the ESP-r moisture transfer scheme, the average curve of adsorption and desorption curves is used for both processes. This can be modified in the future by assuming, for example, adsorption as the default process. In this way, the moisture equation is solved. If desorption occurred instead of adsorption then the equation will be resolved with respect to desorption. This should also be considered in the moisture data file by assigning a different index requiring double the associated data items.

The numerical representation of the moisture transport equation requires the evaluation of the moisture storage coefficient at the nodes, and the moisture transport coefficients between adjacent nodes. This requires specifying an acceptable profile for each variable. A stepwise profile (i.e. the value of the variable at the node prevails over its associated control volume) is assumed for the moisture storage term in ESP-r. Therefore, the estimation of the moisture storage capacity, ξ, for a homogeneous control volume is straightforward. The moisture storage capacity for a control volume at the interface of adjacent layers is determined from a solid mass weighting as

$$\bar{\xi}_i = \frac{\sum_{i=1}^{N} (\rho_o)_i \, \Delta x_i \, \xi_i}{\sum_{i=1}^{N} (\rho_o)_i \, \Delta x_i} \tag{5.11}$$

where N refer to the number of materials in the control volume (N=2 for a 1D simulation). Similarly, the moisture capacity coefficient for the air node is determined by

$$\xi = \frac{\partial u_{air}}{\partial \phi} = \frac{R_a \, P_s \, P_t}{R_v \, P_a^2} \tag{5.12}$$

where the vapour ratio u_{air} is defined by

$$u_{air} = \frac{R_a \, P_v}{R_v \, P_a} = \frac{R_a \, \phi \, P_s}{R_v \, (P_t - \phi \, P_s)}$$

Alternatively, the storage term for vapour transfer in air can be written as

$$\rho_o \, \frac{\partial u}{\partial t} = \rho_o \, \frac{\partial u}{\partial P_v} \, \frac{\partial P_v}{\partial t} = \rho_o \, \frac{R_a \, P_t}{R_v \, P_a^2} \, \frac{\partial P_v}{\partial t}$$

which is similar to the former approach. Numerical differentiation can also be used in deriving the storage term.

Similarly, various formulae are available to define vapour permeability. The upgraded version of the IEA Annex 14 catalogue of material properties presents the following equation to estimate vapour permeability

$$\delta = \frac{\delta_a}{\mu} = \frac{1.89923e-10}{\mu} \qquad @ \ (25^oC) \tag{5.13a}$$

where the vapour resistance factor, μ , is given by

$$\mu = \frac{1}{a + b\ e^{c\phi}} \quad 0 \le \phi \le 1 \tag{5.13b}$$

or

$$\mu = \frac{1}{a + b\ \phi^{\ n}} \quad 0 \le \phi \le 1 \tag{5.13c}$$

Ricken (1989) proposes the following formula to estimate the vapour resistance factor

$$\mu = \mu_o - a\ \phi^b \quad 0 \le \phi \le 1 \tag{5.13d}$$

Equations (5.12a) and (5.12b) are used in ESP-r to estimate the vapour permeability on the basis that the IEA catalogue provides coefficients for a variety of building materials. If a piecewise, linear profile is assumed for the relative humidity then the numerical representation of the permeability of a homogeneous material at the interface of two adjacent control volumes ($i + 1$, and i) is defined by

$$\delta_{i+1/2} = \frac{\delta_i\ \Delta x_{i+1 \to i+1/2} + \delta_{i+1}\ \Delta x_{i \to i+1/2}}{\Delta x_{i \to i+1}} \tag{5.14}$$

No function is required to determine the permeability through a non-homogeneous material as the gridding technique ensures the existence of a node at the interface of the construction layers (this is mainly done to reduce the truncation error as shown in chapter 3). The thermal vapour diffusion coefficient is assumed to be constant throughout the homogeneous layers due to lack of data.

As mentioned in Chapter 2, the diffusion of vapour in air can be described by

$$\vec{J}_v^D = - D_{\rho_v} \nabla \rho_v$$

or

$$\vec{J}_v^D = - \frac{D_{\rho_v}}{R_v T} \nabla P_v + \frac{D_{\rho_v} P_v}{R_v T^2} \nabla T$$

Several empirical expressions for the vapour diffusion coefficient in air are given elsewhere (Galbraith, 1992). However, for the normal range of conditions encountered in buildings, a value of 0.000025 m^2/s for D_{ρ_v} is generally acceptable (McLean, 1988). This value can be used to describe vapour flow through air gaps.

Several methods exist to calculate the convective moisture transfer coefficient , β, of which some are a functions of the convective heat transfer coefficient , h. Using Lewis relation (Webb, 1991), the convective moisture transfer coefficient is defined by

$$\beta_p = \frac{h_c\ M_w}{c_p\ R\ T}\left(\frac{Sc}{Pr}\right)^{n-1} \tag{5.15}$$

where the Schmidt number, Sc, and the Prandtl number, Pr, are defined by

$$Sc = \frac{\nu}{D_{va}}\ ; \qquad Pr = \frac{\nu}{\alpha} = \frac{\nu\ \rho\ c_p}{\lambda}$$

According to Laan (1994), the ratio (Sc/Pr) is constant and equal to 0.79 for the temperature range ($0 - 40^oC$). Webb (1991) suggested a value of 1/3 (i.e. turbulent flow) for the exponent n. The IEA (1991) suggested another equation to estimate the convective moisture transfer coefficient:

$$\beta_p = \frac{h_c}{c_p\ R_a\ T\ \rho_a}\left(\frac{c_p\ R_a\ T\ \delta}{\lambda_a}\right)^{0.67}$$

For building applications, this equation can be simplified to

$$\beta_p = \frac{h_c\ \delta}{\lambda_a} = 7.4\ E-9\ h_c$$

Furthermore, several psychrometric functions are also used to perform the simulation; the psychrometric library is shown elsewhere (ASHRAE, 1993).

On the other hand, the heat sub-matrix should be modified to account for moisture transport. In order to maintain the flexibility of the ESP-r structure, the moisture transport related modifications are performed within a separate routine and correspond to a different space discretisation scheme. The moisture content for a heat control volume is the algebraic sum of the moisture content for all the moisture nodes within that heat volume. The latent heat of evaporation or condensation is estimated by calculating the change in the liquid mass for each moisture volume within the heat volume, based on that the heat volume total latent heat is determined. Moisture flow related enthalpy is estimated on the basis of the moisture flow between the two adjacent moisture volumes. Accordingly, the enthalpy is estimated on the basis of the moisture node's temperatures.

5.4 Solution method

The two sets of equations are coupled and have to be solved simultaneously within one global matrix. That is

$$\begin{bmatrix} \mathbf{E} \\ \mathbf{M} \end{bmatrix}\begin{bmatrix} \mathbf{T} \\ \mathbf{P} \end{bmatrix} = \begin{bmatrix} \mathbf{B}_e \\ \mathbf{B}_m \end{bmatrix} \tag{5.16}$$

where **E** and **M** are the energy and moisture coefficients sub-matrices respectively. These are not square matrices. **T** and **P** are the temperature and vapour pressure sub-vectors respectively. The heat

and moisture future source variables are included in these sub-vectors. The energy and moisture boundary sub-vectors are denoted by $\mathbf{B}_e$ and $\mathbf{B}_m$ respectively.

Iterative methods must be used to solve the global system since

- Both equations (energy and moisture) are non-linear, and some terms (especially in the moisture equation) are strongly dependent on the variables, such as the moisture capacity of building materials which may be an exponential functions of the temperature and vapour pressure. Therefore, linearisation techniques are not acceptable for these coefficients.
- Both equations contain coefficients which are dependent on the variables of the other equation. This requires that the two sets of equations be contained within one global matrix for direct solution. This is complicated for different discretisation schemes.

Because of the strong interaction between the heat flow and moisture transport, the global set of equations should be solved within one global iteration loop as shown in Figure 5.4. However, the adopted solution approach is shown in Figure 5.5. This is because the existing energy matrix solver in ESP-r is based on direct solution method. Because of nonlinearities, the Gauss-Seidel method is used to solve the moisture sub-matrix. The adopted solution method includes a global iteration loop which is invoked whenever the liquid mass variations exceed the convergence limit. In that case, the energy matrix is resolved with the new moisture variables while the energy terms are not recalculated. Because of the multi-level linking between ESP-r's different modules and schemes, the adoption of energy terms recalculation within the global iteration loop requires lengthy validation work. This was not possible because of time constraints. For cases which may involve higher energy flow dependence on moisture flow, smaller time step can be used. However, for high dependencies the energy sub-matrix should be solved at each iteration (i.e. equivalent to the first solution approach).

The Gauss-Siedal method is used to solve the moisture sub-matrix. However, it cannot be directly applied for the simultaneous solution of a set of non-linear equations. Under-relaxation factors should be used in order to prevent divergence and minimise or eliminate convergence instabilities. In order to define the most appropriate under-relaxation factors, the source(s) of divergence and convergence instabilities should be defined. There are three such sources:

- Strong non-linearity (e.g. exponential function) in the moisture flow coefficients. To overcome the effect of this source a linear under-relaxation factor can be used. If employed, its effect should be considered within the convergence test. Otherwise, false convergence will be detected.
- Discontinuity in the moisture transfer rate at the maximum relative humidity due to condensation. a linear under-relaxation factor is also convenient for this source.
- Usually, the future self-coupling term ($\rho_o \, \xi \, V \, / \, P_s$) is relatively small. Thus, changes in the connected node's variable has a strong effect on the node's future value. To control this

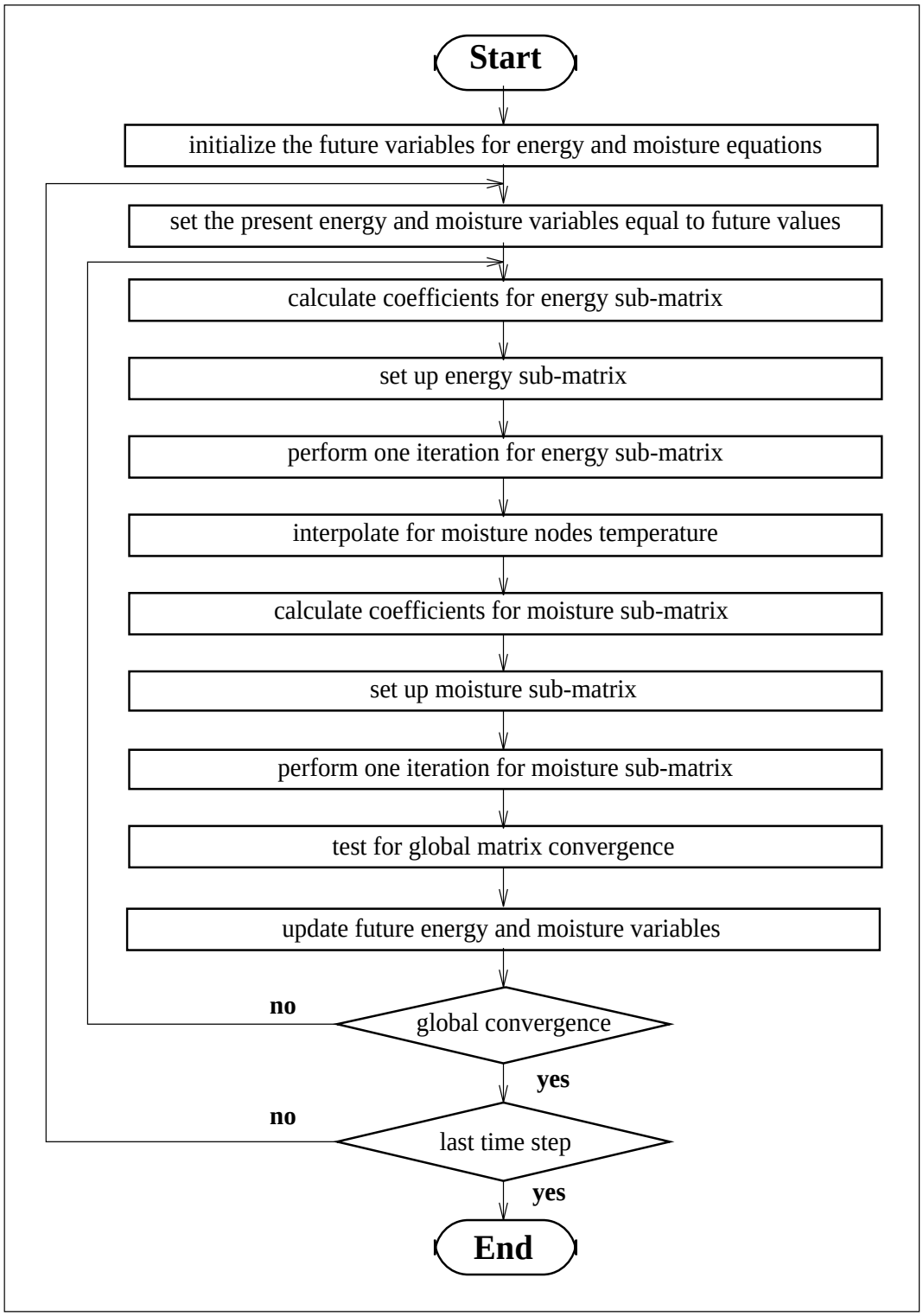

Figure 5.4 First solution method flow chart.

source a false time step (inertia) relaxation factor can be used. This works by magnifying

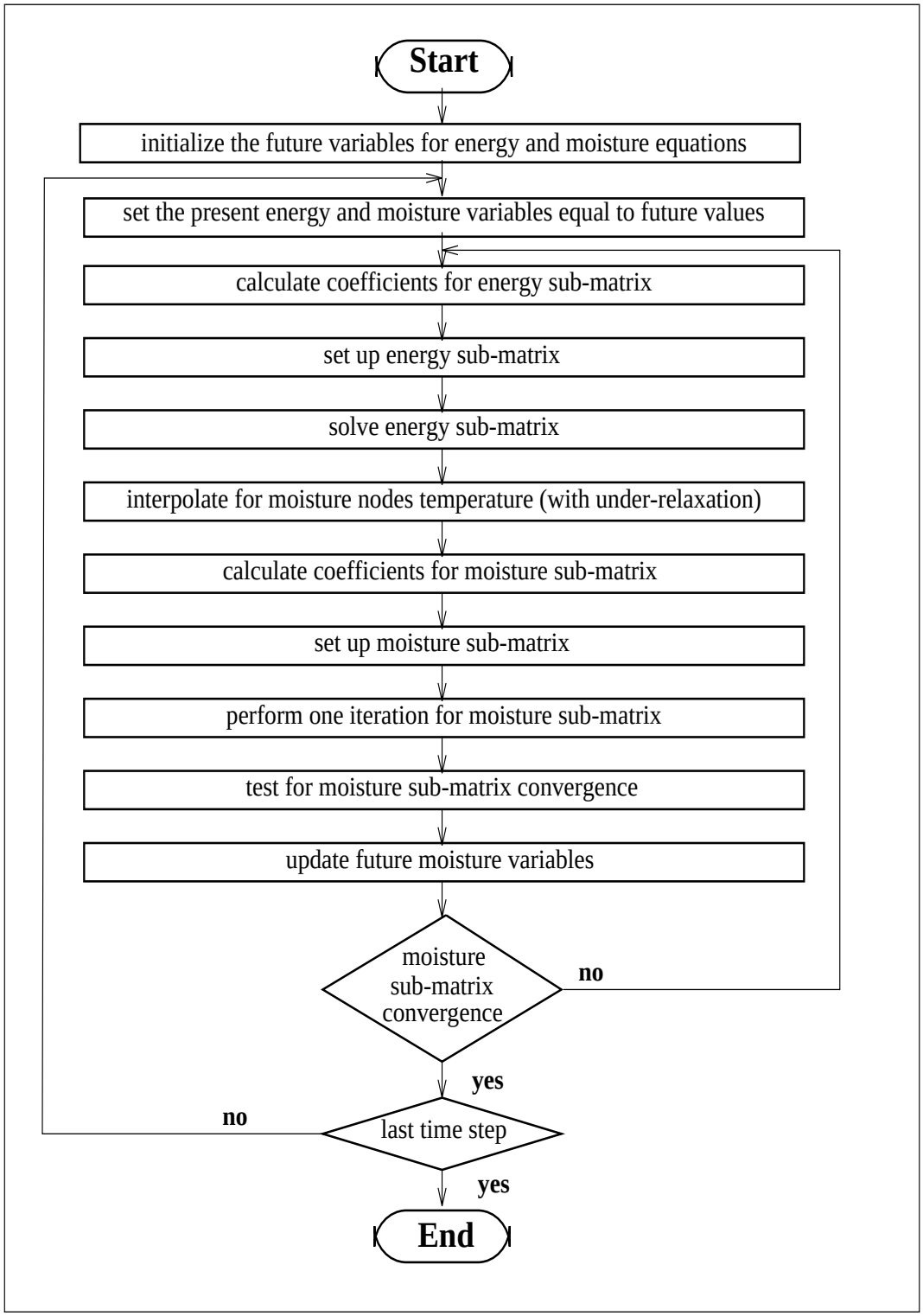

Figure 5.5 Second solution method flow chart.

the future storage term. From a physical point of view, this means that for the same source

and flux combination, the change in the dependent variable value is less as the storage capacity is higher. From a numerical view point, increasing the self-coupling coefficient reduces the difference between the present and future dependent variable values. In other words, the source of divergence is minimised or removed. This is done by adding the under-relaxation term to the future self-coupling coefficient. In order to maintain the validity of the equation, the same term multiplied by the variable's latest future value is added to the right hand side of the equation. In addition, the inertia under-relaxation factor partially absorbs the fluctuations in the moisture storage coefficient as it increases the magnitude of the future self coupling term.

The false time step under-relaxation factor is equal to the future self-coupling term except that the time step is replaced by the false time step. Therefore, for the moisture finite difference equation shown above, the false time step under-relaxation factor is defined by

$$RLX_{false} = \frac{\rho_o \ \xi_i \ V \ \Delta t}{(P_s)_i^{n+1} \ (\Delta t)_{false}} \tag{5.17}$$

Introducing a false time step under-relaxation factor into equation (5.5) produces

$$(RLX_{false} + a_i^{n+1}) \ P_i^{n+1} + \sum_{j=1}^{2} a_j^{n+1} \ P_j^{n+1} + (m_l)_i^{n+1} - \gamma \ \Delta t \ S_i^{n+1} =$$

$$RLX_{false} \ (P_i^{n+1})_{latest} + a_i^n \ P_i^n + \sum_{j=1}^{2} a_j^n \ P_j^n + (m_l)_i^n + (\ 1 - \gamma \ ) \ \Delta t \ S_i^n +$$

$$\sum_{j=1}^{2} b_j^n \ (\ T_j^n - T_i^n \ ) + \sum_{j=1}^{2} b_j^{n+1} \ (\ T_j^{n+1} - T_i^{n+1} \ ) \tag{5.18}$$

Unlike the linear one, the false time step under-relaxation factor is not usually constant throughout the space dimension. The effect of both relaxation factors is expected to vanish (depending on the convergence criteria) as the change in the future variable's values become negligible. The two relaxation factors are allowed to be applied together because the three source of divergence and convergence instabilities usually exist together in the moisture transfer equations.

On the other hand, the building moisture matrix is divided into zone based sub-matrices. This will allow future implementation of the first solution method as the same technique is used for the system heat matrix. Hence, for each zone the present and future variable values for external ambient should be known. This is done on the basis of a one time step lag. Otherwise, an iterative loop will be required to assure the conservation of mass and energy through partitions. Figure 5.6 shows the electrical analog of the moisture connections through a construction. The external ambient node is **not** assigned a capacitance. Otherwise, an iterative loop will be required to ensure the conservation of

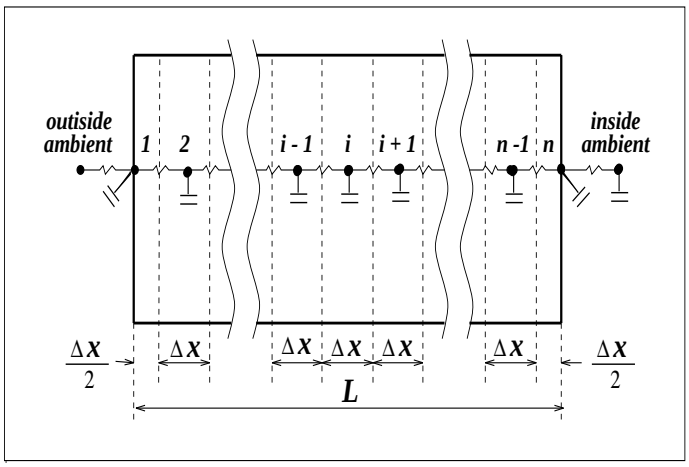

Figure 5.6 Electrical analog of moisture transport through a construction.

mass and energy.

5.5 Conclusion

A computer model has been developed for the moisture transport through building multi-layered constructions. Temperature and partial vapour pressure are used as the transport potentials for moisture. This model is integrated into ESP-r in order to combine the moisture transport with other related domains in buildings such as heat flow, air flow and plant. The physical, mathematical, numerical and computational basis of a 1-dimensional, transient, control volume model for combined heat and moisture transfer in buildings had been presented. A 1-dimensional, transient model was then developed with an extensible structure. The type of integration is mixed sequential/simultaneous. A fully simultaneous integration between heat and moisture transfer has been presented. This should be adopted when liquid transfer is included. The current model considers most of the effective interactions between heat and moisture transfer. For example, the dependence of the transport and storage properties of each equation on the dependent variable of the other equation is included.

The developed moisture model not only facilitates simulation of moisture content dependence for building materials thermophysical properties, but also provides better estimate for inside air moisture content for the air flow and plant modules.

The validation of the developed model is presented in Chapter 6 and an application of the integrated model is shown in Chapter 7.

References

American society of Heating, Refrigeration, and Air-Conditioning Engineers 1993. in *ASHRAE HANDBOOK: Fundamentals,* Atlanta,USA.

Clarke, J. A. 1985. *Energy simulation in building design,* Adam Hilger Ltd, Bristol,UK.

Galbraith, G1992. , *Heat and Mass Transfer Within Porous Building Materials*, Glasgow. PhD University of Strathclyde

Hansen, K K 1986. ‘‘Sorption isotherms: A catalogue,’’ *Technical report 162/86, Technical University of Denmark.*

IEA 1991. ‘‘Condensation and energy: Catalogue of Material Properties, Report Annex XIV,’’ *International Energy Agency, Energy Conservation in Buildings and Community System Programme*, vol. 3.

IEA 1994. ‘‘Catalogue of Material Properties, upgraded version,’’ *International Energy Agency, Energy Conservation in Buildings and Community System Programme, IEA annex 24 HAMTIE*.

Laan, M J van der 1994. ‘‘A model for combined heat and vapour transfer in building constructions,’’ *PhD Progress Report, Einhoven University of Technology*.

Patankar, S V 1980. *Numerical Heat Transfer and Fluid Flow,* Hemisphere Publishing Corporation, USA.

Ricken, D. 1989. ‘‘Ein einfaches Berechnungsverfahren für die eindimensionale, instationäre Wasserdampfdiffusion in mehrschichtigen Bauteilen,’’ Dissertation, Universität Dortmund.

Smith, G. D. 1985. *Numerical Solution of Partial Differential Equations: Finite Difference Methods,* Clarendon Press, Oxford.

Webb, R L 1991. ‘‘standard nomenclature for mass transfer process,’’ *ASHREA Transactions*, vol. 97, pp. 114-117.

CHAPTER 6

Validation

The schemes developed in Chapters 3, 4 and 5 are validated in this chapter. This is done by first defining the validation methodology. Then, the validation of the developed schemes is performed in the same sequence they were introduced. Finally, conclusions related to the validation process are given.

6.1 Validation methodology

As was mentioned in Chapter 1, quality of the prediction tools can be improved via three major approaches. First, by developing new mathematical models for better representation of the heat and mass transfer processes occurring within the building/plant system. Second, by increasing the simulation resolution in order to reduce the number of simplifying assumptions. Third, by elaborating comprehensive validation methodology which includes all stages of simulation program development. While the first two approaches were considered in Chapters 2, 3, 4 and 5, the third approach is considered in this chapter.

According to Judkoff *et al* (1983), the sources of inaccuracy in building energy simulation programs can be divided into two groups external and internal. External errors are independent of the internal working of the method of analysis, such as errors in the input data. Internal errors are directly linked to the internal workings of a prediction technique. Therefore, internal errors sources include the development of physical, mathematical and numerical models, beside the coding errors. In other words, internal errors are related to the process of developing a simulation program, and external errors are related to the process of using these simulation tools.

The current work is concerned with internal errors only. Some errors related to the development of physical, mathematical and numerical models were considered in Chapters 2, 3, 4 and 5. Furthermore, errors related to the process of model generation were considered by means of other documentations (Nakhi, 1993a; Nakhi, 1993b; Hensen and Nakhi, 1994; Strachan, Nakhi and Sanders, 1995). In this chapter, coding errors are investigated. For that purpose, the robust PASSYS validation

methodology (Jensen, 1994) is adopted. It was produced by the Commission of the European Communities PASSYS project. It includes all stages of simulation program development. It comprises five components, not all of which need to be applied in a given context:

- theory checking: the theory of the developed computer model is examined to confirm that the theory is appropriate in terms of its application and scope (refer to Chapters 2,3,4 and 5).
- source code inspection: the code should be checked to insure that the selected algorithms are correctly implemented. Structured programming, and documentation ease this process (code checking tools (for syntax errors) and debugging tools (for logic errors) have been used).
- analytical verification: the output of the whole package or part of it is compared with the analytical solution for relatively simple heat transfer problems.
- inter-model comparisons: the calculated results from the developed scheme is compared with other schemes within the program itself, or other programs which are considered to be better validated.
- empirical validation: the output of the program is compared with monitored results from a real structure such as test cells.

From practitioners point of view, the empirical validation is the most important one as practitioners are mainly concerned with the overall simulation result accuracy. However, analytical verification (when possible) is the most suitable for validating codes related to specific processes in isolation since acceptable overall simulation accuracy does not necessarily mean acceptable accuracy for all processes in isolation.

6.2 Adaptive Gridding

The adaptive gridding scheme developed in Chapter 3, was tested via the analytical, inter-model and empirical validation procedures. For the analytical test, the ESP-r results from the default 1-D nodal scheme and the new 3-D nodal scheme (Approaches 1 and 4 respectively in Figure 3.15) were compared with the analytical solution for a 1-D transient heat conduction problem.

The test domain (shown in Figure 6.1) is a slab with an adiabatic boundary at one side and a convective boundary on the other side. The effect of a step change from 50°C to 0°C in the ambient temperature was monitored. The convective boundary surface temperature was selected as the validation variable, as maximum error is expected at that location. The mathematical model is defined by the following partial differential equation with its associated boundary and initial conditions.

$$\frac{\partial^2 T(x,t)}{\partial x^2} = \frac{1}{\alpha}\,\frac{\partial T(x,t)}{\partial t} \quad , \qquad 0 < x < d \quad , \quad t > 0 \tag{6.1a}$$

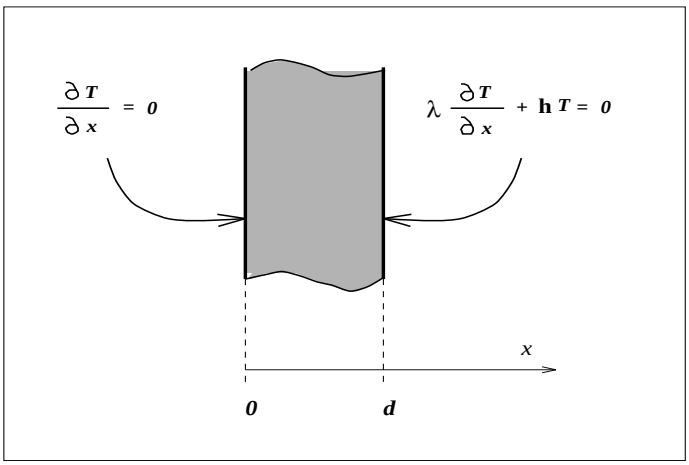

Figure 6.1 Analytical validation domain.

$$T = T(x,0) \quad , \quad 0 < x < d \ , \ t = 0 \tag{6.1b}$$

$$\frac{\partial T}{\partial x} = 0 \quad , \quad x = 0 \ , \ t > 0 \tag{6.1c}$$

$$\lambda \frac{\partial T}{\partial x} + h\, T = 0 \ , \quad x = d \ , \ t > 0 \tag{6.1d}$$

The analytical solution for that problem is given by Appendix B as

$$T(x,t) = 2T_0 \sum_{m=1}^{\infty} \frac{e^{-\alpha \omega_m^2 t} \cos(\omega_m x) \sin(\omega_m d)}{\omega_m \left[\dfrac{\sin(\omega_m d)\cos(\omega_m d)}{\omega_m} + d \right]} \tag{6.2}$$

where ω_m are the roots of the following equation

$$\omega_m \tan(\omega_m d) = \frac{h}{\lambda} \tag{6.3}$$

Based on equations (6.2) and (6.3) a FORTRAN program was written to performing the required calculations. Before that, the roots, ω_m, should be determined. Equation (6.3) can be re-arranged to simplify this process.

$$\psi_m \tan(\psi_m) = \frac{h\, d}{\lambda} \tag{6.4}$$

where,

$$\omega_m = \frac{\psi_m}{d}$$

The mathematical package Maple (Abell and Braselton,1994)§ was used to determine the roots of equation (6.4).

The measured and predicted results when plotted on the usual time decay basis are close. For this reason they are plotted in the format of Figure 6.2 to accentuate the differences. The predictions from the 3-D scheme are considered acceptable; the 3-D scheme with massless boundary nodes gives a better response for the surface temperature, but the default 1-D scheme prediction became slightly more accurate as the rate of temperature variation decreased. This is probably the effect of a higher heat storage term for the neighbouring control volume in the 3-D scheme. These simulations were undertaken against a 1 hour time step; agreement with the analytical solution is improved if smaller time steps are used.

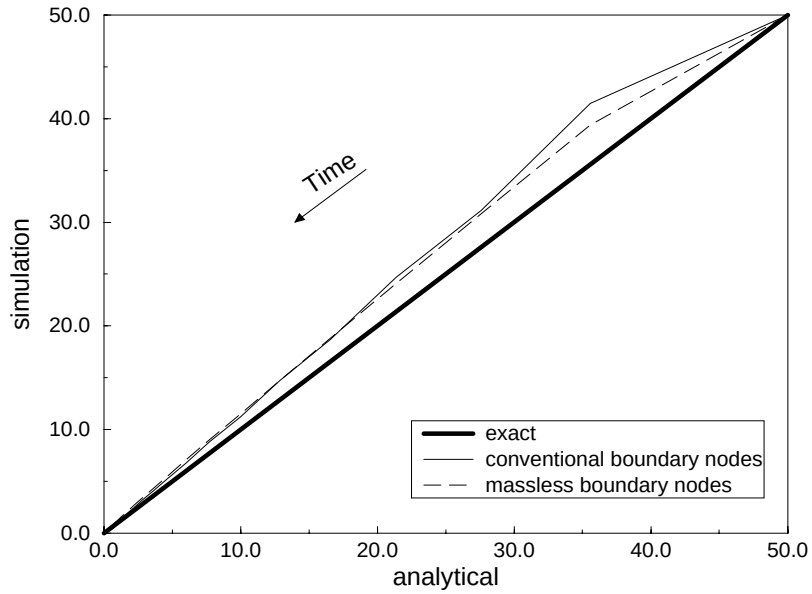

Figure 6.2 Analytical Comparison: Decay from Step Change

Two inter-model comparisons were performed. In the first, a comparison was made between the default 1-D scheme for ESP-r and the new 3-D scheme on a 1-D zone model. Minor changes were required within the 3-D code so that the same nodal scheme (approach 1 in Figure 3.15) was used in both cases. The predicted temperatures were in agreement to better than 0.001°C. In the second inter-

§ Maple is a mathematical tool of Waterloo Maple Software for symbolic mathematical calculation

model comparison, ESP-r's 3-D results were compared with results from the computational fluid dynamics package PHOENICS (refer to Appendix D). A cubic room with a homogeneous one layer construction was used. The thermophysical and geometrical symmetry was required to cancel the effect of internal longwave radiation effects which are treated in ESP-r but not in PHOENICS. Due to the symmetry only one eighth of the room was modelled by PHOENICS. The effect of step excitation in the indoor air temperature was examined. The predicted nodal temperatures with ESP-r and PHOENICS were in agreement to within 0.001°C.

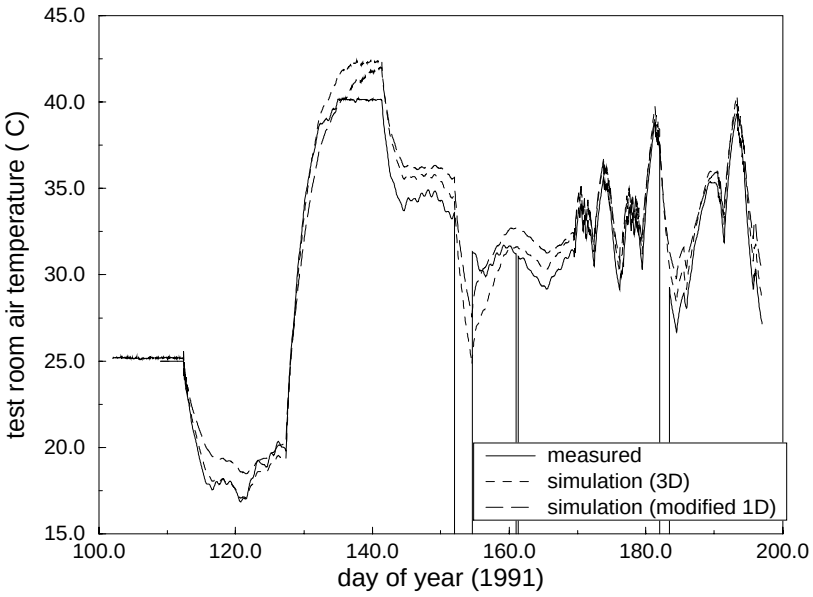

Figure 6.3 Measured, Modified 1-D and 3-D Air Temperatures

Finally, results from a PASSYS test cell experiments (Baker *et al*, 1992) were used for empirical validation. Figure 6.3 shows the measured results, with the modified 1-D (refer to appendix E) and then full 3-D simulations. At lower temperatures, the 3-D simulation results are in better agreement with the measured data, and in general the dynamic response is improved. At high temperatures, the measured and predicted temperatures still differ. This is thought to be mainly due to the effect of temperature on the thermophysical properties, particularly conductivity, for which the model inputs were based on measured conductivity at the standard 10°C. Currently, the ESP-r 3-D scheme is not capable of considering the temperature dependence of thermophysical properties. However, for the default 1-D simulation, the impact of adopting a linear temperature dependence for thermal conductivity for the insulating materials in the test cell is shown in the next section. The application of such dependence would improve agreement with the measured data at high temperatures.

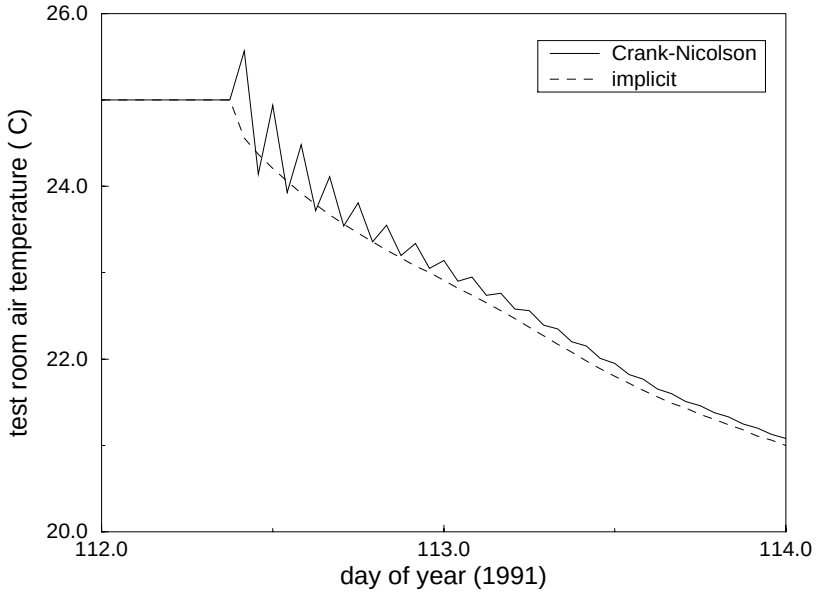

Figure 6.4 Simulation results for Crank-Nicolson and fully implicit methods.

The full 3-D simulation mentioned above was performed using the Crank-Nicolson method. Due to stability errors some stable oscillations occurred during that run. This is shown in Figure 6.4 which compares the simulation results for two implicitness degrees 0.5 and 1.0 (Crank-Nicolson and fully implicit methods, respectively). The oscillation was eradicated by applying the fully implicit method.

6.3 Variable thermophysical properties

After performing the theory validation, the variable thermophysical properties scheme code was validated via inter-model and empirical methods. First, the result of constant thermophysical properties simulation was compared with the result of variable thermophysical properties simulation for which the dependences were all set to zero. Similarly, the results of adopting linear conductivity were compared with those of adopting nonlinear thermophysical properties for linear thermal conductivity simulation. All the results were satisfactory.

In addition, a model[§] was developed to simulate heat conduction through a two layered construction. The boundaries can be defined as being of the second or third kind. And thermophysical properties were defined as a polynomial function of temperature. A fully iterative solution technique,

§ This conduction model will be part of the ESP-r validation bench mark which will be used for validating the main processes for each new version of ESP-r.

with a linear under-relaxation factor, was adopted. In order to allow different accuracy levels, two linearisation schemes are available: one time step in arrears, and the first extrapolation scheme introduced in the previous section. Of course, the most accurate option is when none of these linearisation schemes are used, as the default fully iterative technique will be employed.

This model was used to investigate the validity of the linearisation schemes discussed Chapter 4. On the other hand, this model was used for inter-model validation for the variable thermophysical properties scheme. As expected, the variable thermophysical properties scheme results were valid for low temperature fluctuations. However, the ESP-r time step controller can be used to prevent high temperature variations.

On the other hand, empirical validation was performed. One of the UK PASSYS test cells in Glasgow was selected for that purpose. Since, only the temperature dependence of the insulation's thermal conductivity were provided by PASSYS, and the insulation layer's thickness approximately equals to 90% of wall's total thickness; only the temperature dependence of insulation's thermal conductivity was considered during the investigation. Further, only the linear dependence was considered because only three readings where supplied by PASSYS per insulation type. Table 6.1 shows the linear dependence equations for the insulations, derived by using the method of least squares.

Table 6.1 Thermal conductivity temperature dependence formulaes

Description	Thermal Conductivity
foamed polystyrene (styropor)	$\lambda = 0.0331 + 0.000183\ T_m$
extruded polystyrene (styrodur)	$\lambda = 0.0244 + 0.000175\ T_m$

Similar to PASSYS, the air temperature of the test room was considered as a reference for the investigation. Figure 6.5 shows the test room air temperature for the three cases: as measured by PASSYS, simulation result for the constant conductivity case, and the simulation result for the linearly temperature dependent thermal conductivity case. As can be seen from the figure, the prediction of the air temperature can be improved by adopting a variable thermal conductivity. It should also be noticed that the variable thermal conductivity curve is always overlapping or below the constant thermal conductivity curve. This is because the heat flow within the simulation period is usually to the outside (as can be seen from Figure 6.6 the outside temperature is always lower than the inside temperature) and the actual thermal conductivity value for the insulation layers is usually higher than their reference values, since their mean temperature is always higher than the insulation's thermal conductivity reference temperature (i.e. 10^oC). In addition, the difference between the two simulation curves increases as the room temperature increases. This is because the rise in the room temperature is

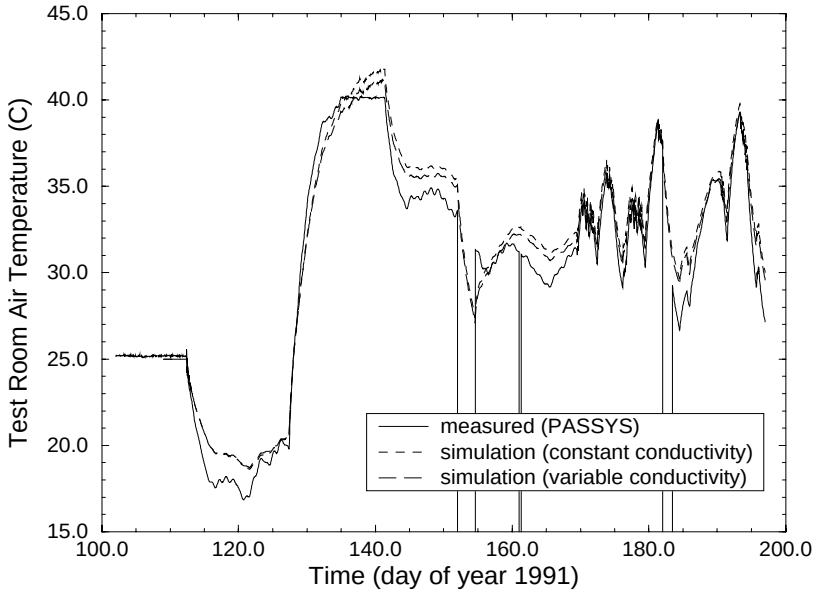

Figure 6.5 Test room air temperature vs time.

associated with the increase in the construction material's temperature. And the higher the layer's temperature, the more deviation from the reference temperature.

It should be noted that better simulation results can be achieved by selecting a better reference thermal conductivity, or temperature, value. However, this usually means that for each investigation there should be two runs; the first run used to determine the average temperature through the simulation period, and the second one used to obtain the required result. This method not only means higher computation cost and effort but also, when the temperature difference within required simulation period is relatively large, it requires dividing the simulation period into sub-periods, with different reference magnitudes for the thermal conductivity of most, if not all, construction materials. In addition, the simulation period portioning method becomes completely inadequate when the frequency of temperature fluctuation is relatively high. This is the case for passive building elements where daily fluctuation is expected.

On the other hand, the thermal conductivity of some materials, such as aluminium, varies with temperature but not in a near to linear manner. For this type of temperature dependence, the linear technique is valid only over a certain range of temperature changes, and its validity is questionable for large temperature differences.

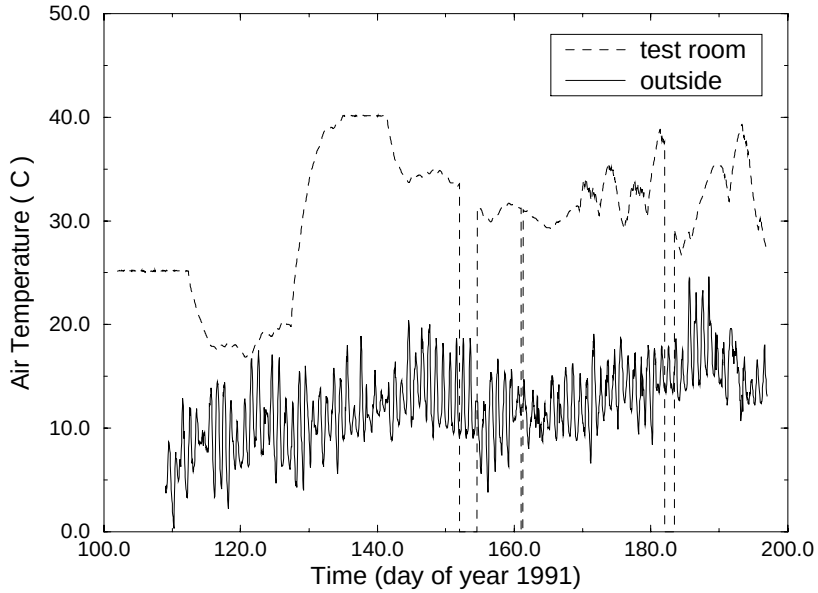

Figure 6.6 Outside and test room temperatures vs time.

6.4 Combined heat and moisture transfer

Beside the theory and code validation works, an analytical validation was also performed for the combined heat and moisture transfer scheme. In order to obtain a simplified case for which analytical solution for combined moisture and energy flows exist, the temperature is set to constant in both space and time dimensions. This will reduce the problem to moisture only flow problem. In addition, the moisture transport and storage coefficients were assumed to be constant. No heat or moisture generation were considered. Finally, the initial and boundary conditions were defined in such a way that moisture condensation was not possible. For this problem the moisture transfer equation reduces to

$$\frac{\partial P}{\partial t} = \alpha_v \frac{\partial^2 P}{\partial x^2} \tag{6.5a}$$

Where,the vapour diffusivity α_v is defined by

$$\alpha_v = \frac{\delta_P^T \; P_s}{\rho_o \; \xi}$$

For this validation test to be most beneficial, very minor modifications were made to the ESP-r to enable the simulation of constant vapour transport and storage coefficients. The test case shown in Figure 6.7 is a homogeneous slab ($0 \le x \le d$) initially at a constant pressure $P_0 = 1000(Pa)$. The

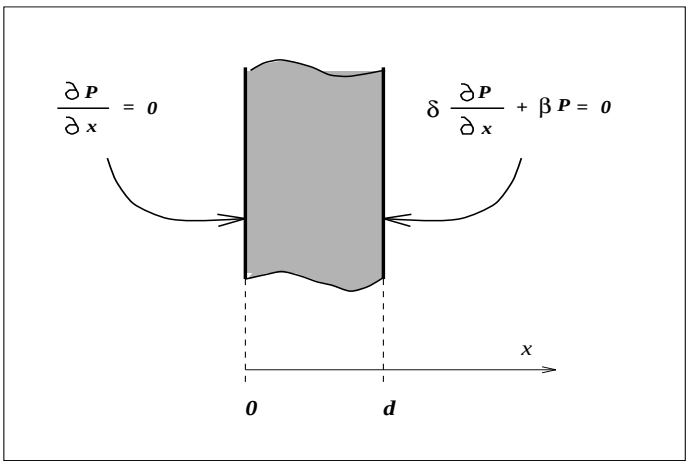

Figure 6.7 Analytical validation domain.

boundary at x=0 is kept insulated (i.e, no moisture flow). While the boundary at x=d is exposed to an environment whose vapour pressure changes in a stepwise manner from P_0 to zero (Pa). The temperature every where remains constant (T= 20^oC). This problem can be defined by equation (6.5a), whose boundary conditions are defined by

$$P(x,t) = 1000.0 \qquad ,0 \le x \le d \ , \ t = 0 \tag{6.5b}$$

$$\frac{\partial P}{\partial x} = 0 \qquad , x = 0 \ , \ t > 0 \tag{6.5c}$$

$$\delta_P^T \frac{\partial P}{\partial x} + \beta \ P = 0 \qquad , x = d \ , \ t > 0 \tag{6.5e}$$

$$T(x,t) = 20.0 \qquad ,0 \le x \le d \ , \ t \ge 0 \tag{6.5f}$$

The analytical solution for that problem is given by Appendix B as

$$P(x,t) = 2000.0 \ \sum_{m=1}^{\infty} \frac{e^{-\alpha_v \omega_m^2 t} \cos(\omega_m x) \sin(\omega_m d)}{\omega_m \left[\frac{\sin(\omega_m d)\cos(\omega_m d)}{\omega_m} + d \right]} \tag{6.6}$$

where ω_m are the roots of the following equation

$$\omega_m \tan(\omega_m d) = \frac{\beta}{\delta_P^T} \tag{6.7}$$

or

$$\psi_m \tan(\psi_m) = \frac{\beta\, d}{\delta_P^T} \tag{6.8}$$

where,

$$\omega_m = \frac{\psi_m}{d}$$

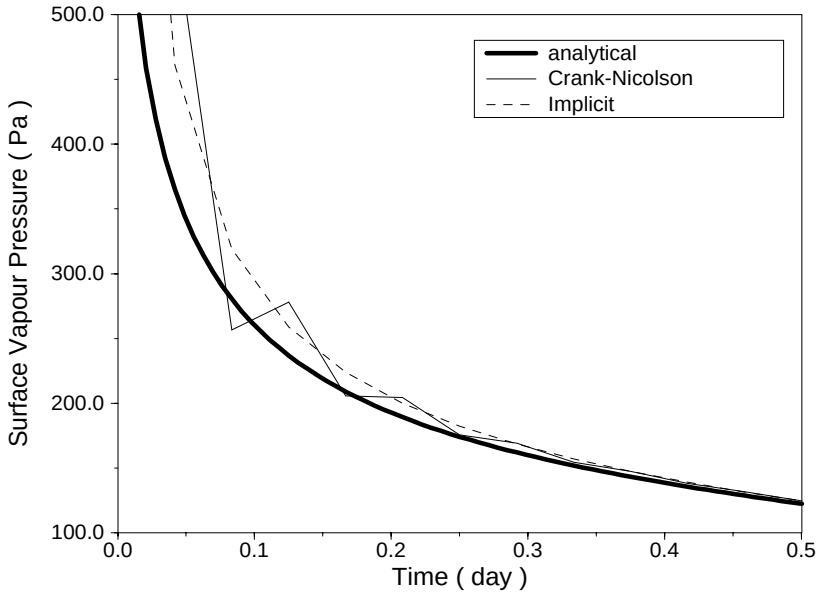

Figure 6.8 Damping oscillation.

As the maximum local error is expected to occur at the internal surface node (x = d), its vapour pressure was selected as the validation variable. Furthermore, the fully implicit method was selected as it is unconditionally stable, and no damping oscillation is expected. From the truncation error point of view , more accurate numerical representations can be obtained using for example the Crank-Nicolson method. However, this method was not employed for the validation test due to the possibility of damping oscillation occurrence as shown in Figure 6.8.

The effect of time step is clarified by Figure 6.9 which shows the variation of internal surface vapour pressure as a function of time for three different time steps. The accuracy of simulation improves as the time step is reduced. But the rate of improvement decreases. This is because the time step total error is composed of three sources (truncation, round off, and stability) which behave differently with time step reduction. In Figure 6.10 the effect of space step reduction is investigated. Similarly, the accuracy of the simulation improves as the space step is reduced (i.e., number of nodes per

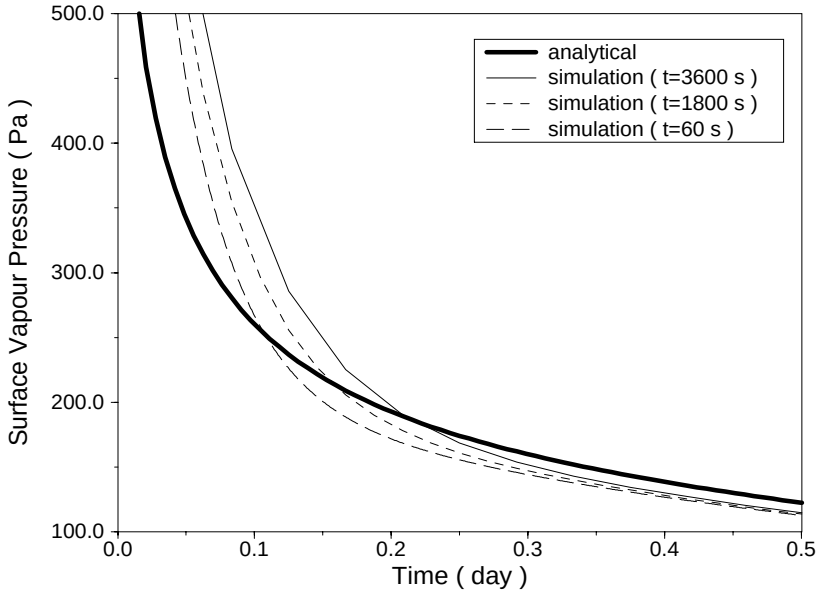

Figure 6.9 The effect of time step on the accuracy of simulation.

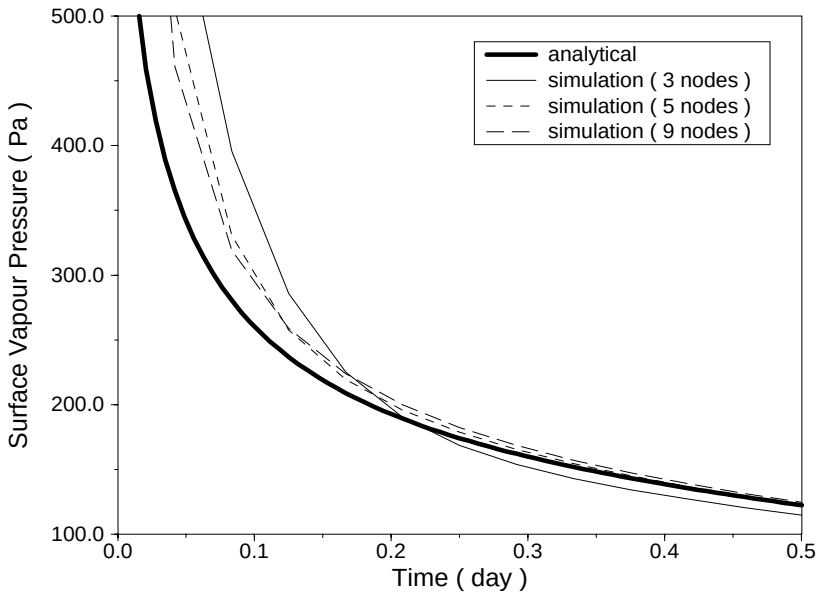

Figure 6.10 The effect of space step on the accuracy of simulation.

layer increased) with decreasing rate. In order to visualise the effect of varying the time or space

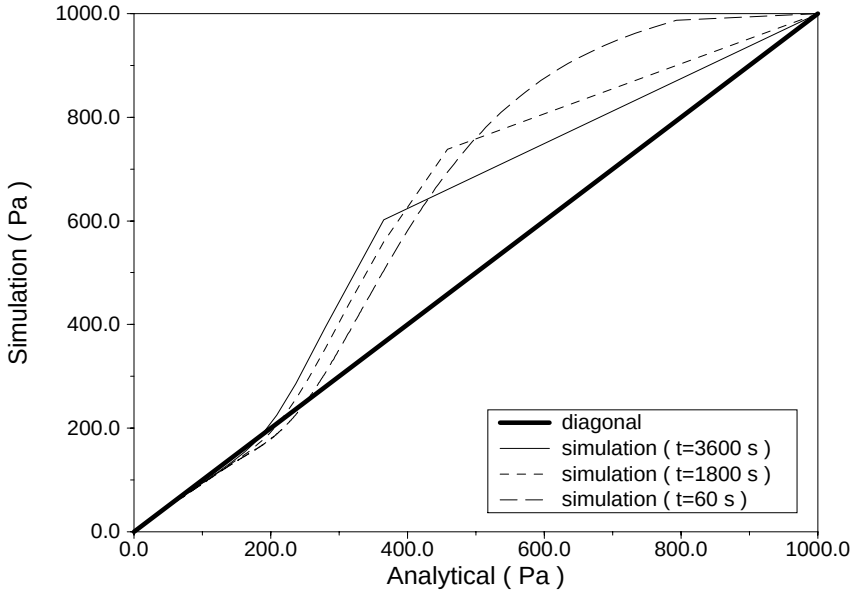

Figure 6.11 The effect of time step on the accuracy of simulation.

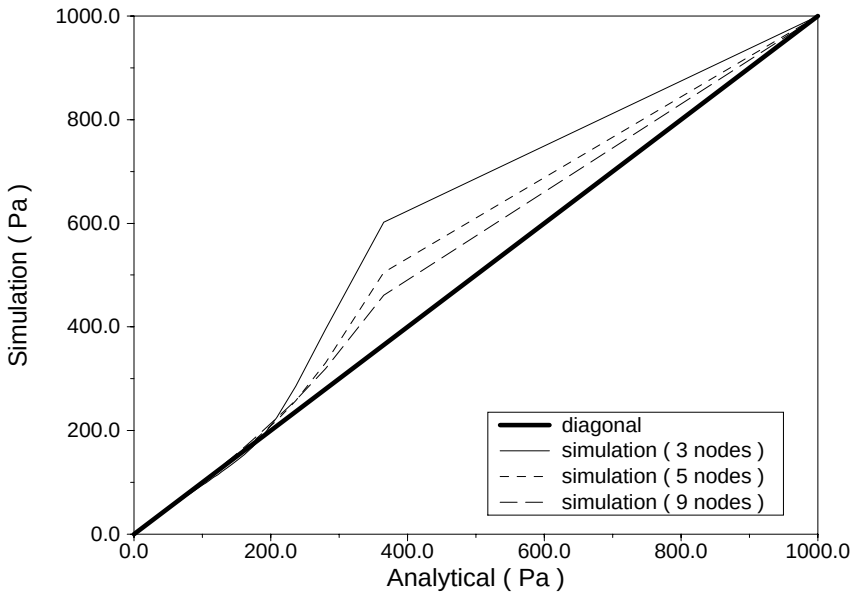

Figure 6.12 The effect of space step on the accuracy of simulation.

steps, Figures 6.11 and 6.12 can be used, respectively. These figures show that the accuracy of

simulation should be control by considering both the time and space steps since the way each step reduction improves the accuracy in different. Furthermore, the accuracy can be improved by several other means such as by altering the degree of implicitness (as was shown in Chapter 3)

6.5 Conclusions

The developed schemes validation results are satisfactory. However, more work is required to reduce the external error sources in order to bridge the gap between simulation tools and the building design practice.

The developed schemes are ready for operation after the validation process. The use of the developed schemes in practice is presented in the next Chapter.

References

Aasem, E., J. Clarke, J. Hand, J. Hensen, C. Pernot, and P. Stachan 1993. ‘‘ESP-r A program for building energy simulation, Version 8 series,’’ ESRU Manual U93/1.

Abell, M and J Braselton1994. , *The Maple V handbook*, Boston.

Baker, P., J. Clarke, A. Guy, P. Owens, K. Pearson, P. Strachan, and J. Twidell 1992. ‘‘Final report of the UK consortium,’’ *PASSYS*, vol. 2.

Hensen, J.L.M. 1991. ‘‘On the thermal interaction of building structure and heating and ventilating system,’’ Ph.D. Thesis, Eindhoven University of Technology.

Hensen, J.L.M. and A.E. Nakhi 1994. ‘‘Fourier and Biot Numbers and the Accuracy of Conduction Modelling,’’ in *Proceedings of Building Environmental Performance*, pp. 247-256.

Jensen, S O1993. , *The PASSYS Project: Subgroup Model Validation and Development*, Brussels. Final Report, Part I and II 1986-1992. Commission of the European Comunities. DGX1I,EUR 15115 EN.

Jensen, S O1994. , *Validation of Building Energy Simulation Programs*, Brussels. Research Report PASSYS Subgroup Model Validation and Development, Commission of the European Comunities, Directorate General XII for Science, Research and Development

Nakhi, A1993. , *Dynamically adaptive gridding for numerical modelling of thermal capacity and insulation systems*. ESRU Occasional Paper, University of Strathclyde

Nakhi, A1993. , *The impact of adapting variable thermal conductivity within building energy simulation*. ESRU Occasional Paper, University of Strathclyde

Strachan, P, A Nakhi, and C Sanders 1995. ‘‘Thermal Bridge Assessment,’’ *Proc. Building Simulation ’95*, USA.

CHAPTER 7

Applications

The developed schemes described in Chapters 3, 4 and 5 were integrated into an environmental building performance program ESP-r (refer to Appendix A). This chapter describes how the developed schemes can be used in practice. In addition it shows the effect of these schemes on the robustness and applicability of ESP-r.

Applications of the developed schemes can best be demonstrated by means of realistic case studies. All the applications will be performed with the same problem. This helps the reader to concentrate on the problem description associated with the developed schemes. Although most of the developed schemes can be applied together within a simulation, they are presented in isolation for clarity. However, combining them is a straightforward process.

In general, the problem description for all developed schemes are created via the ESP-r Project Manager with the support from other ESP-r modules as required (e.g. databases of material properties). The description of the simulation problem is given in Section 7.1. In Section 7.2, modelling systems with large temperature variation is presented. Design problems involving 3-dimensional conduction effects are shown in Section 7.3. Finally, a condensation risk assessment case is dealt with in Section 7.4

7.1 Problem description

The problem presented here concerns the modelling of a house at a site in Glasgow. It is attached to similar houses at the East and West sides. The building model comprises 12 thermal zones, each representing a distinct room in the building. The building is shown in Figure 7.1. The ground floor comprises five zones: bin, hall 1, stairs, kitchen and living room. The first floor consists of six zones: hall 2, water heater cupboard, bathroom, bedroom 1, bedroom 2, and bedroom 3. The remaining zone is the loft.

The geometry of the individual zones is held within the zone geometry file. All the files associated with this problem are shown in the appendices. The dwelling accommodates a family of 6

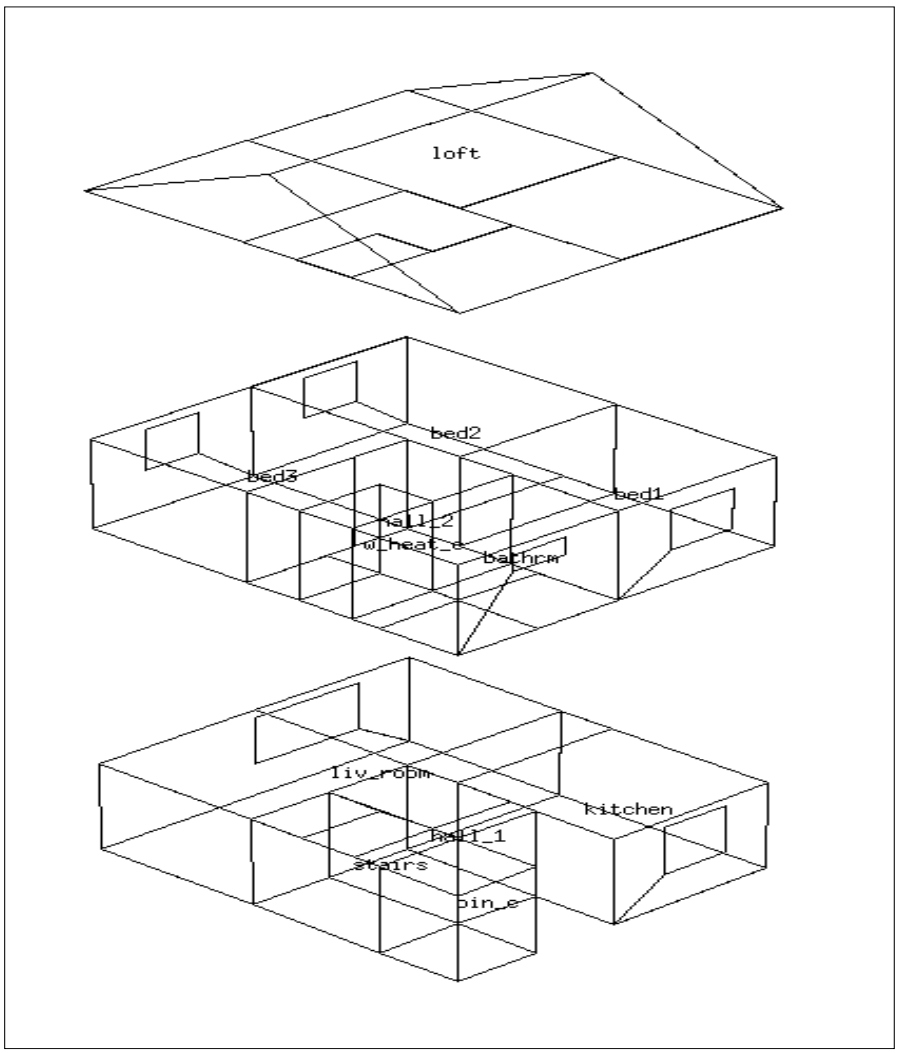

Figure 7.1 A perspective view of the applications building.

persons: one parent works while the other remains at home, and two children are of pre-school age. The associated sensible and latent energy gains due to people and equipment is described within the problem operation files. The building is made of medium weight and insulated construction and has air tight double glazed windows. The detailed construction informations are held within the construction and transparent multi-layered construction files.

In order to better represent the air infiltration and inter-zonal air coupling, an air flow network file is constructed. This is used to define the building's air leakage distribution in terms of flow components (such as cracks) due to temperature and pressure effects as elaborated by Hensen (1991). The constructed air flow network consists of 15 nodes representing outside air and all thermal zones (except "bin_c" which does not have a direct air flow contact with the other zones). For each external

facade two nodes are defined with different elevation and exposure types to better model air infiltration. The internal air flow nodes are connected with each other via five types of air flow components: door, crack, stairs, roof vent and window. The constructed network contains 18 connections as shown in Figure 7.2.

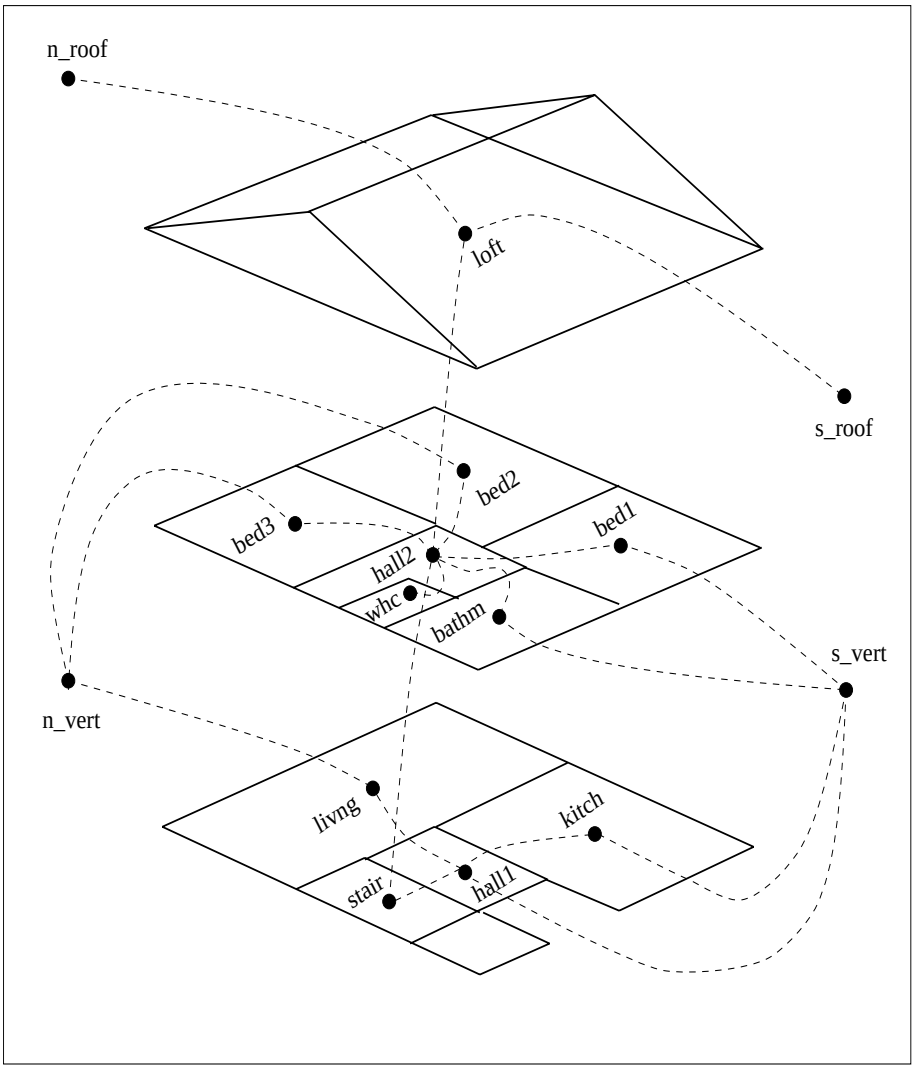

Figure 7.2 Mass flow network for the applications building.

To keep the problem relatively simple, ideal control laws and plant representation (i.e., plant equipment with no inertia or time dependent characteristics) are used[§].

Two building control functions and one controlled air flow component are specified. The sensor for the first control function measures the dry bulb temperature in zone 5 (living room) and the

§ Other levels of control algorithms (such as PID control) and detailed plant simulation (Aasem *et al*, 1994) can also be modelled by ESP-r.

actuator for this function is the air node in the same zone. Only one day type is defined for the first control function. This day type is valid all year round, and contains four control periods as shown in Table 7.1.

Table 7.1 The control periods details for the first control function

Period number	Start time	Sensed property	Actuated property	Control law
1	0.00	T_{db}	flux	free floating
2	6.00	T_{db}	flux	ideal control at 21^oC
3	9.00	T_{db}	flux	free floating
4	17.00	T_{db}	flux	ideal control at 21^oC

The second control function is similar to the first one except that it is associated with zone 9 (hall 2), and the start time for the fourth control period is 20.00. On the other hand, the air flow control contains one day type which is valid all year round and comprises one control period valid all day. The sensed condition is the dry bulb temperature of the air flow nodes, with actuation on the fifth air flow component type (window) as shown in Table 7.2. Basically, the defined mass flow function will open the associated window when the dry bulb of the mass flow node defined by the sensor location exceeds 23^oC.

Table 7.2 The controlled mass flow connections

Connection Details				sensor location
number	+ve node	-ve node	component	
1	kitch	n_vert	windw	kitch
2	bed1	n_vert	windw	bed1
3	bathm	n_vert	windw	bathm
4	livng	s_vert	windw	livng
5	bed2	s_vert	windw	bed2
6	bed3	s_vert	windw	bed3

7.2 Modelling systems with large temperature variation

Although other mechanisms can be used to reduce the indoor vapour condensation risk, such as reducing moisture production, dehumidification, increasing heat generation rate and increasing ventilation rate, insulation is the most robust method because it is independent of occupants behaviour, and more efficient in reducing energy consumption and amending thermal comfort. Transparent insulation materials TIM increase the thermal resistance of walls and, unlike conventional insulation, allows the transmission and absorption of solar energy. For that reason, the use of TIM in buildings not only reduces the possibility of surface water condensation but may also terminate it since the wall's internal surface temperature is expected to be higher than that of the inside air. Furthermore, TIM converts the wall into a heat source which is a form of renewable energy.

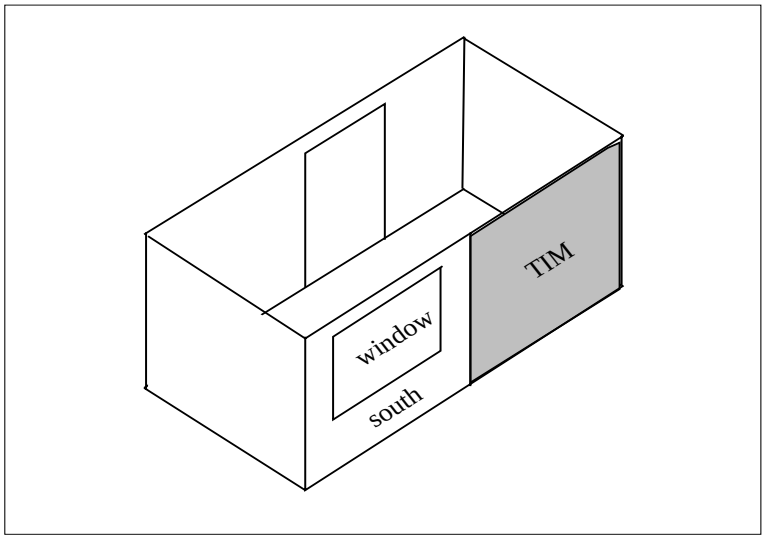

Figure 7.3 The TIM wall location in the living room.

The dynamic simulation of TIM requires the adoption of variable thermophysical properties since it involves high temperature ranges (Strachan, 1995). For the case studied, TIM is installed on the external wall of the living room as shown in Figure 7.3. In order to model the TIM in detail, separate thermal zone (zone 13) is created. The new thermal zone is called TIM and represents the air between the polycarbonate backing sheet and the block as shown in Figure 7.4. According to PASSYS project, this method is expected to lead to good agreement between measured and predicted results for temperature profiles through the TIM facade (Jensen, 1993). The blind operation strategy ensured that the blind covers the facade if the incident solar radiation is less than 100 W/m^2 in order to provide extra insulation at night and in low light conditions.

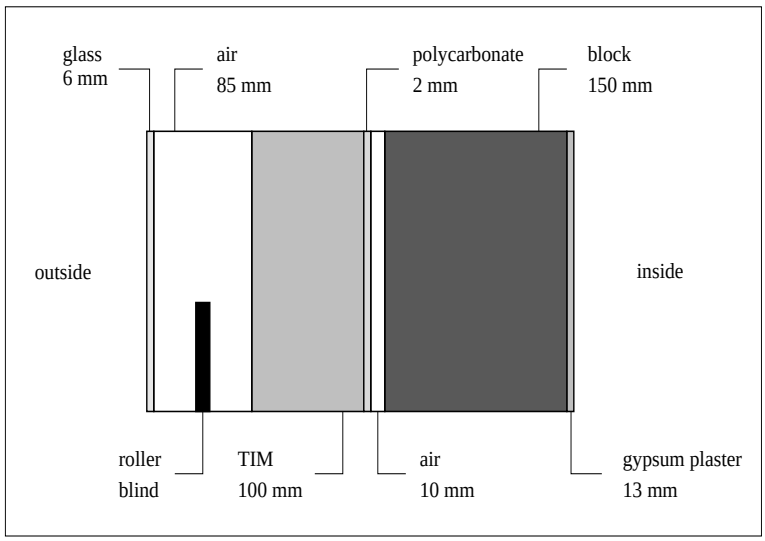

Figure 7.4 Cross-section of the transparently insulated facade (from Strachan and Johnstone, 1994).

The thermal conductivity of of TIM used within the PASSYS (Jensen, 1993) is 0.097 W / (m ^oC) at 20 ^oC and 0.16 W / (m ^oC) at 60 ^oC. Assuming a linear relation, the TIM thermal conductivity can be modelled either via the linear temperature dependence option, or the non-linear thermophysical properties option. If the linear conductivity option is used, the reference temperature can be chosen as 20 ^oC. Accordingly, the reference conductivity is 0.097 W / (m ^oC) and the temperature dependence is 0.00158 W / (m $^oC^2$). A section of the construction file relating to the TIM is shown in Table 7.3.

Table 7.3 Linear conductivity representation of the 3rd layer in 1st surface.

# conduc- # tivity	density	specific heat	thick- ness(m)	dpnd type	ref. temp	temp. factor	moisture factor	surf		lyr
1.0500	2500.0	750.0	0.0040	0	0.00	0.00000	0.00000	#	1	1
0.0000	0.0	0.0	0.0850	0	0.00	0.00000	0.00000	#		2
0.0970	36.0	1028.0	0.1000	1	20.00	0.00158	0.00000	#		3
0.2300	115.0	1028.0	0.0020	0	0.00	0.00000	0.00000	#		4

On the other hand, if the non-linear thermophysical properties option is used, the same dependence information can be fed to the Simulator via the thermal configuration file as shown in Table 7.4.

Table 7.4 Non-linear conductivity representation of the 3rd layer in the 8th surface of the 4th zone.

1			#	TOTAL THERMAL FUNCTIONS									
1			#	thermal function No.									
13	1	3	#	thermal actuator location									
1			#	Total thermal equations									
#	No	T	MIN(Temp)	MAX	A	B	b	C	c	D	d	E	e
	1	1	20.0	60.0	0.097	0.00158	1.0	0.0000	0.0	0.0000	0.0	0.0000	0.0

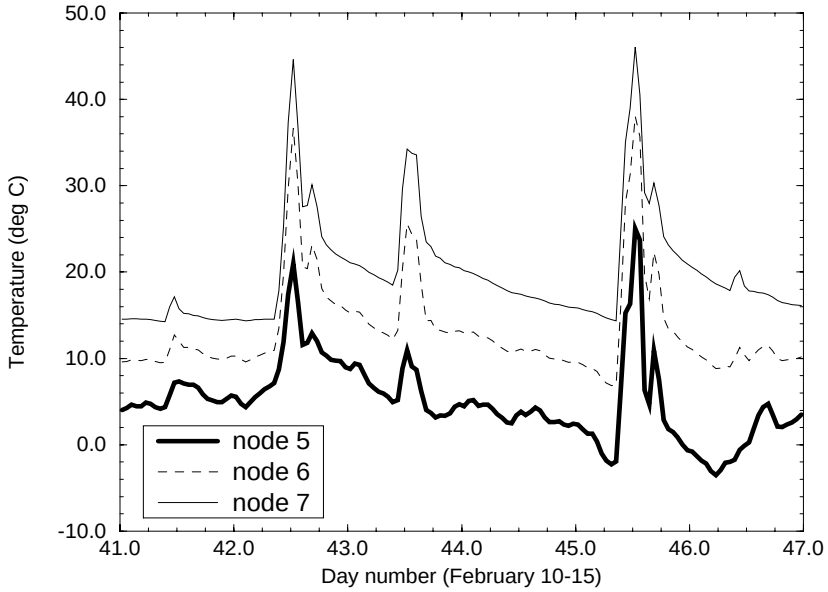

Figure 7.5 The TIM homogeneous node temperature fluctuation.

The temperature profiles for the three nodes (5, 6 and 7) within the TIM layer are shown in Figure 7.5. Higher temperature variations are expected for longer simulation periods. This is because higher solar radiation and clearer skies are expected in the other seasons. However, the difference between temperatures of the two nodes bounding the TIM layer (nodes 5 and 7) is clear. Therefore, thermal conductivity between nodes 5 and 6 should be different from that between nodes 6 and 7. For that reason, the variable thermophysical properties scheme estimates thermal conductivity between each two nodes based on their mean temperature as described in Chapter 4.

7.3 Design involving 3-dimensional effects

In this section two 3-dimensional phenomenon are considered: thermal bridging and heat flow through building slab on the ground. The adaptive gridding scheme is used to simulate these 3-dimensional phenomenon.

7.3.1 Thermal bridging

ESP-r is used to investigate the effectiveness of the insulation layer at an external wall intersection. As an example, the edge at the intersection of the north and east walls in the kitchen is selected. Figure 7.6 shows the details for that edge. Since the 3-dimensional temperature distribution for the kitchen is updated at each time step, a dynamic 3-dimensional temperature distribution can be created for the simulation period. However, this is not available within the current version of ESP-r. The effect of heat flow through the edge on 1-dimensional surface temperature of both north and east walls is shown in Figure 7.7.

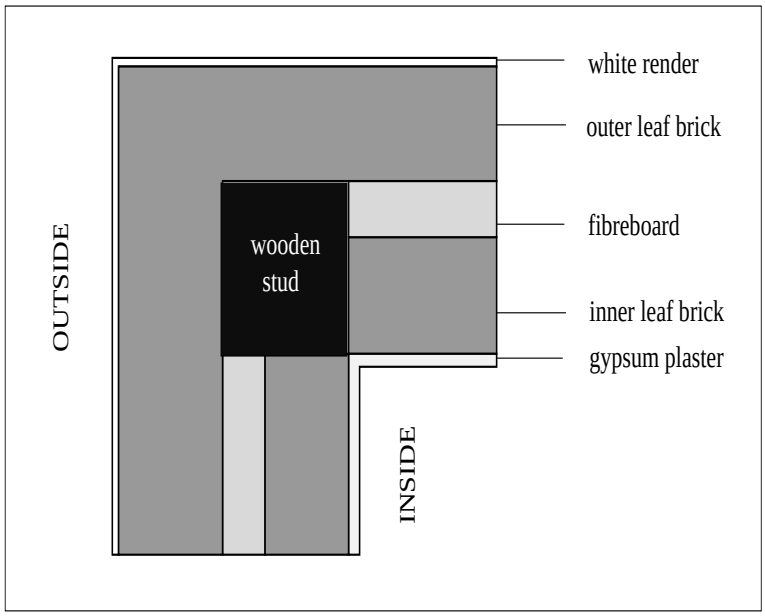

Figure 7.6 Edge details for 3-dimensional model.

7.3.2 Heat flow through ground slab

The boundary conditions at the ground surfaces are defined to be similar to the boundary conditions for surfaces within building zones. If the required boundary condition is not available, an imaginary building zone can be created with the required boundary condition. The geometry and construction details for this zone is expected to be simple. In addition, this zone should be thermally

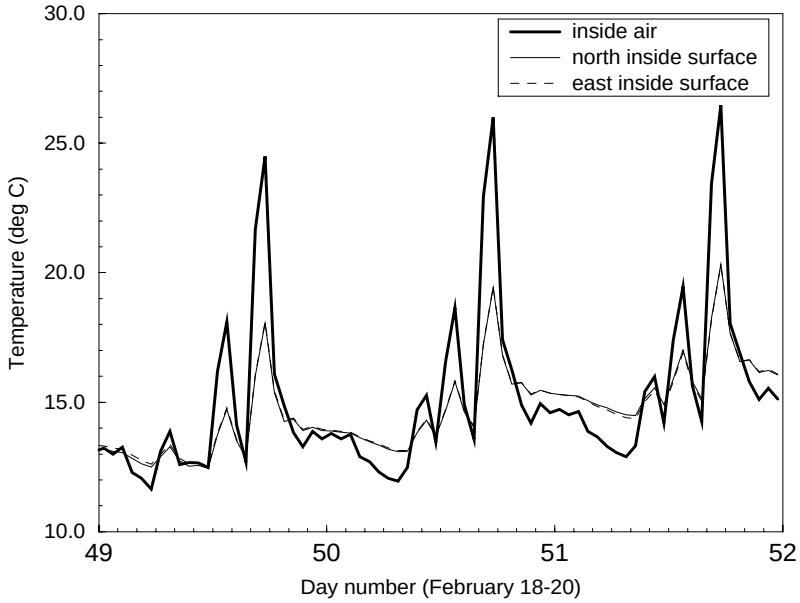

Figure 7.7 Surface temperatures profiles for north and east walls in the kitchen.

unconnected to any real zone within the building in order to prevent an affect on the simulation results.

Furthermore, a more detailed representation of ground boundaries can be modelled. For example, the effect on the current building and adjacent building shading can be considered within the simulation by means of obstruction blocks[§]. In this case, the imaginary zone geometry should account for the geometry of the ground boundaries. That is, the number and shape of the surfaces in the imaginary zone should be similar to the 3-dimensional ground boundary surfaces.

The default boundary condition for the ground is adiabatic. At adiabatic boundaries there is no heat flow between the surface nodes and the boundary. Therefore, these connections are not saved in the connections file (refer to Chapter 3). The boundary can be connected to a node within a 1-dimensional building zone as well as a multi-dimensional zone as shown in Table 3.3.

Since there is no zone with a horizontal roof, an imaginary zone (zone 13) is created in order to model the ground for the building as shown in Figure 7.8. An adiabatic boundary condition is assumed for all bounding surfaces except the top one. The boundary conditions for that surface is shown in Figure 7.9. The ground surface nodes are linked with the external floor nodes of the zones indicated in the Figure. Accordingly, ground gridding should match the floor geometry of the

§ obstruction blocks can be created via the geometry menu of the ESP-r Project Manager.

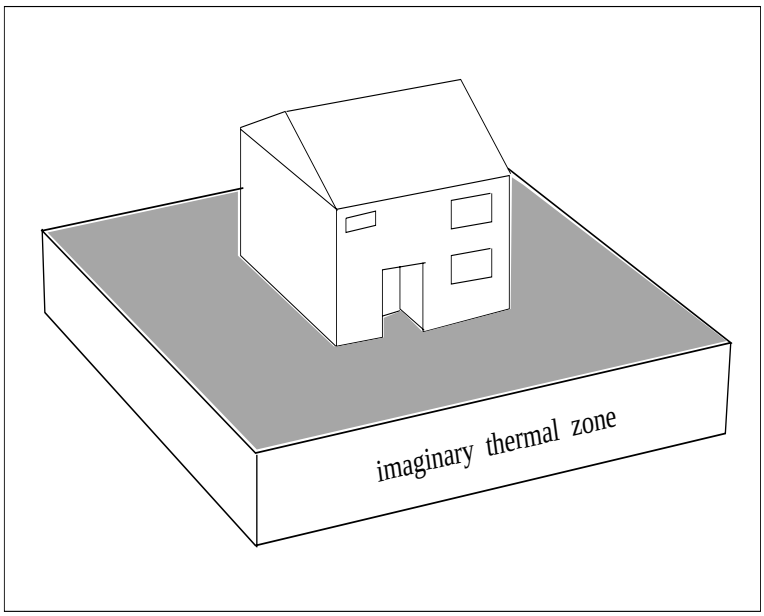

Figure 7.8 Imaginary thermal zone providing required boundary conditions for 3-dimensional ground model.

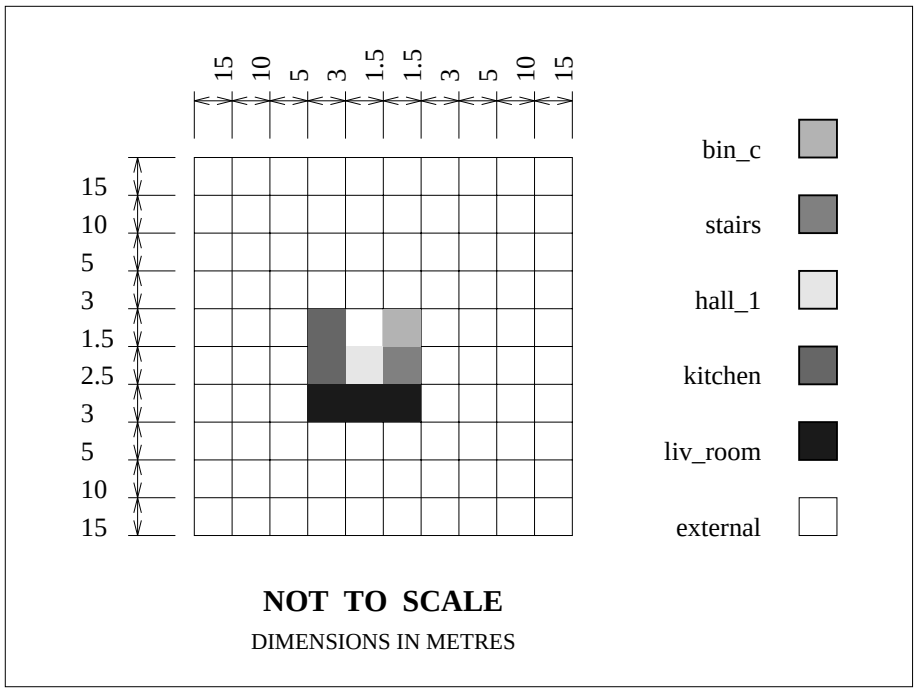

Figure 7.9 3-dimensional ground boundaries.

building zones at the ground level. The remaining area is set to have boundary conditions similar to the external boundary condition for the roof of the imaginary zone (zone 13).

On the other hand, the floor construction for zones connected to the ground should be modified. This is because the 1-dimensional modelling connect the floor construction with a point deep in the ground. However, the 3-dimensional ground modelling allows connection with the ground surface beneath the zone. Furthermore, the system topology should be updated by connecting the floor surfaces to the 3-dimensional ground model (i.e. connection 4 -3 0).

The start up period for 3-dimensional ground simulation is estimated by the gridding module and passed to the Simulator via the ground connections file. The start up period for the ground may be altered by the user via the Simulator. Within the ground start up period, all the invoked options are considered except the multi-dimensional conduction simulation which is replaced by the default 1-dimensional assumption.

Because of the large thermal storage capacity of the ground, the start up period required for a 3-dimensional ground is usually measured in years. In order to overcome this problem, the Simulator initialises the ground temperature distribution on the basis of the ground node temperatures file. The node temperatures file created from previous runs for the same problem can be used as the input file for new runs with much shorter start up period.

The temperature profiles for outside air, living room air, and ground surface are shown in Figure 7.10. The impact of outside air on the ground surface (floor external node) temperature can be noticed. A lower impact with greater time lag is expected if the temperature of a node within the ground is monitored.

7.4 Condensation risk assessment

Dampness and associated mould growth are recognised as a major problem affecting a significant population of houses in the UK as well as many other countries (Rowan *et al*, 1995). In this application, dynamic vapour distribution in the case building is predicted. The output of this simulation can be used to predict dampness and/or mould growth occurrences.

The hygric properties and node distribution details required for moisture flow simulation is fed into the Simulator via a moisture file. This file is zone based. It is created by the 1-dimensional moisture gridding scheme in the gridding module. Within this scheme, moisture node distribution and hygric properties are defined by menu driven options. Because hygric properties are material based, they can be stored in the primitive data base with thermal properties. This will simplify problem definition for moisture flow since hygric properties will be supplied automatically. However, this was not adopted due to lack in hygric properties and internationally standardised formulae for describing hygric properties.

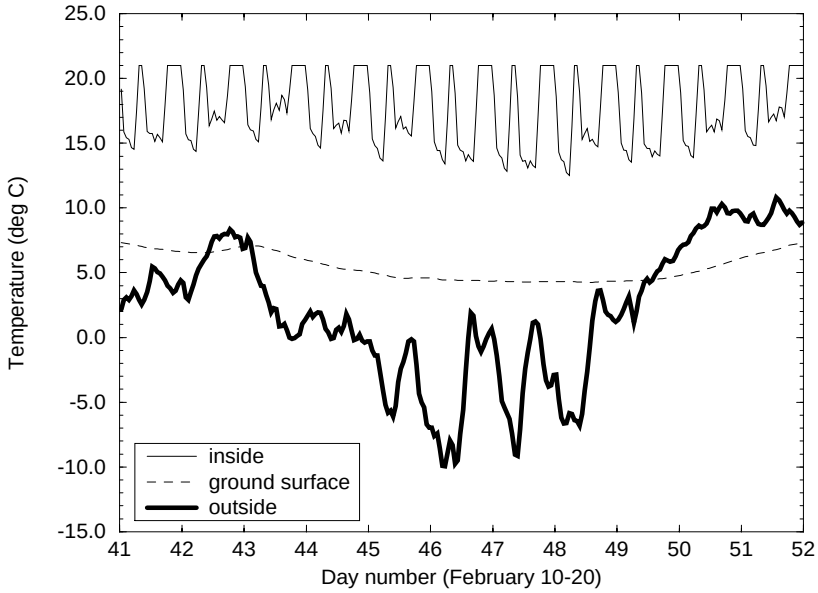

Figure 7.10 Floor exterior node temperature profile.

The zone moisture file location and name are saved in the zone utility file. It has the following format:

- for each surface, number of moisture nodes per layer.
- for each layer, vapour permeability index and data.
- for each layer, sorption isotherm index and data.
- for each layer, thermal vapour diffusion index and data.

The index for each hygric property defines the formula to be used by the Simulator. This allows different formulae to be used for the same property based on the available data. The number of data required for each hygric property is based on the formula index. The current version of the Simulator supports only one formula for each hygric property. These formulae are presented in chapter 5.

Because of the high degree of non-linearity, the Simulator allows the user to change all convergence parameters. In addition, it warns the user if convergence did not occur, or occurred after one iteration. This warning informs the user about the time step and zone number associated with the warning.

The current version of the Simulator saves the relative humidity and the amount of stored condensed vapour at the air nodes. In addition, a commented subroutine call exists for saving relative

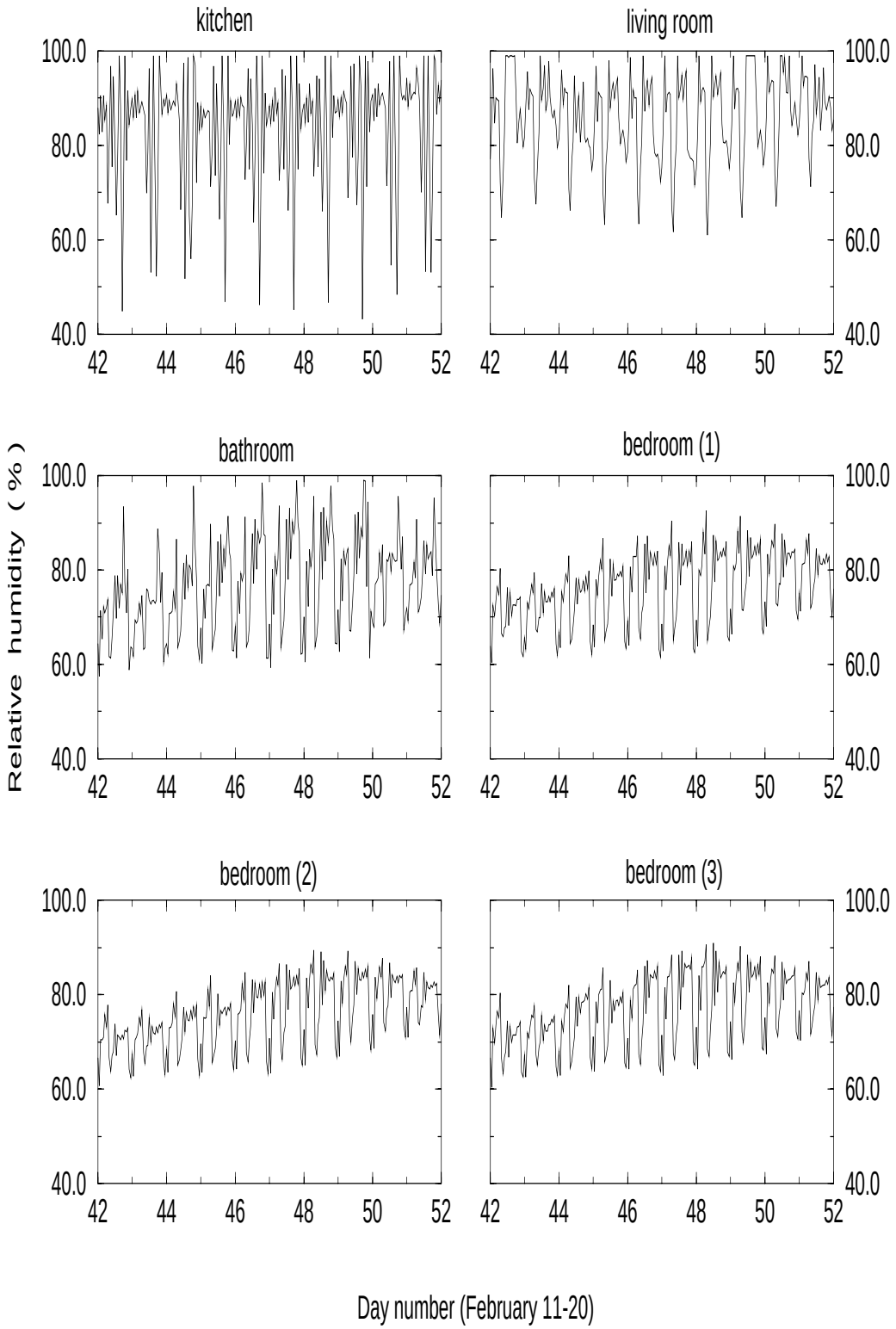

Figure 7.11 Space air relative humidity.

humidity at all internal surfaces in a default file. Graphical tools can be used to display these data after extracting the results for the required location by using UNIX^{TM} commands or small codes for

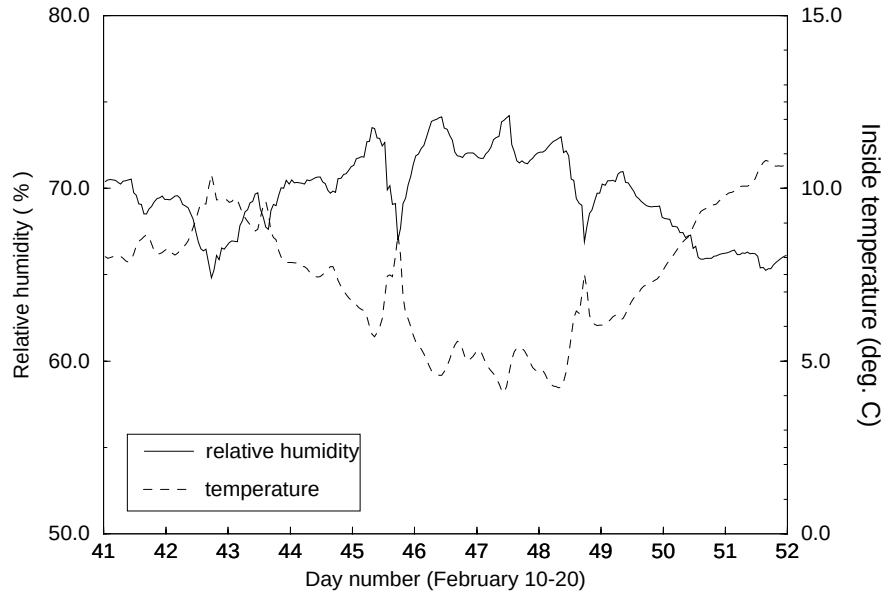

Figure 7.12 Relative humidity and temperature profiles for bin_c.

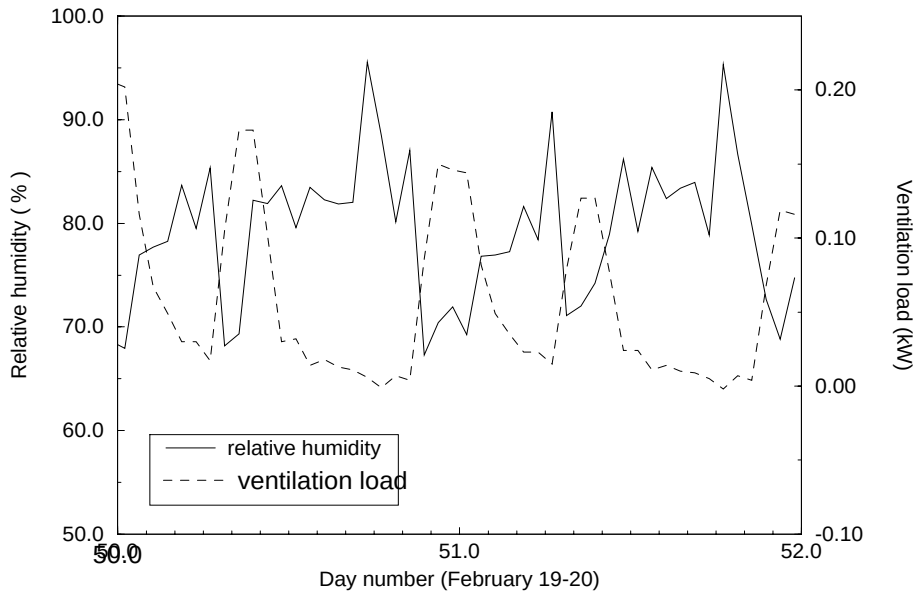

Figure 7.13 Relative humidity, and ventilation profiles for bedroom (3).

data manipulation.

The relative humidity profile for the kitchen, living room, bathroom, bedroom 1, bedroom 2, and bedroom 3 are shown in Figure 7.11. The rapid fluctuation in relative humidity values is because of variation in the dry bulb temperature as shown in Figure 7.12 and air infiltration and ventilation as shown in Figure 7.13.

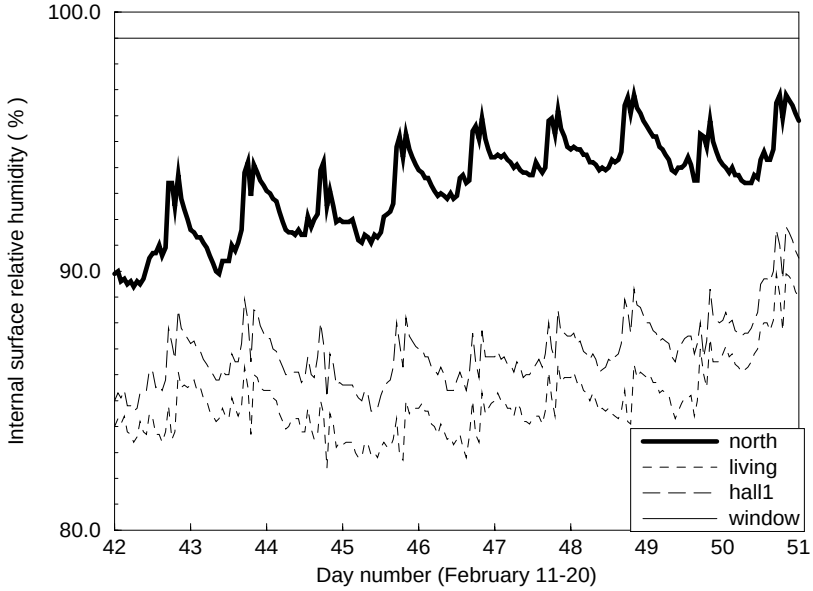

Figure 7.14 Relative humidity profiles for kitchen internal surfaces.

Although condensation did not occur at the kitchen air node for the simulation period, condensation did occur at the window's internal surface as shown in Figure 7.14. This is mainly due to lower temperatures at window's internal surface. On the other hand, the fluctuation of relative humidity for the other surfaces in the kitchen is slower than that at inside air. This is because vapour flow by means of air flow is faster than that through constructions. In addition, heat and vapour produced by cooking is linked to the air node.

7.5 Conclusions

Although the robustness and applicability of ESP-r is significantly increased by the developed schemes within the current work, much work is required with respect to data input, such as hygrothermal properties, and result analysis, such 4-dimensional result display for the multi-dimensional conduction modelling. These points should be considered in the future.

References

Aasem, E., J. Clarke, J. Hand, J. Hensen, C. Pernot, and P. Stachan 1993. ‘‘ESP-r A program for building energy simulation, Version 8 series,’’ ESRU Manual U93/1.

Aasem, E O1993. , *Practical simulation of buildings and air-conditioning systems in the transient domain*, Glasgow. PhD thesis University of Strathclyde

Aasem, E O, J A Clarke, J L M Hensen, N J Kelly, J McQueen, and C O R Negrao1994. , *Current Building Systems Modelling Potential of ESP-r*. System Simulation in Buildings

Hensen, J.L.M. 1991. ‘‘On the thermal interaction of building structure and heating and ventilating system,’’ Ph.D. Thesis, Eindhoven University of Technology.

Jensen, S O1993. , *The PASSYS Project: Subgroup Model Validation and Development*, Brussels. Final Report, Part I and II 1986-1992. Commission of the European Comunities. DGX1I,EUR 15115 EN.

Rowan, N, J A Clarke, J E Smith, J G A Anderson, A Nakhi, N Kelly, R McClain, and J L M Hensen1995. , *Development of a prototype technique for the prediction/alleviation of conditions leading to mould growth in houses*, Glasgow. ESRU report

Strachan, P1995. , *Personal communication*.

CHAPTER 8

Conclusions and Future Work

8.1 Conclusions

Energy conservation has become of increased importance, not only because of economic reasons or scarcity, but, more importantly, because of the effect of energy-related activities on the environment such as global warming. The building sector has been recognised as having potential for energy conservation, mainly in the use of heating, ventilating, and air-conditioning (HVAC) systems. Energy conservation in buildings can be achieved at the design stage through HVAC optimisation, and through improved building thermal performance.

However, buildings and their environmental control systems are complex, making this optimisation task non-trivial. In order to accommodate this complexity, and provide effective design decision support, environmental building performance programs can be used. Intensive research is being performed by the research community in order to ensure the quality of these tools.

While the state-of-the-art for environmental building performance simulation has been substantially enhanced for most building processes, building construction modelling is not well performed. Accordingly, the main goal of this work was to enable adaptive fabric modelling within whole building dynamic energy simulation in order to improve its robustness and applicability. Three approaches were considered to reduce internal simulation error sources: adaptive gridding, variable thermophysical properties simulation and combined heat and moisture transport simulation.

For the adaptive gridding, two approaches were considered: adaptive 1-dimensional and multi-dimensional gridding. The former scheme is designed to reduce or control 1-dimensional heat conduction simulation internal errors. This is done by relating the node distribution to the variable gradient and thermophysical properties distribution. The purpose of the latter scheme is to enable better modelling of multi-dimensional phenomenon such as thermal bridging. In addition, this scheme was used to simulate ground heat flow in 3-dimensional. In order to reduce the computation effort, this scheme allows 3-dimensional conduction modelling with variable resolution throughout the building.

Furthermore, matrix reordering, based on the number of connections and sparse storage and solution techniques, is employed.

A scheme has been developed to simulate the temperature and/or moisture content dependence of material thermophysical properties. This scheme is integrated within a whole building energy simulation environment, ESP-r, and provides two types of dependencies. First, a linear temperature and/or moisture content dependence of thermal conductivity. Second, a nonlinear temperature dependence of all the thermophysical properties. The impact of adopting variable thermophysical properties within building energy simulation has been shown and proved to be important for some cases.

On the other hand, a scheme has been developed to simulate moisture transfer through porous building materials. This scheme is integrated within ESP-r in such a way as to enable combined heat and moisture transport simulation. In addition, it allows modular-simultaneous simulation of heat, air and moisture flow in a combined building/plant context.

The robust PASSYS validation methodology was employed for the validation of the developed schemes. It included all stages of simulation program development. Accordingly, the validity of the developed schemes was concluded.

On the other hand, the developed schemes were used to model real world cases for a typical Scottish house. Not only was the applicability of the developed schemes demonstrated, but also the need to employ these schemes in environmental building performance programs was shown by the cases considered.

8.2 Future work

Although the developed schemes improved the robustness of building fabric modelling, further work is required. Beside the work related to reducing internal simulation error sources, there is a potential to develop and enhance other related areas. For example, the analysis of the multi-dimensional modelling results can be enhanced by incorporating a 4-dimensional (x,y,z and T) graphical tool, and the capabilities of the ESP-r gridding module (/fIgrd/fP) can be improved to allow multi-dimensional gridding of more complicated zone shapes.

8.2.1 Software structure

In order to accommodate the size and complexity of whole building dynamic simulation, the program should be support with a highly modular software structure. This structure should allow different levels of integration through the adoption of a network of integration and accuracy checking loops. Such a structure should provide the user with control on the type of integration and on the accuracy of the simulation. This should ease future developments and facilitate the integration of other simulation tools (e.g. power simulation) into whole building simulation environments.

8.2.2 Explicit air gap modelling

Air gaps are very common in some building constructions. They are used as thermal insulation layers. However, they are usually not well modelled within building energy simulation tools. While heat flow through air gaps takes place via one or more of the three heat flow modes (i.e. conduction, convection and radiation), these are often approximated by an equivalent heat conduction. In other words, the air gap is replaced by an equivalent solid layer.

In order to ensure the quality of simulations, air gaps should be modelled explicitly. That is, the convective and radiative terms should be considered. Although the inclusion of these terms in the system matrix is a straightforward step, it complicates the matrix solution process. For example, ESP-r employs a fast, sparse, direct solver which assumes two connections for each interconstructional node. Therefore, this solver cannot be used if air gaps are explicitly modelled as this will require more than two connections for air gap surface nodes. The adoption of a general, sparse, direct solver (such as the one used for multi-dimensional fabric modelling) will allow an unlimited number of coefficients for each node.

8.2.3 Dynamically adaptive 1-dimensional gridding

The accuracy of heat conduction through multi-layered building constructions can be maximised or controlled by means of the gridding process. However, node distribution is dependent on thermophysical properties of the building, including the heat transfer coefficient for convective boundaries. Since these properties are usually dynamic within a simulation period, dynamically adaptive 1-dimensional gridding is required to update the gridding each time step, or at least each time a relatively large variation in one or more of the thermophysical property values occurs.

8.2.4 Matrix reordering

Unlike the iterative solution methods, the direct methods for the simultaneous solution of a set of linear equations do not preserve the original sparseness of the system matrix. For example, within the Gausian elimination process new non-zero elements are generated in place of zero elements making sparse direct solution techniques more lengthy. The number of non-zero elements can be minimised via the selection of the pivot element. Therefore, matrix reordering can be used to minimised the number of non-zero elements.

On the other hand, matrix reordering can be employed to minimise the round off errors (i.e. maintain mathematical stability). This is usually performed by partial or full pivoting techniques.

8.2.5 3-dimensional control algorithms

The current version of the multi-dimensional gridding scheme supports only free floating and ideal control algorithms. This is because the control related subroutines employ the 1-dimensional

variables (i.e. temperature and heat flux) directly. If the global 1-dimensional variables are replaced by local variables within the control related subroutines, all the available control algorithms can be supported by the multi-dimensional gridding scheme.

8.2.6 CFD and multi-dimensional fabric modelling

The ESP-r environment is capable of multi-dimensional modelling of heat flow through the building fabric. On the other hand, Negrao (1995) has coupled computational fluid dynamics (CFD) with ESP-r in order to simulate air spaces with higher resolution. The multi-dimensional fabric modelling and CFD model may be integrated via the 1-dimensional gridding scheme variables. In other words, the multi-dimensional fabric modelling is performed by employing 1-dimensional heat transfer coefficients which are estimated by the CFD model, and the CFD model requires 1-dimensional internal surface temperatures, as boundary conditions, which are calculated by the multi-dimensional fabric scheme.

ESP-r's simulation potential can be improved by integrating the multi-dimensional scheme with the CFD model in a more direct manner. For example, a new connection type in the multi-dimensional fabric modelling can be used to define a connection with a CFD node.

8.2.7 3-dimensional ground start up period

While almost all buildings are on the ground, empirical validation test cells are usually isolated from the ground in order to reduce the simulation uncertainties. Therefore, the adoption of a proper ground model is of some importance. Numerical ground models are advantageous because of their flexibility. However, they require long start-up periods due to the large thermal capacitance. In order to overcome this problem, the 3-dimensional ground model's initial conditions (i.e. temperature distribution) can be defined by a temperature file generated by a previous run. However, new 3-dimensional ground models will be associated with very long start up periods. Hence, their is a need for an approach which will reduce the start up period of numerical ground models.

8.2.8 Multi-dimensional variable thermophysical properties

This work has shown the impact of adopting multi-dimensional gridding and variable thermophysical properties within building energy simulation. This was concluded from the PASSYS test cell empirical validation of both schemes. Furthermore, the empirical validation of the multi-dimensional gridding scheme has highlighted the importance of adopting both multi-dimensional gridding and variable thermophysical properties within a simulation. This can be achieved by updating thermophysical properties provided by the control volumes and connections files at each time step based on the location of the control volumes which is defined by the supplementary data in the control volume file.

8.2.9 Hygrothermal properties database

The accuracy of heat and moisture transport through the building fabric is strongly dependent on the thermal and hygroscopic transport and storage properties. Therefore, the generation of a standardised hygrothermal property database will reduce the possibility of external error source in building dynamic simulation. In order to allow temperature and moisture content dependent simulation, this database should also include dependence associated data.

8.2.10 Validation of combined heat and moisture transport scheme

While the developed scheme is analytically validated for a simple case, additional validation work is required. For example, the results of the developed scheme can be compared (i.e. inter-model comparison) against another model which has already been the subject of rigorous validation, such as MATCH (Pedersen, 1990).

8.2.11 Explicit fluid transport modelling

The model developed for combined heat and moisture transport through porous building material assumed the fluid flow as vapour because of the lack in experimental data. The explicit inclusion of fluid flow in the model requires both experimental and numerical work. Furthermore, it requires a comprehensive review of existing literature.

8.2.12 HAM models

While the current version of ESP-r allows simulation of heat, air and moisture flow in a building/plant context, it only models combined heat and moisture flow through porous building materials. On the other hand, air flow through porous building materials can be modelled via the air flow network module of ESP-r. However, their is a need for combined heat, air and moisture (HAM) flow through porous building materials because the design impact on thermal quality and durability is large (Hens, 1994).

References

Hens, H 1994. ‘‘Heat+Air+Moisture (HAM) Transport in Envelope Parts, The Annex 24 Enquiry on HAM-Codes,’’ in *Proceedings of Building Environmental Performance*, pp. 373-380, York.

Negrao, C 1995. ‘‘Conflation of Computational Fluid Dynamics and Building Thermal Simulation,’’ *Phd thesis, University of Strathclyde.*

Pedersen, C.R. 1990. ‘‘Combined heat and moisture transfer in building constructions,’’ Ph.D. Thesis, Technical University of Denmark.